THE THERMAL CONDUCTANCE OF BOLTED JOINTS

Final Report
on
NASA Grant No. 19-001-035

Submitted by

The Division of Engineering Research
Louisiana State University
Baton Rouge, La.
May 1968

Prepared Under the Direction of

C. A. Whitehurst, Ph. D.
Associate Professor of Research
Division of Engineering Research
Louisiana State University

THE THERMAL CONDUCTANCE OF BOLTED JOINTS

A Dissertation

Submitted to the Graduate Faculty of the
Louisiana State University and
Agricultural and Mechanical College
in partial fulfillment of the
requirements for the degree of
Doctor of Philosophy

in

The Department of Mechanical, Aerospace
and Industrial Engineering

by
John Elton Fontenot, Jr.
B.S., Loyola University of New Orleans, 1956
M.S., University of Maryland, 1962
February 1968

ACKNOWLEDGMENT

This research was conducted under the guidance of Dr. Charles A. Whitehurst, Associate Professor of Research. I want to express my gratitude to him for the encouragement, counsel and consideration rendered throughout this study. I wish also to thank Drs. G. D. Whitehouse and D. R. Carver for their helpful suggestions.

The assistance of undergraduates W. Thomas Durbin and Kamyar Arjomand with the experimental work is greatly appreciated. Special thanks are extended to Charles Hill for his excellent photographic work and to Tom Durbin again, for his very capable assistance with the computer programming.

Thanks are extended to Shell Development Company for typing of the manuscript and for assistance in the preparation of the figures.

The financial assistance of the National Science Foundation and the National Aeronautics and Space Administration is gratefully acknowledged. This study was supported by funds provided under NASA Grant Number 19-001-35.

Special acknowledgment is given to my wife, Barbara, for her help and her consistent patience without which this work would not have been possible.

TABLE OF CONTENTS

LIST OF TABLES

LIST OF FIGURES

LIST OF ILLUSTRATIONS

NOMENCLATURE

Latin Letters

$\bar{a}$	Average radius of contact points (spots)
A	Apparent contact surface area (equation II-1); also represents surface area of plate 1
A_i	Coefficient in polynomial expression for $\sigma(r)$ (equation IV-4)
b	Plate thickness
b_1	Thickness of plate 1
b_2	Thickness of plate 2
C	Thermal conductance
C_a	Thermal conductance of contact points (equation II-1)
C_D	Thermal conductance due to conduction
C_f	Thermal conductance of interface fluid (equation II-2)
C_g	Thermal conductance across interface gap
C_R	Thermal conductance due to radiation (equation II-6)
C_t	Total conductance of joint contact area
C_V	Thermal conductance due to convection
d_h	Diameter of fastener head
D	Plate flexural rigidity (equation II-27)
E	Modulus of elasticity
Gr	Grashof Number; defined on p. 486 of reference 5
h	Convective film coefficient
h_{e_1}	Total heat transfer coefficient for heat exchange between edge of plate 1 (Illustration V-3) and surroundings
h_{e_2}	Total heat transfer coefficient for heat exchange between edge of plate 2 (Illustration V-3) and surroundings
h_{t_1}	Total heat transfer coefficient for heat exchange between top of plate 1 (Illustration V-3) and surroundings

h_{t_2}	Total heat transfer coefficient for heat exchange between bottom of plate 2 (Illustration V-3) and surroundings
H	Meyer hardness
He	Chemical symbol for helium
H_0	Nominal Meyer hardness (equation II-13)
H_2	Chemical symbol for hydrogen
i_A	R.M.S. of surface irregularity - surface A
i_B	R.M.S. of surface irregularity - surface B
k	Thermal conductivity
k_a	Thermal conductivity of dry air
k_f	Thermal conductivity of interface fluid
k_M	Mean thermal conductivity between two surfaces in slip flow (equation II-10); also mean thermal conductivity defined for equation II-13
k_1	Thermal conductivity of plate 1
k_2	Thermal conductivity of plate 2
L	Length of joint
m	Variable defined for equation II-27 (Plotted in Figure II-8)
M	Molecular weight of interface gas
n	Number of contact points per unit area
P	Pressure
P_f	Pressure of interface fluid
P_1, P_2, P_3, P_4	Points of interest (Illustration I-1)
q	Heat flux
q_a	Heat flux across contact points

q_f	Heat flux across interface fluid
q_R	Heat flux across interface due to radiation
q_t	Total heat flux across interface
q_1	Input heat flux (Illustration V-3)
q_2	Output heat flux (Illustration V-3)
Q_a	Heat transfer rate across contacts
Q_f	Heat transfer rate across fluid
Q_t	Total heat transfer rate across joint
Q_1	Heat input rate (Illustration I-1)
Q_2	Heat output rate (Illustration I-1)
r	Radial coordinate
r_e	One-half of average value of distance between contact points (equation II-14)
r_h	Radius of fastener head
r_L	Radius of loaded area (Illustration IV-2)
r_s	Radius of fastener shank
r_σ	Radius at point of zero interface stress
R	Radius of idealized joint
S_L	Slope of plate at $r = r_L$
S_1, S_2, S_3, S_4, S_5, S_6	Summations (equation IV-13)
T	Temperature
T_A	Absolute temperature of surface A, plate 1
T_B	Absolute temperature of surface B, plate 2

T_f	Absolute temperature of interface fluid
T_M	Average temperature of joint interface (equation II-7)
T_1, T_2, T_3, T_4	Temperatures of points P_1, P_2, P_3, P_4 (Illustration I-1)
T_1	Absolute temperature of plate 1 (Illustration V-3)
T_2	Absolute temperature of plate 2 (Illustration V-3)
V, W, X, Y, Z	Coefficients defined by equation II-29
w	Plate deflection measured from interface plane
w_L	Plate deflection at $r = r_L$
w_1	Deflection of ring 1
w_2	Deflection of ring 2
x, y, z	Rectangular coordinates
x_1	One-half the joint length (Illustration V-3)
X, Y, Z	Rectangular coordinates
y_1	One-half the joint width (Illustration V-3)

Greek Letters

α	Accommodation coefficient; also a parameter defined by equation IV-12
β	Defined in terms of the accommodation coefficient in equation II-11; also a parameter defined by equation IV-12
γ	Ratio of specific heats; also a variable defined by equation IV-12
δ	Interface gap thickness
$\bar{\delta}$	Average interface gap thickness

δ_R	Equivalent interface gap for radiation
ϵ	Emittance
ϵ_A	Emittance of surface A
ϵ_B	Emittance of surface B
ζ	Empirical constant used in equation II-14
η	Empirical constant used in equation II-31
θ	Angle measured from z axis in clyindrical coordinates
λ_A	Wavelength of surface waviness, surface A
λ_B	Wavelength of surface waviness, surface B
Λ	Free-molecule heat conductivity (equation II-9)
μ	Poisson's ratio
ν	Empirical constant in equation II-20
ρ	Ratio - - - r/r_s
$\overline{\rho}$	Ratio - - - r/r_L
ρ_A	R.M.S. value of surface roughness, surface A
ρ_B	R.M.S. value of surface roughness, surface B
ρ_h	Ratio - - - r_h/r_s
$\overline{\rho}_h$	Ratio - - - r_h/r_L
$\overline{\rho}_R$	Ratio - - - R/r_L
$\overline{\rho}_s$	Ratio - - - r_s/r_L
ρ_σ	Ratio - - - r_σ/r_s
$\overline{\rho}_\sigma$	Ratio - - - r_σ/r_L
σ	Stefan-Boltzmann constant
$\sigma(r)$	Interface stress as a function of r
σ_h	Normal stress under fastener head

Nomenclature (cont'd)

σ_I	Normal stress at interface plane
σ_{I_o}	Interface stress at r = 0
Φ	Stress function (equation IV-1)
ψ	Empirical constant in equation II-14
ω	Empirical constant in equation II-20

ABSTRACT

The primary objective of this investigation was the development of a practical analytical method of determining the interface thermal conductance of a bolted joint from a minimum of design information. Such a method was developed and its validity demonstrated with experimental data.

In reviewing the literature, it was found that the development of a completely analytical method was hampered by a number of factors. These included the lack of: (1) experimental data for the stress distribution under boltheads, (2) an experimentally verified method for obtaining the stress distribution in the interface of a bolted joint and the region of apparent contact, and (3) a theoretical method for predicting the interface gap when the stresses are known. A comprehensive program combining experimental analysis with theory and digital computer calculations was undertaken to eliminate the unknowns and to provide the necessary analytical techniques.

Normal stress distributions under button-head and fillister-head bolts were measured and the results indicate that the common assumption of a uniform stress is not always valid.

Measurements of the interface stress distribution between thin bolted plates were made and the results for the extent of the stress region were found to disagree with Sneddon's theory developed for a simplified configuration. This disagreement was found to be important when calculating deflections of bolted plates. Fernlund's simplified approach to determining the interface stress distribution, previously verified for

thick plates, was shown to be invalid for thin plates. A new approximate method was developed to replace Fernlund's simplified method for thin plates and was shown to yield interface stress distributions which, when used to calculate plate deflections, produced deflections in good agreement with experimental measurements. The goodness of the agreement was found to depend upon the exact value used for the extent of the interface stress region.

An analytical technique, employing the method of superposition, was developed to describe the deflection of thin circular plates with center holes, subject to non-uniform partial loading. The resulting equations were programmed for solution on a digital computer. The validity of this analysis was checked experimentally for thin circular and square plates. Using the computer program, the deflection of thin bolted plates was shown to be extremely sensitive to the interface stress distribution. Fernlund's simplified method to determine the interface stress distribution, when used with the digital program was found to yield plate deflections more than an order of magnitude too large for thin plates. Plate deflection calculations, based upon experimental data obtained in this study for the radial extent of the interface stress and an approximate method developed to describe the interface stresses between thin plates, were shown to agree well with measured values of plate deflection.

The interface pressures and plate deflections, determined from the study of bolthead and joint interface stresses, were used in equations previously developed to determine the thermal conductance of two bolted joints in the region of interfacial contact, and in the zone of interfacial separation. The computed values of thermal conductance were used

in a finite-difference heat transfer analysis to determine the steady-state temperature gradients across aluminum and stainless-steel bolted joints in air and vacuum. These computed gradients were found to agree with experimentally determined gradients within 2°F. The experimental gradients were obtained in 5 tests in air at ambient pressure and 4 tests in vacuum.

CHAPTER I

INTRODUCTION

The determination of accurate temperature distributions and heat transfer rates in highly-stressed structures is of great importance, particularly in the aerospace industry. High temperatures are produced in high performance aircraft and rockets by either aerodynamic heating or heat transfer from products of combustion; in spacecraft, by solar heating. Very low temperatures are also produced in these same vehicles, owing primarily to the cooling action of cryogenic propellants. At certain times, one part of a structure is being severely heated and an adjacent part is being cryogenically cooled. This combination results in large temperature gradients and correspondingly high heat transfer rates.

In the majority of structural temperature studies, the temperature distribution in structural members that are bolted or riveted together is determined by assuming that the fasteners are not present and that the members are in perfect physical contact, i.e., thermally they act as a uniform solid. However, when the need for accurate temperature distributions is combined with high heat transfer rates, the discontinuity of the real joint may no longer be ignored. This is also true in spacecraft structures when the need for accurate temperature distributions is combined with only moderate heat transfer rates. This latter problem occurs frequently in spacecraft structures which are adjacent to astronomical experiments.

The following is an example of a transient heat transfer problem in which joint discontinuity must be considered.

Consider the simple, two-dimensional lap joint depicted in Illustration I-1. If T_3 and T_4 are fixed temperatures at points P_3 and P_4 and heat is flowing into the joint only at P_3 and leaving only at P_4, a transient temperature analysis can be obtained with a digital computer. The thermal properties of the materials and the thermal conductance of the interface must be known. The value of the interface thermal conductance can have a pronounced effect on the temperature at points 1 and 2 as well as on the transient heat rejection rate.

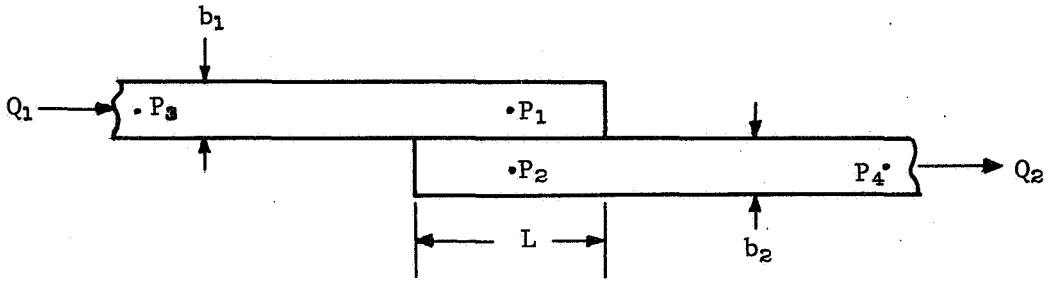

ILLUSTRATION I-1 Two-Dimensional Lap Joint

This effect is demonstrated in the results of a short study, graphically presented in Figures I-1 and I-2, which was conducted with the digital program described in reference 1. The pertinent physical data is also given in these two figures. The value of the interface thermal conductance used--6.7×10^{-5} BTU/in^2 sec °F--admittedly is quite low. Values of this order have been experimentally measured, however, in the case of riveted lap joints by Coulbert and Liu (2). A low value was purposely chosen to emphasize the large errors that can sometimes occur if the joint discontinuity is neglected. In many spacecraft, a temperature

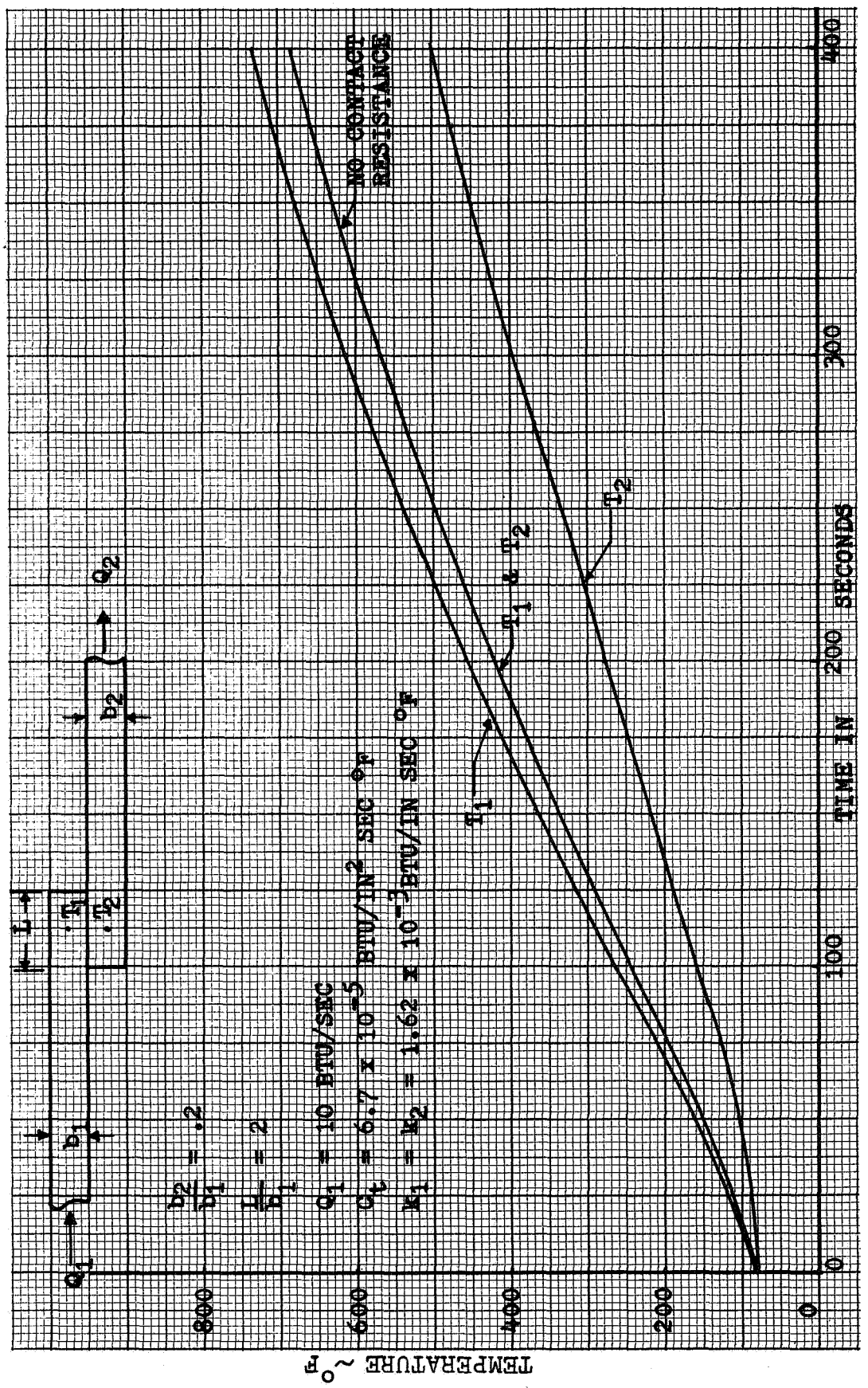

FIGURE I-1 TEMPERATURE DISTRIBUTION IN A LAP JOINT WITH AND WITHOUT CONTACT RESISTANCE

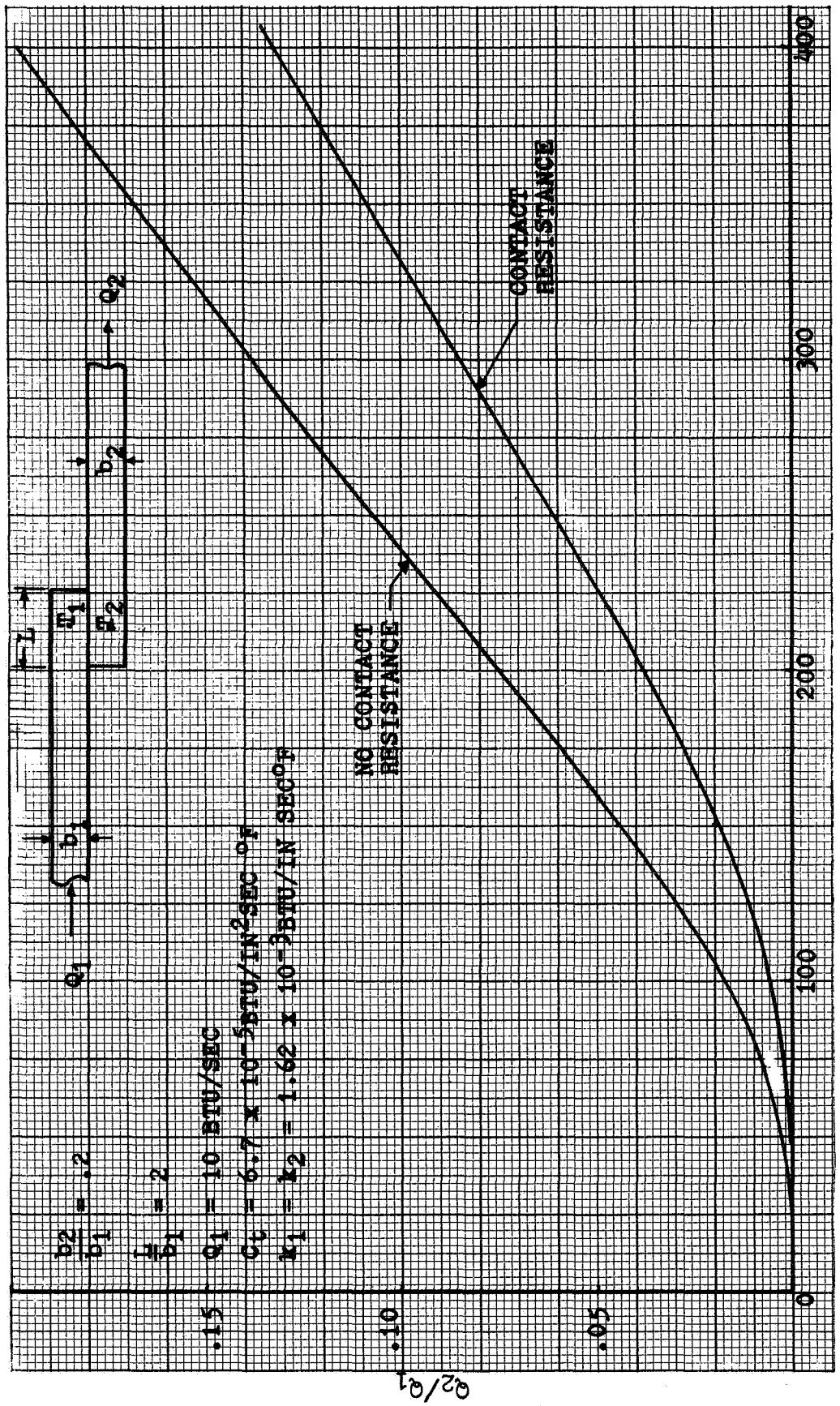

FIGURE I-2 RATIO OF HEATING RATES IN A LAP JOINT WITH AND WITHOUT CONTACT RESISTANCE

error of 10 degrees or a 10 percent error in heat transfer rate can be serious.

The purpose of this investigation was to provide a means of analytically determining the interface thermal conductance of a bolted joint from a minimum of design information. Until the present time, this was not possible, as a discussion of the present state-of-the-art will show in Chapter II.

The investigation was both theoretical and experimental. The experimental work was intended both to provide empirical data for bolthead and joint interface stress distributions where current theory is inadequate, and to verify the heat transfer analysis.

CHAPTER II

BACKGROUND, LITERATURE SURVEY, AND PROBLEM DEFINITION

A discussion of the underlying physical mechanisms and a review of the current state of affairs pertaining to joint thermal conductance is required before this investigation can be described. A systematic treatment of the various aspects is necessary because of the complexity of the overall problem. This will be done according to the following outline:

A. The differences between an idealized joint (or contacts) and an actual mechanical joint, either bolted or riveted, will be explained.

B. The heat transfer mechanisms involved in interfacial heat transfer will be described and their magnitudes compared.

C. Previous research pertaining to heat transfer across contacts and actual mechanical joints will be discussed.

D. The specific problem under investigation will be defined and the work done will be outlined.

A. Idealized Joint Versus an Actual Mechanical Joint

In most of the work that has been done to measure either the heat transfer across or the thermal conductance of an interface, many simplifying assumptions have been made. The mechanical fastener was eliminated and the problem worked as if the two joint members were pressed together by a uniformly distributed load. The simplification is demonstrated by Illustration II-1.

There are important differences between the heat transfer problems of actual joints and of contacts. In the actual joint, the width of the interface (interface gap) is a function of fastener and joint geometry as well as the torque applied to the fastener. The width of this gap

varies considerably along the interface. In the idealized joint, the applied load is uniform and the interface stress is macroscopically uniform. The interface stress varies on a microscopic scale because of irregularities on the contact surfaces. Of primary importance in a study of the thermal conductance of contacts is the consideration of the microscopic roughness. A study of the thermal conductance of an actual mechanical joint involves primarily the determination of the macroscopic contact zone, which is a function of the stresses induced in the joint members by the fastener.

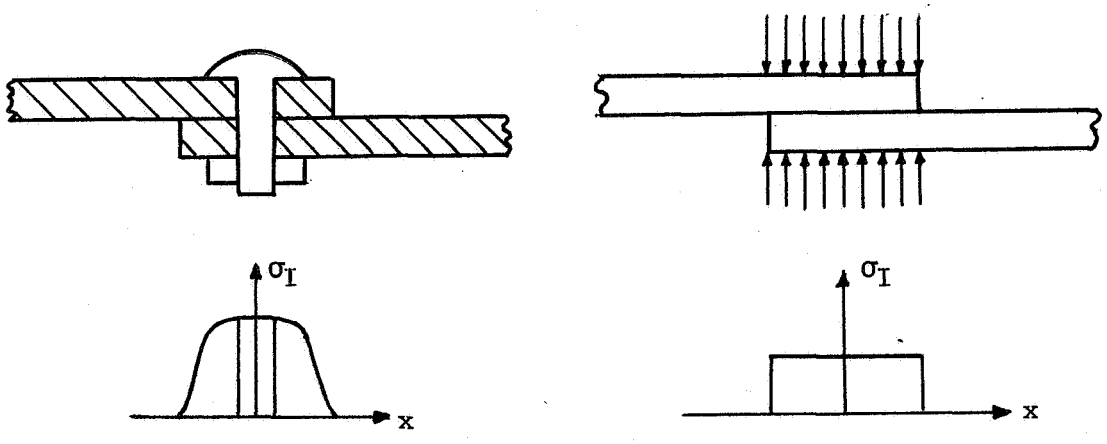

Actual Joint Idealized Joint or Contacts

ILLUSTRATION II-1

B. Interfacial Heat Transfer Mechanisms

The essential problem in the study of interfacial heat transfer is to determine either the effective thermal conductivity or the thermal resistivity of the interface. Since the basic mechanisms of heat transfer across actual mechanical joints and contacts are the same, the following discussion will be initially confined to contacts. The problem of the actual joint will be considered later.

Consider two plates that are placed together and held in position by a uniformly applied force. To the unaided eye, the two plates might appear to be in perfect contact, especially if the surfaces in contact are highly polished. On the contrary, because microscopic irregularities do exist, even in the most highly polished surfaces, the two plates do not meet over the entire area of the interface. Especially at low contact pressures, the surfaces may touch at very few places (as few as three are possible). Although the interface gap varies from point to point (Illustration II-2) an average value of this gap can be used to represent the proximity of the two surfaces. If the outside surface of plate 1 in Illustration II-2 is heated and the outside surface of plate 2 is cooled, a temperature gradient will exist across the width of

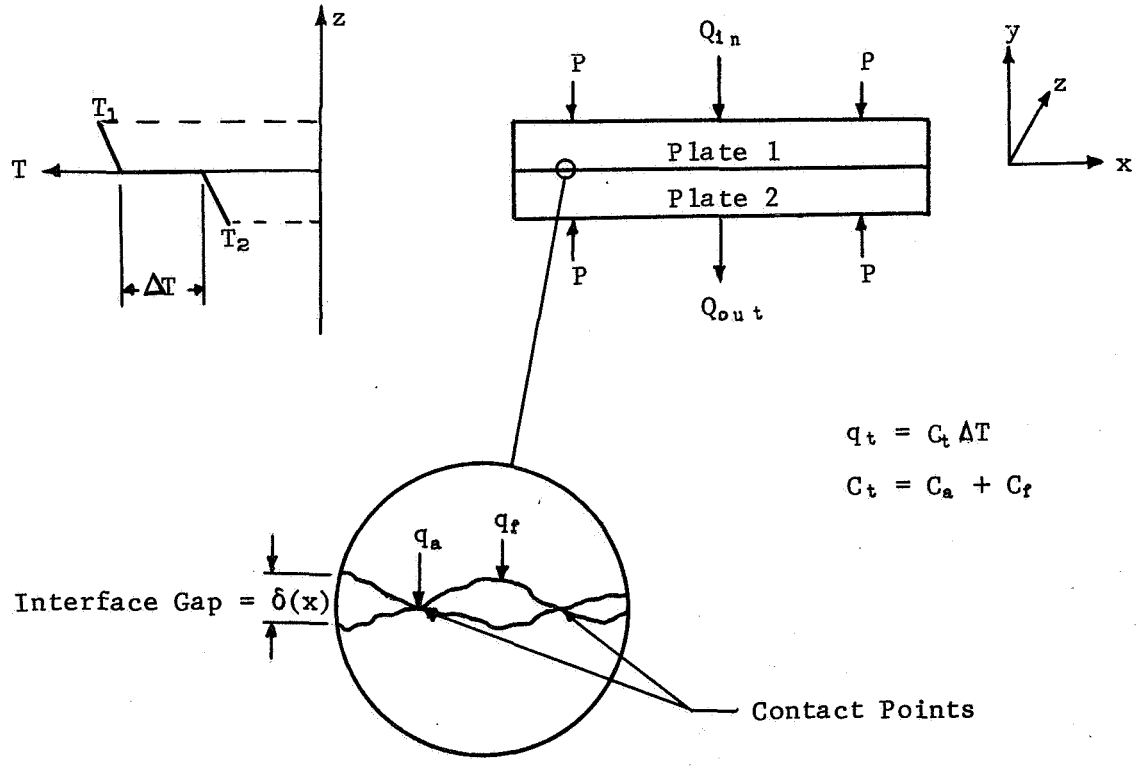

ILLUSTRATION II-2 Heat Transfer across Contacts

the plates. This gradient will be the summation of the gradients across each plate and the temperature drop (ΔT) that occurs at the interface. This temperature drop is the result of a finite interface gap.

The total heat transfer between the surfaces will be due to the heat conducted across the actual contact points and that transferred across any interstitial fluid. If the total heat transfer rate is denoted by Q_t, the heat transfer rate across the contact points by Q_a; and the rate across the fluid by Q_f:

$$Q_t = Q_a + Q_f = (q_a + q_f)A = A(C_a + C_f)\Delta T \qquad \text{(II-1)}$$

where C_a and C_f denote the thermal conductance of the contact points and the fluid, respectively, and A is the apparent contact surface area.

1) Fluid Conductance:

The conductance of the interstitial fluid, if one is present, depends on several factors, since heat transfer across the fluid may occur by conduction, convection, radiation or a combination of these. Therefore C_f may be expressed as

$$C_f = C_D + C_V + C_R \qquad \text{(II-2)}$$

where C_D, C_V, and C_R are the thermal conductances of the fluid due to conduction, convection, and radiation, respectively. These conductances need discussion in some detail. It will be shown that, at moderate temperature levels, radiation and convection can be neglected, in most contacts and joints.

Radiation. First compare heat transfer across an interface gap by radiation and fluid conduction. The heat flux by radiation can be expressed as

$$q_R = C_R (T_A - T_B) \qquad \text{(II-3)}$$

where T_A and T_B are the absolute temperatures of the contact surfaces. The Stefan-Boltzmann equation applied to this situation is shown by Eckert and Drake (3) to be

$$q_R = \frac{\sigma(T_A^4 - T_B^4)}{\frac{1}{\epsilon_A} + \frac{1}{\epsilon_B} - 1} \qquad \text{(II-4)}$$

where σ = Stefan-Boltzmann constant and ϵ_A and ϵ_B are the emittances of the contact surfaces. A combination of equations II-3 and II-4 gives

$$C_R = \frac{\sigma(T_A + T_B)(T_A^2 + T_B^2)}{\frac{1}{\epsilon_A} + \frac{1}{\epsilon_B} - 1} . \qquad \text{(II-5)}$$

Assume now an equivalent interface gap for radiation; this is a gap thickness that would have the same conductance by fluid conduction. Then

$$C_R = k_f / \delta_R \qquad \text{(II-6)}$$

where k_f is the thermal conductivity of the interface fluid for the average temperature and pressure of the gap. If it is assumed that $\epsilon_A = \epsilon_B = 1$ and $T_A \simeq T_B \simeq \frac{T_A + T_B}{2} = T_M$, then

$$\delta_R = \frac{k_f}{4\sigma T_M^3} . \qquad \text{(II-7)}$$

In Figure II-1, this expression is plotted for air at a pressure of one atmosphere. The fluid thermal conductivity is independent of pressure except in the vacuum range; i.e., less than about 0.2 psia [according to R. A. Minzner et al. (4)]. The curve is therefore a conservative estimate for most problems (since $\epsilon_A = \epsilon_B = 1$) involving air as the interface fluid and is typical for most other gases.

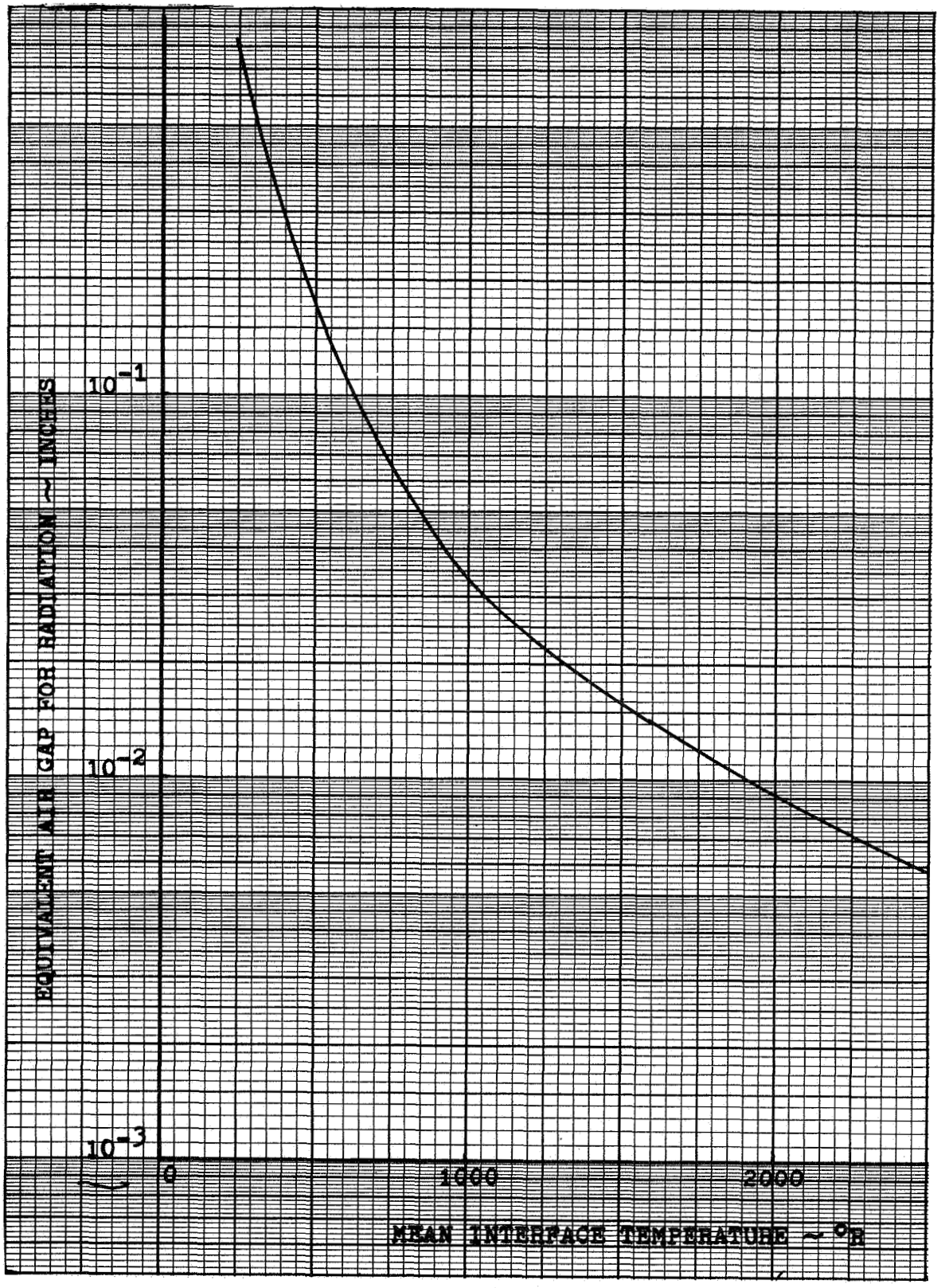

FIGURE II-1 EQUIVALENT AIR GAP FOR RADIATION VERSUS MEAN INTERFACE TEMPERATURE

If, in a particular situation, the maximum interface gap is small compared with δ_R heat transfer by radiation may be neglected. In Figure II-1 again, for an interface temperature of 1000°R, it can be seen that the equivalent air gap for radiation is 0.034 inches. Since a nominal value for large gaps is actually about 0.001 inches, the heat transfer due to radiation would only be about three percent of that due to fluid conduction. Of course, when there is no fluid in the gap, the conductance due to radiant heat transfer has to be compared with the value of the conductance of the contact points to determine if radiation must be considered.

Convection. Consider now the problem of convective heat transfer in the interface gap. To determine whether convection across a particular interface may be neglected, the ratio $C_V/C_D = C_V\bar{\delta}/k_f$ is convenient, where $\bar{\delta}$ is the average value of the interface gap. Jacob (5) gives values of the ratio for air determined by various investigators. These values are presented in graphical form as a function of the Grashof Number, Gr.

To apply this data to the immediate problem, the properties of air are evaluated at T_M. The expression $C_V\bar{\delta}/k_f$ is the ratio of the conductance for heat transfer by convection to that for conduction only. McAdams (6) indicates that, for a vertical interface gap (the orientation most conducive to convection), free convection can be ignored for $Gr < 2000$. For a horizontal gap, the limiting Grashof Number is 1000.

Figure II-2 (from reference 7) is useful for determining whether natural convection should be considered in a particular case. This figure is a plot of the minimum interface gap thickness for free convection versus the temperature drop across the gap, with T_M as a parameter.

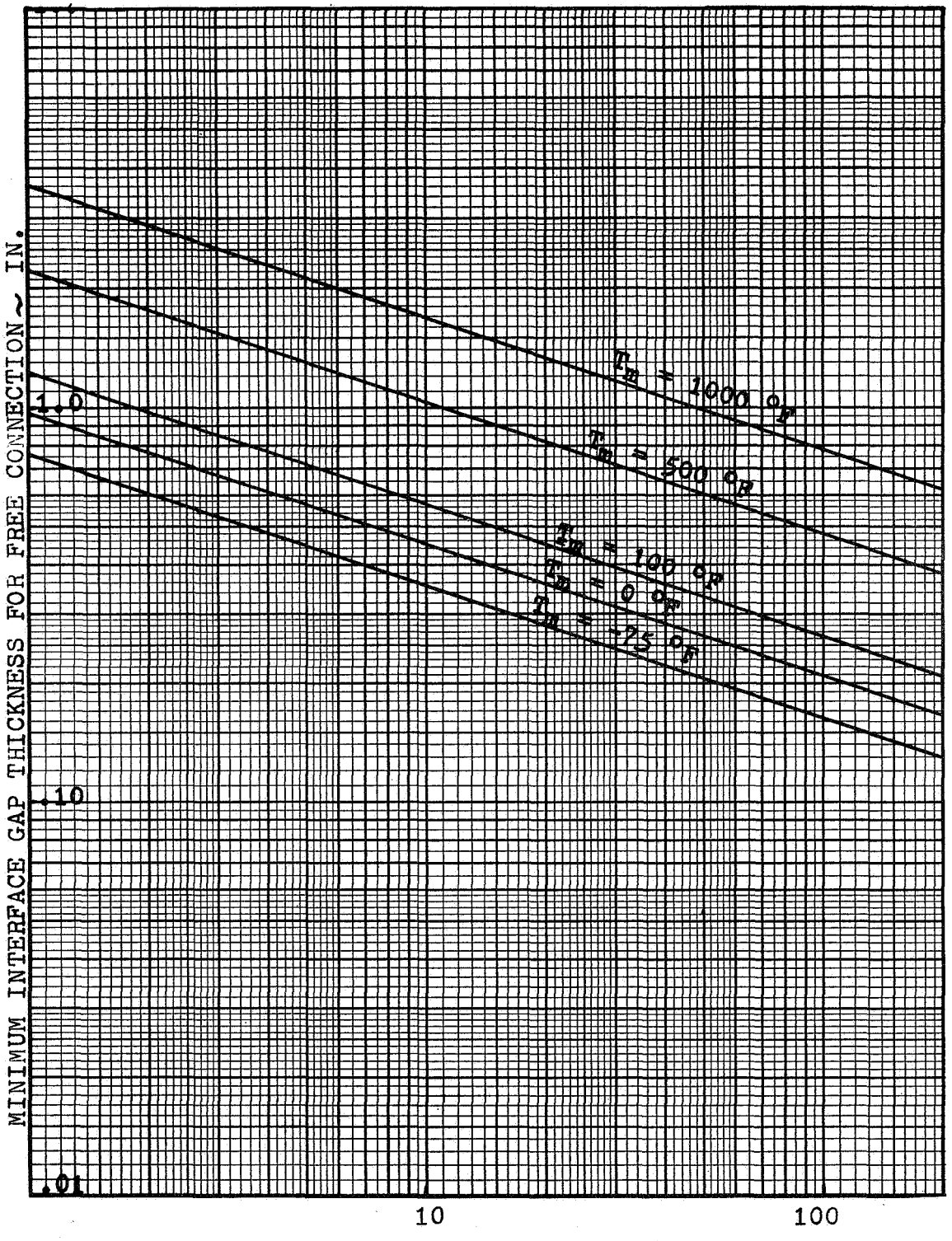

FIGURE II-2 MINIMUM INTERFACE GAP THICKNESS FOR FREE CONVECTION VS. TEMP. DROP ACROSS INTERFACE

It is based on a limiting Grashof Number of 2000, an ambient pressure of one atmosphere, and air as the interface fluid. If the interface pressure is less than one atmosphere, the minimum gap thickness for free convection increases. From Figure II-2 it can be seen that in most cases, heat transfer by convection will be only a small percentage of that by fluid conduction.

Conduction. From the foregoing discussion, it can be concluded that the dominant mode of heat transfer across the fluid in the interface gap will be conduction, in most cases.

Previously it was noted that conductive heat transfer across the gap is proportional directly with the fluid conductivity and inversely with the average value of gap thickness. Thus, the conductance due to fluid conductivity is

$$C_D = \frac{k_f}{\bar{\delta}} \quad . \qquad \text{(II-8)}$$

The value of C_D can be determined if k_f and $\bar{\delta}$ are known. (Methods of determining $\bar{\delta}$ will be discussed later.) The value of k_f is dependent upon the fluid, the interface temperature, and, in some cases, the ambient pressure. Since air is the most common fluid, the value of k_f for air will be considered here.

The thermal conductivity of dry air, k_a, is plotted as a function of temperature at a pressure of one atmosphere in Figure II-3. Experimentally, k_a has been found to be independent of pressure, except at very low pressures when the mean free path of the air molecules approaches the width of the interface gap (8). At these low pressures, continuum theory ceases to be applicable. Free-molecule heat conductivity must be used.

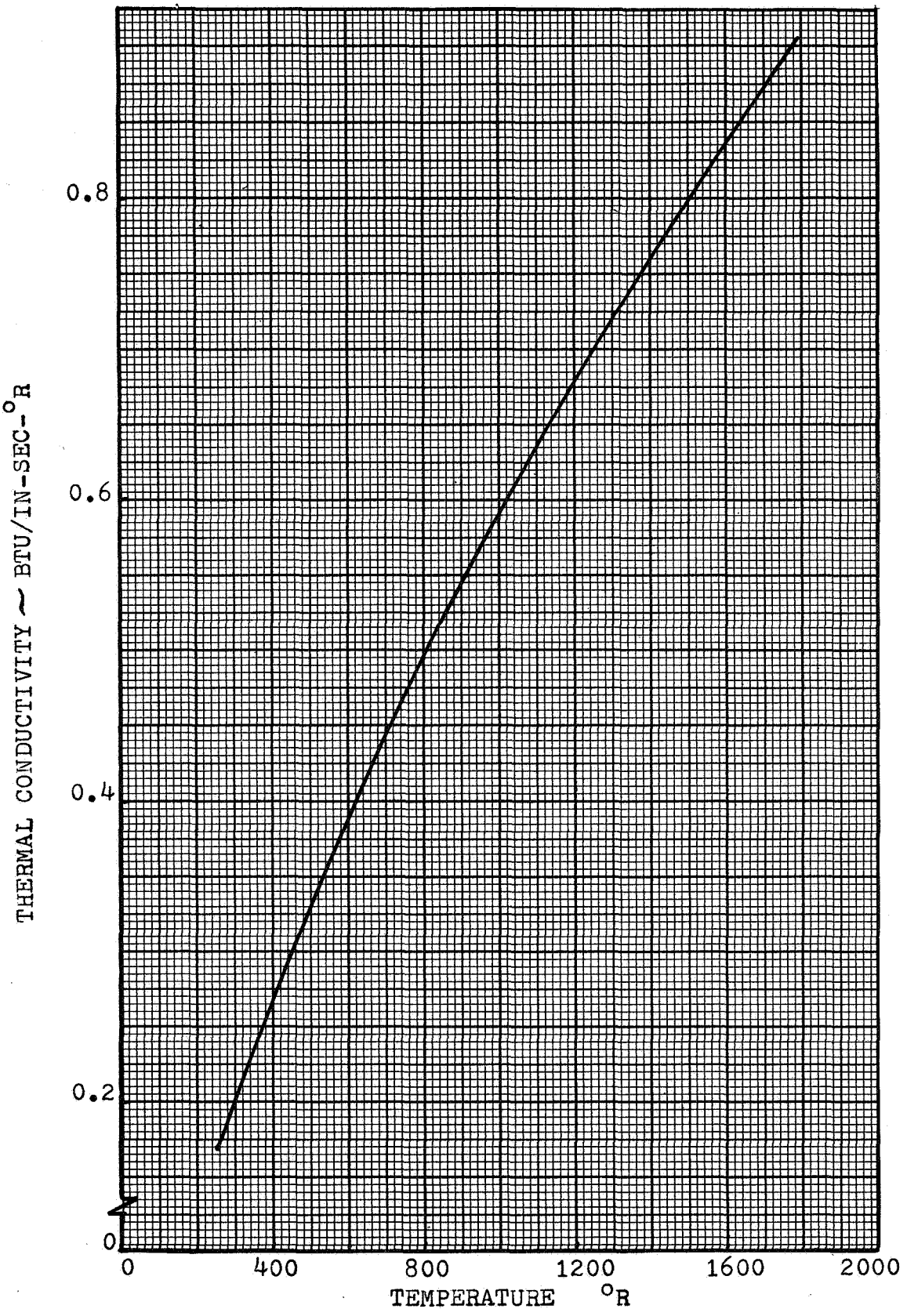

FIGURE II-3 THERMAL CONDUCTIVITY OF DRY AIR VS. TEMPERATURE

Dushman (9) gives the free-molecule heat conductivity of a gas at 32°F as

$$\Lambda = \frac{2.58 \times 10^{-3}}{M^{0.5}} \left(\frac{\gamma + 1}{\gamma - 1}\right) \frac{\text{BTU}}{\text{sec °R lb}_f} \qquad \text{(II-9)}$$

where M is the molecular weight of the gas and γ is the ratio of specific heats. Dushman also gives the mean thermal conductivity between two surfaces in slip flow as

$$k_M\left(\frac{\text{BTU}}{\text{in. sec °R}}\right) = 2\beta\bar{\delta}P_f \Lambda\left(\frac{\alpha}{2 - \alpha}\right)\left(\frac{460}{T_f}\right)^{\frac{1}{2}} \qquad \text{(II-10)}$$

where P_f is the pressure (psia) and T_f is the temperature (°R) of the fluid between the surfaces. Dushman shows that

$$\beta\left(\frac{\alpha}{2 - \alpha}\right) = \frac{9\gamma - 5}{2(\gamma + 1)} \qquad \text{(II-11)}$$

and if this equation is combined with equations II-9, II-10 and II-11, the result is

$$k_M\left(\frac{\text{BTU}}{\text{in. sec °R}}\right) = 5.53 \times 10^{-2} \frac{9\gamma - 5}{\gamma - 1} \frac{\bar{\delta}P_f}{\sqrt{MT_f}} . \qquad \text{(II-12)}$$

This equation is plotted in Figure II-4 for air at five values of T_f. When a value for the thermal conductivity of air is needed at pressures lower than those available from Figure II-4, equation II-12 may be used with the appropriate value of the molecular weight.

With a knowledge of the fluid conductivity and the average value of the interface gap thickness, the fluid conductance due to conduction can be determined. If radiation and convection may be neglected, then this is the total value of fluid conductance. With a known value of C_f, a determination of C_a will give the total conductance of the interface.

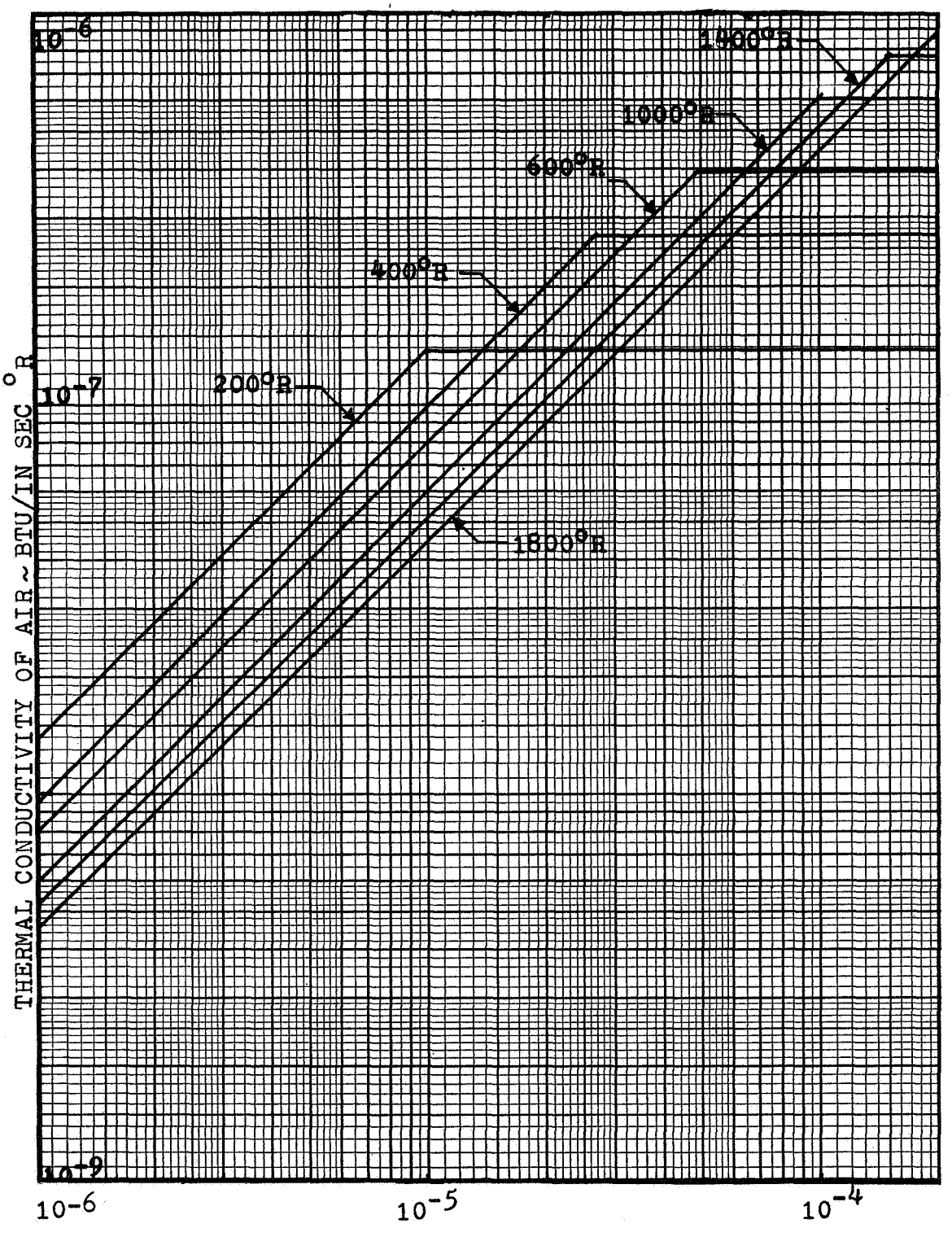

FIGURE II-4 THERMAL CONDUCTIVITY OF AIR AT VERY LOW PRESSURE

2) Contact Point Conductance:

Much work, both theoretical and experimental, has been and is currently being done to define the nature and magnitude of the contact point conductance for idealized joints. In order to adequately discuss this problem, it is necessary to consider some of the theoretical approaches that have been taken and the results of the numerous experimental investigations. This will be done in the following paragraphs.

C. Literature Survey

The problem of determining the thermal gradients across surfaces in contact (or its equivalent, the thermal conductance of contacts) was of concern as far back as 1913, when Northrup (10), in discussing this problem in relation to the measurement of the thermal conductivity of metals, presented some experimental data. He measured the thermal contact resistance of the interface between two solid-copper cylinders, 3.8 cm in diameter, pressed together and found that at a pressure of 1.6 kg the interface resistance is equal to the thermal resistance of a section of the copper bar, 31.2 cm long. In 1919, Taylor (11) accounted for contact thermal resistance to design an apparatus to measure the thermal conductivity of various building materials; in 1922, Van Dusen (12) measured the thermal resistance of contacts as a function of the physical condition of the interface and the type of filler material employed in the interface.

Jacobs and Starr (13), in 1939, measured the thermal conductance of gold, silver, and copper contacts as a function of interface temperature and pressure. Theirs was the first work in the modern era. In the same year, Bowden and Tabor (14) measured the area of contact between two

contacting surfaces by electrical conductance measurements. Their primary interest was the electrical resistance problem. In 1940-41, three more papers (15, 16, 17) appeared which gave experimental data related to the electrical resistance problem. In 1944, Karush (18) presented one of the first mathematical approaches to the contact heat transfer problem.

Since the late forties, many more papers have been published which discuss the contact conductance problem. A very comprehensive bibliography of these was compiled by Atkins (19) in 1965, and a fairly comprehensive review of this literature was prepared by Minges (20) in 1966. A detailed discussion of some experimental results and of three theoretical approaches will be made in later paragraphs, but no discussion will be given here of the papers during the period from 1945 to 1965. However, some of the very recent work will be briefly touched upon.

Most of the very recent papers have been concerned with experimental data for the thermal conductance of metal joints in a vacuum. During 1965-66, the results of at least seven experimental studies in vacua were published (21, 22, 23, 24, 25, 26, 27). These dealt primarily with metals: aluminum and its alloys, copper, iron, stainless steel, beryllium, and magnesium. In most cases, the contact bearing pressure was the significant independent parameter. Koh and John (28) investigated the effect of soft metal foils in the interface on the thermal contact resistance. Williams (29) performed more basic experiments which aimed at measuring the influence of the number of contact points and of the applied load on the contact resistance. Mendolsohn (30) conducted an analysis to determine the influence of the contact resistance problem on the efficiency of a space thermal radiator.

Besides the afore-mentioned papers which contained experimental data, at least five other recent papers are primarily theoretical or analytical. Blum and Moore (31) investigated the transient effects in the contact conductance problem that included changes in the contact temperature and in the physical structure of the contact. Dutkiewicz (32) developed a statistical method for determining the interaction between two randomly-rough surfaces placed face to face. Yovanovich (33) developed an idealized theory to describe the contact resistance between smooth rigid planes and deformable smooth spheres. To solve a simplified version of the contact heat conduction problem, Hultberg (34) developed a theoretical approach. Ozisik and Hughes (35) developed a simple analytical relation to predict the thermal contact conductance of a smooth surface in contact with a rough surface. This analysis requires that certain test data on the actual contact be available.

In the preceding paragraphs it has been seen that the thermal conductance problem involving contacts (idealized joints) has been of interest since the early part of this century. However, with respect to actual mechanical joints involving some sort of fastener, the first known publication was that of Jelinek (36), in 1949, who measured the conductance of eight riveted structural joints for the rocket package of the F-86D airplane. It appears that the thermal conductance problem of a mechanically fastened joint was ignored until the advent of high-performance aircraft and missiles, when aerodynamic heating became a problem and the interface conductance of riveted and bolted joints required consideration. As technology has advanced toward higher speed aircraft, missiles, rocket boosters, and spacecraft, increasing emphasis has been placed on this problem.

In the early and middle 1950's, there were several publications on the subject of riveted and bolted joints. Coulbert and Liu (37) measured the interface conductance of sixteen riveted and one welded aluminum joint in 1953, but they presented no analytical correlation. UCLA, in the same year, began extensive series of experiments involving both riveted and welded aircraft structural joints. These studies, which involved aluminum, stainless steel, and titanium joints, are documented in references 38, 39, 40, 41, and 42. The report published by Lindh et al. (42) will be discussed more fully in later paragraphs, since it was by far the most complete study up to that time and, in some respects, still is. Apparently this was the first time a complete analytical treatment had been attempted.

In 1954, Holloway (43) measured the transient temperature distribution in fifteen riveted aluminum alloy skin-stringer combinations. He also investigated the possibility of generalizing the interface conductance problem. Four other publications appeared between 1955 and 1957. Two of these (44 and 45) dealt primarily with experimental results; two (46 and 47), with analyses of the effects of thermal resistance on temperature and stress distributions.

In addition to these early papers, there have been numerous other publications on the subject of mechanical-joint thermal conductance. An extensive bibliography is available in reference 19. Fontenot (48) reviewed and compiled a large amount of the available experimental data in 1964. Some of the information in his report will be discussed later. During the period 1964-1966, the results of at least five experimental studies were published (49, 50, 51, 52, 53). Considerable efforts to

obtain more data and better analytical solutions are underway in a number of laboratories at the present time.

Several references from the literature will now be discussed in more detail to provide a basis for the problem definition.

1) Contact Conductance:

A review of the literature on the subject of contact thermal conductance leads to the conclusion that there is little practicality in the great majority of theoretical or semi-empirical methods now available. In other words, it is almost impossible for a designer to take this problem into account without an appreciable amount of testing. As an illustration of this point, four approaches outlined in the literature will be discussed here. These are the work of Fenech and Rohsenow (54), Centinkale and Fishenden (55), Laming (56), and Boeschoten and Van der Held (57).

Fenech's and Rohsenow's approach is very rigorous and complex; it agrees well with the experimental data. Unfortunately, this method requires that two recorded surface profiles of each plate in contact be made and analyzed. In lieu of making surface profiles, one would probably find it easier to actually measure the contact conductance. Obviously this theoretical approach is not practical for the prediction of contact thermal conductance. The Centinkale-Fishenden and Laming methods, though not so rigorous as that of Fenech and Rohsenow, require less information about the contact surfaces. In some cases, all the required information may be available. Hence, these two approaches merit greater consideration as possible methods for the theoretical prediction of contact conductance. Therefore, these two methods, along with that

of Boeschoten and Van der Held, will be discussed in more detail. The approach taken by Boeschoten and Van der Held requires very little information about the surface properties and is nearly always applicable.

Centinkale and Fishenden made use of Southwell's relaxation method to derive a theoretical expression for the conductance of metal surfaces in contact. The expression which they obtained for the total conductance is:

$$C_t = C_f + C_a = \frac{k_f}{\bar{\delta}} + \frac{k_M (P/H_o)^{\frac{1}{2}}}{r_e \tan^{-1} \left\{ \left[(H_o/P) \left(1 - \frac{k_f}{C_t \bar{\delta}} \right) \right]^{\frac{1}{2}} - 1 \right\}} \qquad \text{(II-13)}$$

where H_o is the nominal value of Meyer hardness (see Table II-1) of the softer metal, $k_M = \frac{2k_1 k_2}{k_1 + k_2}$, and r_e is one-half the average value of the distance between contact points. Their approximation for r_e was

$$r_e = \psi(\lambda_A + \lambda_B)\left(\frac{P}{H_o}\right)^{-\zeta} \qquad \text{(II-14)}$$

Table II-1

NOMINAL VALUES OF MEYER HARDNESS (H_o)

Metal	H_o (psi)		
	Centinkale and Fishenden (55)	Laming (56)	Boeschoten and Van der Held (57)
Cast Steel	510,000		
Uranium			342,000
Iron			272,000
Mild Steel	238,000	240,000	
Brass	171,000	170,000	
Aluminum Alloy	151,000	151,000	203,000
Pure Aluminum	46,800		

where λ_A and λ_B are the wavelengths of the surface waviness of surfaces A and B, respectively, and ψ and ζ are constants to be determined experimentally.

Centinkale and Fishenden determined ψ and ζ for ground surfaces to be $\psi = 4.8 \times 10^{-3}$ and $\zeta = 5/6$. These values were independent of the plate material and the interstitial fluid. For surfaces finished by other methods than grinding, different values for ψ and ζ may be needed. Centinkale and Fishenden also found experimentally that

$$\overline{\delta} = 0.61(i_A + i_B) \qquad \text{(II-15)}$$

where i_A and i_B are the root-mean-square values of surface irregularity (roughness plus waviness) for surfaces A and B, respectively. They state that no change in $\overline{\delta}$ with pressure was detectable up to 800 psi. Since contact point conductance increasingly predominates over fluid conductance as the pressure is increased, the effects of any change in $\overline{\delta}$ on the contact conductance would become very small. They thus assumed that $\overline{\delta}$ is constant.

With equations II-13 and II-14 combined and the values determined for ψ and ζ inserted, C_a can be written as

$$C_a = \frac{2.08 \times 10^{-4}\ k_M P^{\frac{4}{3}}}{(\lambda_A + \lambda_B) H_O^{\frac{4}{3}} \tan^{-1}\left\{\left[\frac{H_O}{P}\left(1 - \frac{C_a}{C_t}\right)\right]^{\frac{1}{2}} - 1\right\}} \qquad \text{(II-16)}$$

where

$$\frac{C_a}{C_t} = \frac{C_a}{C_f + C_a} = \frac{1}{\frac{C_f}{C_a} + 1} \,. \qquad \text{(II-17)}$$

For equation II-13 to be used, i_A, i_B, λ_A, λ_B must be known. Values of i_A and i_B can be approximated from the specified values of surface

finish. If the surface finish is unknown but the finishing process is known, limiting values can be fixed for i_A and i_B from Figure II-5, which is from Graff (58). If the finishing process is grinding, equation II-16 can be used to determine C_a. For other finishing processes, this equation will at least provide an approximation.

If values for λ_A and λ_B are known in a particular case, then equation II-16 can provide a fair estimate of the conductance due to the contact points. If numerical values are not available (usually the case in design), then this equation is useless. An attempt was made during the present study to determine if a range of possible values for wavelength of surface waviness could be fixed when the quality of surface finish and the machining operation are known. Apparently a correlation between waviness and roughness for a given finishing operation has never been made. The consensus of several experts on metal finishing is that such a correlation is impossible. It is felt that the waviness of a surface is dependent on so many parameters that the only way to obtain it is to measure it.

Laming (56) approaches the problem of determining C_t in a somewhat simpler manner than that of Centinkale and Fishenden. The expression that he obtained for C_t is identical to equation II-13. However, he found $\bar{\delta}$ to be $0.67(i_A + i_B)$ instead of $0.61(i_A + i_B)$, given in equation II-15. This good agreement suggests an average value, $\bar{\delta} = 0.64(i_A + i_B)$. The expression derived by Laming for C_a is somewhat different from that given by equation II-6.

Following a line of intuitive reasoning and incorporating experimental information on electrical contacts given by Holm (59), Laming derived

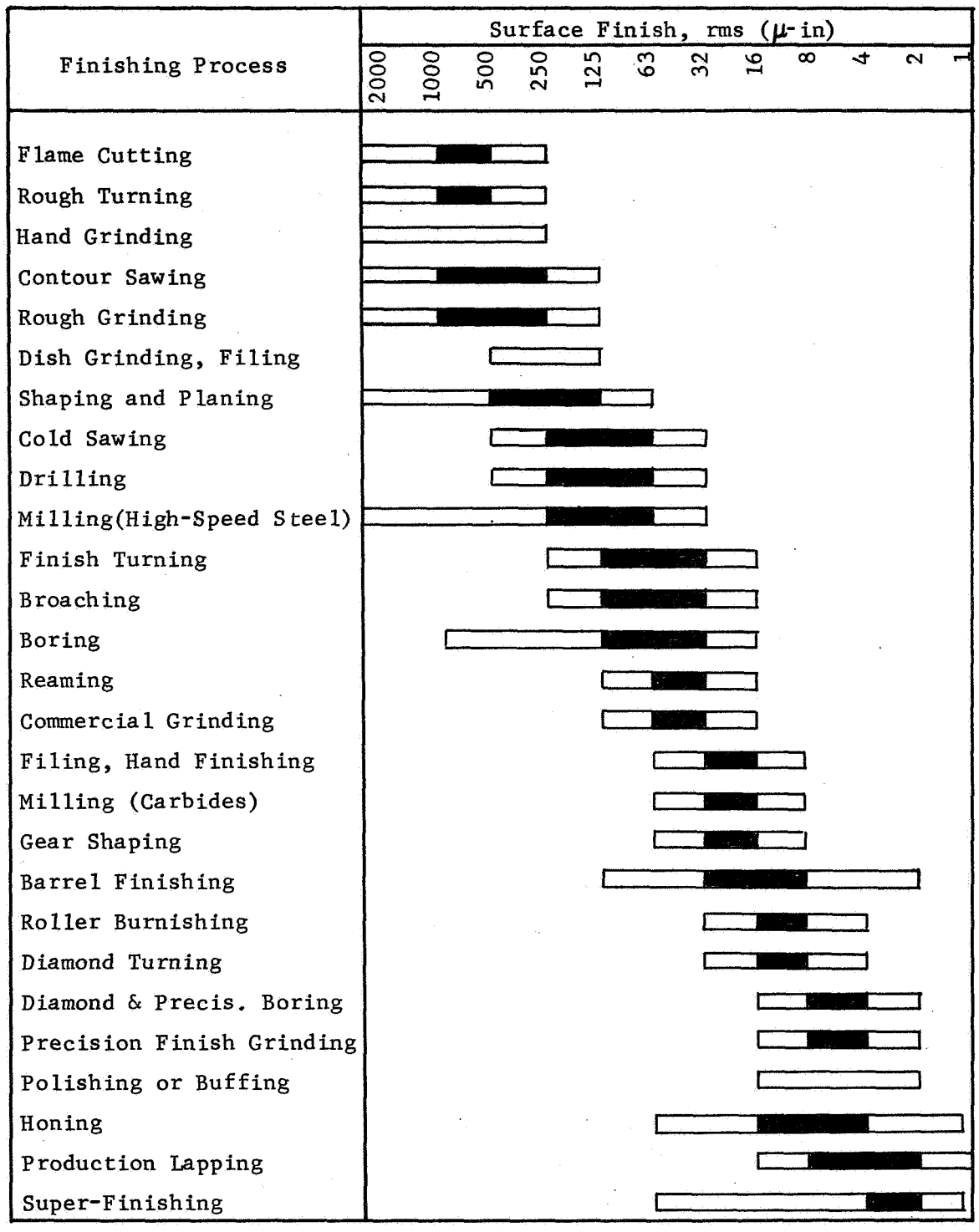

FIGURE II-5 SURFACE ROUGHNESS VERSUS FINISHING PROCESS
(Data Prepared by Graff(58))

$$C_a = \frac{2k_M (P/H)^{\frac{1}{2}}}{(1 - f)(\pi\lambda_A\lambda_B)^{\frac{1}{2}}} \qquad \text{(II-18)}$$

where f is defined as the constriction alleviation factor

$$f = 1.41\left(\frac{P}{H}\right)^{\frac{1}{2}}\left(\frac{C_t}{C_a}\right)^{\frac{1}{2}} . \qquad \text{(II-19)}$$

In equations II-18 and II-19, he introduces the parameter H, the value of the Meyer hardness, which he assumes to be a function of the load. In equations II-13, II-14, and II-16, the parameter H_o was employed. Centinkale and Fishenden did not account for variation in metal hardness with load. Laming, in equation II-18, presumably accounts for a reported variation in Meyer hardness at small loads by writing P/H instead of P/H_o. He gives a dimensionless P/H as

$$\frac{P}{H} = \left(\frac{P}{\omega}\right)^{\frac{1}{\nu}} (\lambda_A\lambda_B)^{\frac{1}{\nu}-1} \qquad \text{(II-20)}$$

where ω and ν are empirically-determined constants. Using experimental data for steel-aluminum, steel-brass, and brass-brass contacts, Laming gives ω = 5280 psi and ν = 2/3. It is thought that these values should be applicable when brass or aluminum is the softer of the two plates in contact at contact pressures up to 10^4 psi. At very high loads; i.e., $P > 10^4$ psi, a value of ν = 1 is expected since at that point the nominal value of Meyer hardness is reached.

If equations II-17 through II-20 are combined and the reported values of ω and ν are used, C_a can be written as

$$C_a = \frac{1.83 \times 10^{-3}\ k_M P^{\frac{3}{4}}}{(\lambda_A\lambda_B)^{\frac{1}{4}}\left[1 - 2.28 \times 10^{-3}(P)^{\frac{3}{4}}(\lambda_A\lambda_B)^{\frac{1}{4}}\left(1 - \frac{C_f}{C_a}\right)^{\frac{1}{2}}\right]} . \qquad \text{(II-21)}$$

A comparison of this with equation II-16 reveals some similarity, but

one striking difference. In equation II-21, C_a is dependent upon $P^{\frac{3}{4}}$; in equation II-16, upon $P^{\frac{4}{3}}$. Fontenot (48) shows that a dimensional analysis will yield an exponent for P of 3/4 and an equation quite similar to equation II-21.

In the work of Centinkale-Fishenden and Laming, the parameter λ appears in the resulting equations. As it was mentioned previously, the value of the wavelength of surface waviness is generally unknown. No way of estimating it is available. Thus, in most practical problems, equations II-16 and II-21 will be of little use. For determining C_a when λ is unknown, a very simple, semi-empirical approach developed by Boeschoten and Van der Held (57) is presented below.

Using intuitive reasoning and an estimation of size and number density of contact spots, Boeschoten and Van der Held derived an expression for C_t. Their expression for C_a is in reality an approximation of that given by Centinkale and Fishenden. Boeschoten and Van der Held approximate the arc-tangent term in equation II-13 with $\pi/2$. This, however, is not the only simplifying assumption. Others must be made to eliminate the dependence upon λ.

As it was before, the total contact conductance is written $C_f + C_a$; C_f is given as $k_f/\overline{\delta}$. The values of $\overline{\delta}$, reported in the same reference for air, hydrogen, and helium are:

$$\overline{\delta}_{air} = 0.36(i_A + i_B) \; ; \quad \overline{\delta}_{H_2} = 0.76(i_A + i_B) \; ; \quad \overline{\delta}_{He} = 0.80(i_A + i_B) \; .$$

The average value of $\overline{\delta}$, found to be $0.64(i_A + i_B)$, is in excellent agreement with the values found by Centinkale and Fishenden and Laming. The apparent dependence of $\overline{\delta}$ upon the fluid, reported by Boeschoten and Van der Held, was not found in the other two investigations (55 and 56),

in which the interface fluids were air, glycerol, water, and spindle oil.

The simplified expression for C_a given by Boeschoten and Van der Held is

$$C_a = 1.06 \frac{k_M}{\bar{a}} \left(\frac{P}{H_O}\right) \qquad \text{(II-22)}$$

where $\bar{a}$ is the average radius of the contact spots. An approximate value for $\bar{a}$ determined by Boeschoten and Van der Held is 1.2×10^{-3} inches. They report that the value of $\bar{a}$ does not depend upon the materials of which the contacts are made or the contact pressure. This is in agreement with Holm (59). Boeschoten and Van der Held conducted tests with aluminum, iron, and uranium contacts at pressures of 498 and 1000 psi. If this average value of $\bar{a}$ is inserted into equation II-22, C_a can be expressed simply as

$$C_a = 8.8 \times 10^{-4} \; k_M \frac{P}{H_O} \; . \qquad \text{(II-23)}$$

Since all the terms in this equation are known quantities, an approximation for C_a may be obtained. If equation II-23 is combined with the previous expression for C_f $[k_f / 0.64(i_A + i_B)]$ a working expression for C_t can be written as

$$C_t = \frac{1.56 k_f}{(i_A + i_B)} + 8.8 \times 10^{-4} \frac{k_M P}{H_O} \; . \qquad \text{(II-24)}$$

In lieu of equation II-24 or one of the more complex expressions, one can go to the literature and attempt to use experimental data. This can be done in many cases, but the end results is not often satisfactory because of the wide divergence of experimental results. This divergence is most apparent in the experimental data compiled by Minges (20) and Fontenot (48).

Fontenot outlines a recommended approach to estimate the thermal conductance of contacts when limited information is available. He rewrites equation II-24 as

$$C_t = C_f + C_a = \frac{1.56k_f}{(i_A + i_B)} + 2n\bar{a}k_M \qquad \text{(II-25)}$$

where n is the number of contact spots per unit area. This equation, combined with Figures II-6 and II-7 (which are taken from reference 48), allows one to obtain very simply an estimate of C_t when the R.M.S. value of surface roughness and k_M are known. This estimate should prove useful whenever experimental data is not available. To employ this method one must know the parameters ρ_A, ρ_B, k_M, k_f, P, and T_f--all of which are generally known.

2) *Joint Conductance:*

Some of the work done in this area was briefly discussed in a previous section of this chapter. To provide a basis for the problem definition which will follow, a detailed discussion of some of the published work is necessary. The work of Lindh et al. (42) and Fernlund (60) will be discussed at length because theirs were the only two concerted attempts to approach the problem analytically from basic elements.

In an earlier part of this chapter, the mechanisms of interfacial heat transfer were discussed. These mechanisms play a part in the heat transfer across actual mechanical joints just as they do in the case of contacts. There is a major difference, however, between the contact thermal conductance problem and the joint thermal conductance problem. For contacts, the total conductance is due to that of the fluid in the interface (if any) and the contact points; for joints, the contact point conductance, when a fluid is present, is of lesser importance. This is

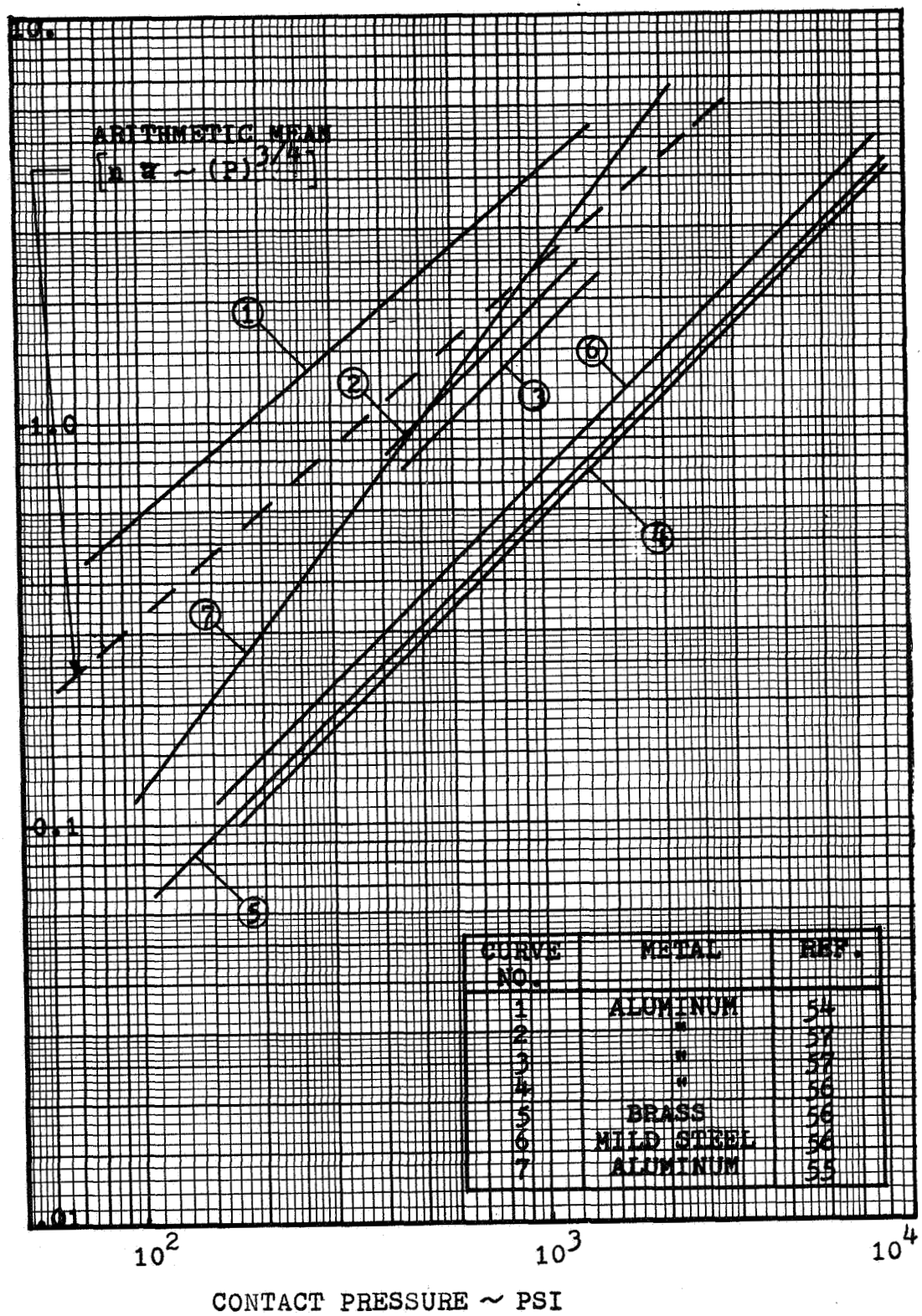

FIGURE II-6 n $\bar{a}$ VERSUS CONTACT PRESSURE

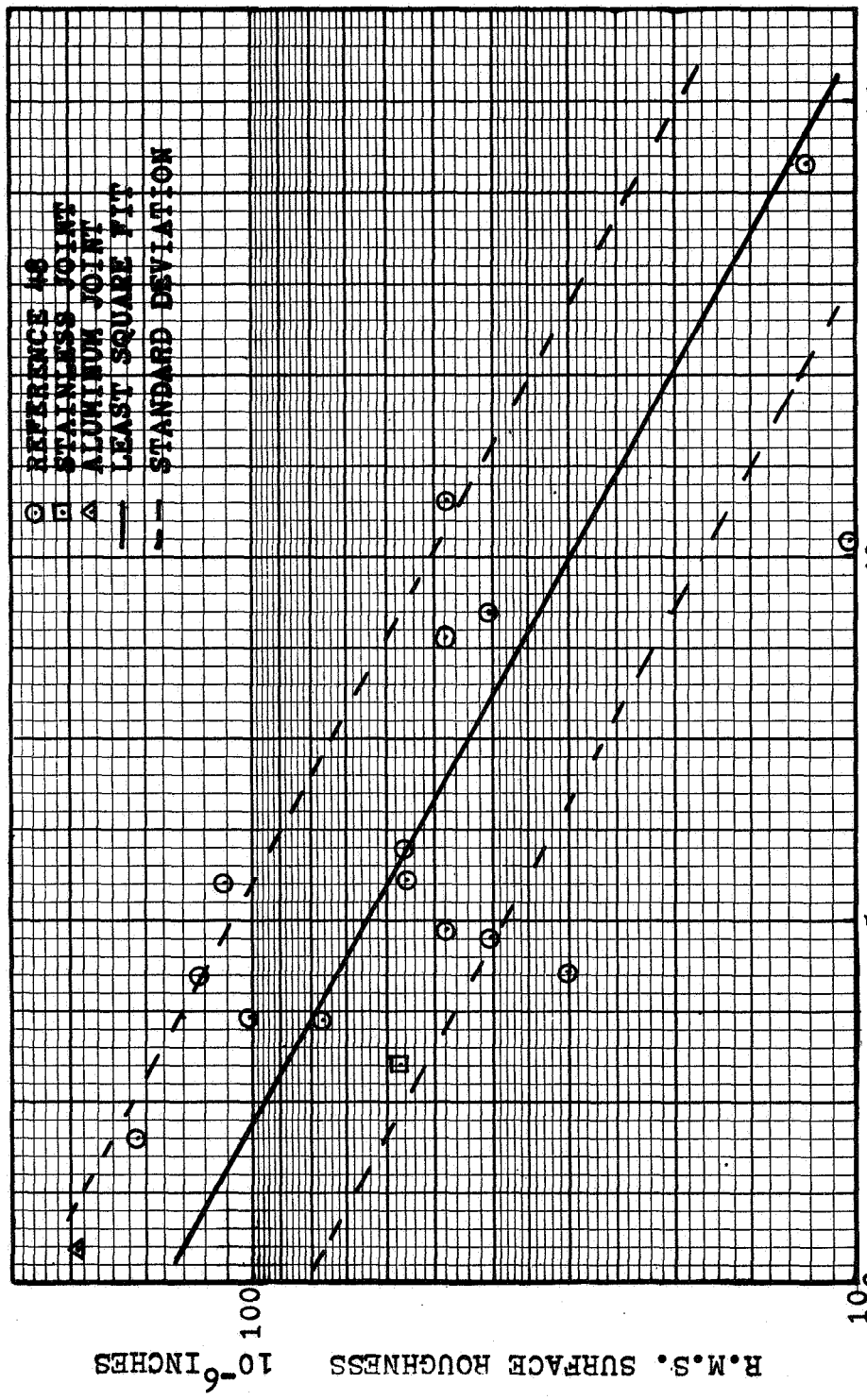

FIGURE II-7 THE RATIO OF AVERAGE SURFACE IRREGULARITY TO R.M.S. SURFACE ROUGHNESS VERSUS R.M.S. SURFACE ROUGHNESS

due to the larger interface gap thickness in actual joints. When no fluid is present in the interface, the problem reduces, in most cases, to determining the apparent area of contact.

In contacts, the area of apparent contact is well defined, although the number of contact points is not. On the other hand, the determination of the contact area in joints is a major problem. For contacts, an estimate of the interface gap thickness can be obtained from a knowledge of the R.M.S. value of surface roughness. For joints, this is not possible because of surface deflections caused by stresses set up in the joint members by the fastener load. These deflections are generally much larger than the surface irregularities and must be taken into account.

Before 1957, no report of an attempt to determine the interface gap thickness of an actual joint appeared in the literature. In that year, the work of Lieb and coworkers (42) was published. Lieb considered the case of a riveted lap joint (Illustration II-3). To permit the problem to be handled mathematically, Lieb employed a simplified configuration, which is shown in Illustration II-4. He then proceeded to derive equations for this physical model to predict the magnitude of the plate deflection, "w", as a function of r for two different end conditions. In one case, he assumed that the plates were free at the ends; in the other, that the slopes of the plates were zero at the ends. The equations given by Lieb (42) are

$$w = \frac{\sigma_{I_o} r_\sigma^4}{16D}\left[\frac{m}{m+4} - \frac{\sigma_h}{\sigma_{I_o}}\left(\frac{r_h}{r_\sigma}\right)^4\right]\left[\frac{(1-\mu)}{(1+\mu)}\left(\frac{r^2 - r_\sigma^2}{2R^2}\right) + \ln\frac{r}{r_\sigma}\right] \qquad \text{(II-26)}$$

for the free plate, and

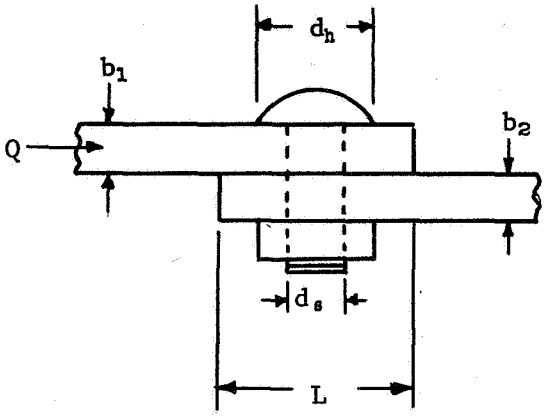

ILLUSTRATION II-3
Two-Dimensional Riveted Lap Joint.

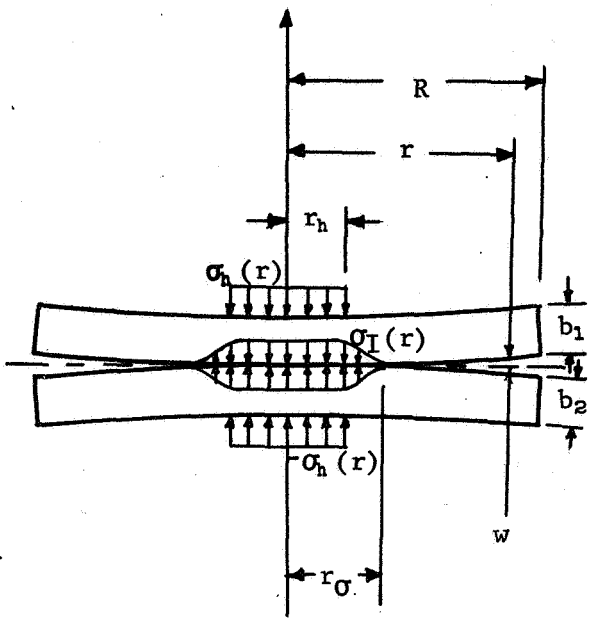

ILLUSTRATION II-4
Lieb's Simplified Model of the Joint - Circular Symmetry Assumed.)

$$w = \frac{\sigma_{I_o} r_\sigma^4}{16D}\left[\frac{m}{m+4} - \frac{\sigma_h}{\sigma_{I_o}}\left(\frac{r_h}{r_\sigma}\right)^4\right]\left[\frac{r_\sigma^2 - r^2}{2R^2} + \ln\left(\frac{r}{r_\sigma}\right)\right] \qquad \text{(II-27)}$$

for the restrained plate; where

$$D = \frac{Eb^3}{12(1 - \mu^2)} \quad \text{and} \quad m = \frac{2}{\frac{\sigma_{I_o}}{\sigma_h}\left(\frac{r_\sigma}{r_h}\right)^2 - 1} .$$

Lieb assumed that σ_h, the normal stress exerted by the bolt or rivet head, is uniform over the entire zone of application and that the stress distribution of the reaction on the interface planes can be written as $\sigma_I = \sigma_{I_o}\left[1 - \left(\frac{r}{r_\sigma}\right)^m\right]$. He evaluated σ_{I_o} and m from Sneddon (61), who treated the case of a single, symmetrically loaded thick plate. The variables r_σ/r_h, m, and σ_{I_o}/σ_h, as determined by Lieb, are plotted as functions of r_h/b in Figure II-8.

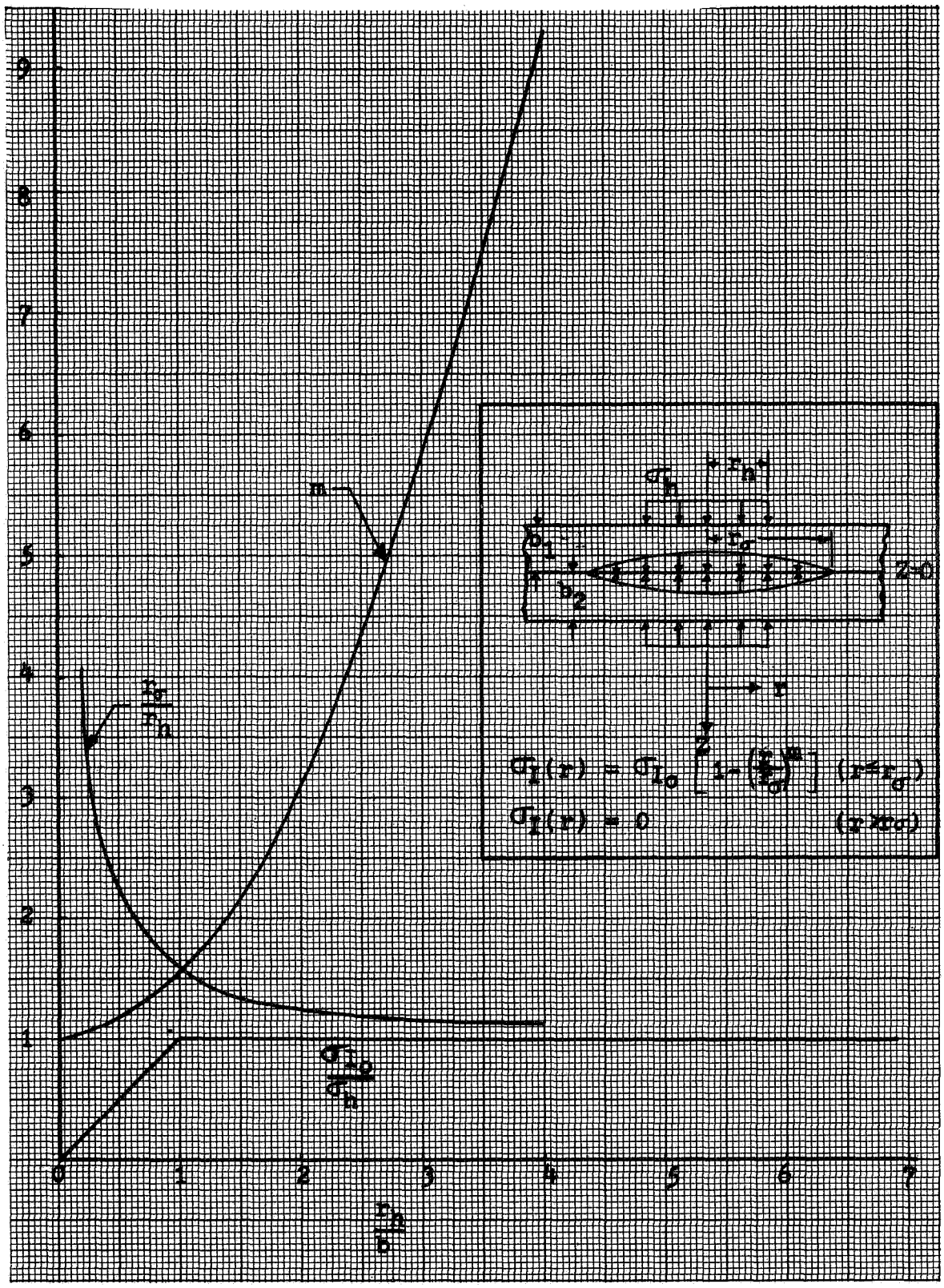

FIGURE II-8 LIEB'S INTERFACE STRESS DISTRIBUTION PARAMETERS

Lieb performed one experiment with two circular plates 8 inches in diameter and 1/16 inches thick. They were bolted together through the center by a No. 10-32 socket-head steel bolt and nut with two washers. He reported that the results of this one test were within 30 percent of the deflection value predicted by his theory. However, no further data was presented to support his theory.

In reference 42, the results of Lindh's experiments to determine the interface gap between actual riveted lap joint specimens are given. Lindh conducted these tests to determine the validity of an analytical technique which would predict the temperature distribution through, and total conductance of, a riveted lap joint. The predicted joint conductances agreed with his experimental measurements within 3 to 25 percent. Since the analytical treatment is dependent upon the measured values of interface gap thickness, approximate correctness of the experimental values of gap thickness is implied. Lieb does not report any attempt to apply his plate deflection theory to these riveted samples.

Because one experiment is not conclusive proof of the validity of a theoretical method, further verification was sought by the author. Correlations between the experimental values of gap thickness reported by Lindh and the values determined from equations II-26 and II-27 were attempted. In all cases the calculated values were at least one order of magnitude smaller. This comparison is shown in Table II-2. As a further check, the gap thicknesses were calculated for riveted joints given in other references. These were then compared to the gap thicknesses obtained indirectly from joint conductance data. Again, the gap thicknesses calculated with equations II-26 and II-27 were much smaller than those obtained from the joint conductance data.

Table II-2

COMPARISON OF VALUES FOR AVERAGE INTERFACE GAP

UCLA Specimen Number	Average Interface Gap $\sim 10^{-3}$ in.		
	Experimental Value	Equations II-26 & II-27	Equations II-33 & II-34
14	3.6	0.11	1.45
21	5.0	0.22	5.94
22	1.8	0.11	1.45
23	1.4	0.04	0.32
27	2.7	0.03	0.32

Subsequent to Lieb's work (42), which was based on a theory of Sneddon (61), calculations were carried out by Fernlund (60) to determine the interface stress distribution between bolted or riveted plates. Fernlund assuming a uniform load distribution on plates of infinite extension, carried out an exact mathematical analysis for one sample case (Illustration II-5). His calculated interface stress distribution for this configuration is shown in Figure II-9. Fernlund restricted his numerical work to this one sample problem due to the complexity of the analysis. However, he proposed an approximate method to provide an estimate of the interface stress without the tedious exact analysis. By comparing the results of the exact and approximate methods for the sample case, he also demonstrated the appropriateness of the approximate method. It involves the representing of the interface stress, $\sigma_I(r)$, by a fourth-order polynomial, which is written

$$\sigma_I(\rho) = V\rho^4 + W\rho^3 + X\rho^2 + Y\rho + Z \qquad \text{(II-28)}$$

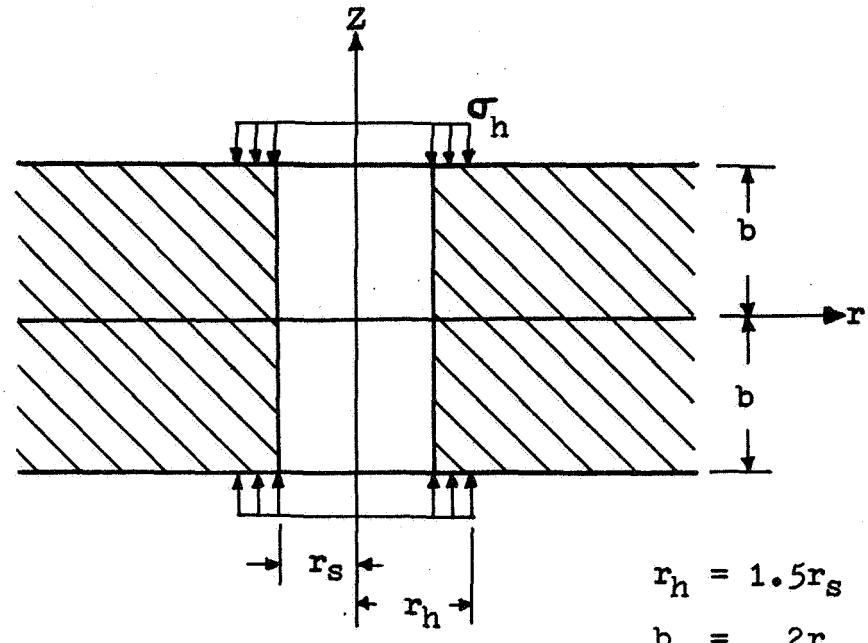

ILLUSTRATION II-5 FERNLUND'S SAMPLE PROBLEM

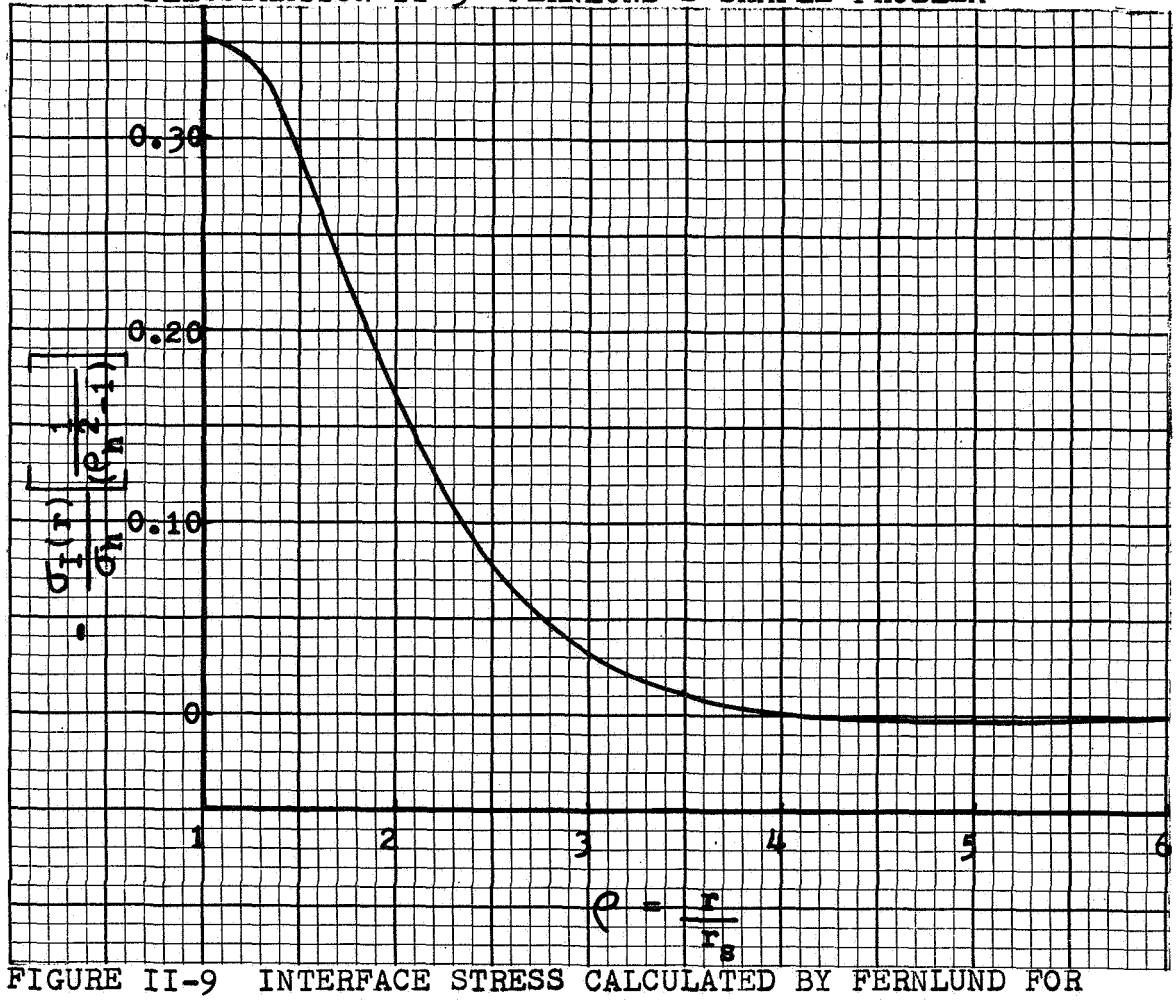

FIGURE II-9 INTERFACE STRESS CALCULATED BY FERNLUND FOR SAMPLE PROBLEM IN ILLUSTRATION II-5

where $\rho = r/r_s$ and the constants are given by:

$$V = \frac{15\sigma_h(\rho_h^2 - 1)}{-\rho_\sigma^6 + 2\rho_\sigma^5 + 5\rho_\sigma^4 - 20\rho_\sigma^3 + 25\rho_\sigma^2 - 14\rho_\sigma + 3}$$

$$W = -\frac{4}{3}(2\rho_\sigma + 1)V$$

$$X = 2\rho_\sigma(\rho_\sigma + 2)V \qquad \text{(II-29)}$$

$$Y = -4\rho_\sigma^2 V$$

$$Z = -\frac{\rho_\sigma^3}{3}(\rho_\sigma - 4)V \ .$$

It can be seen from equation II-29 that the values of all the polynomial coefficients are functions of ρ_σ. Out of curiosity, the author evaluated these coefficients, using equation II-29, for five of the UCLA riveted specimens. The interface stress, $\sigma_I(\rho)$, determined from equations II-28 and II-29 for two extreme cases, is plotted in Figure II-10. As expected, the value of ρ_σ has considerable influence on the interface stress distribution. From Fernlund's work (60), an expression for ρ_σ can be written as

$$\rho_\sigma = (1.09b + r_h)/r_s \ . \qquad \text{(II-30)}$$

Lieb (42), Sneddon (61), and Coker and Filon (62) give an approximate value of 1.3, instead of 1.09, for the coefficient of b. For a plate thinner than those considered by the other investigators, Aron and Colombo (63) found a value of 1.7 for the coefficient of b. Obviously, the value selected for this coefficient will directly affect the calculated plate deflection in any analysis.

To determine if the assumed stress distribution on the interface might be responsible for the poor agreement between the plate deflections calculated from his theory and those experimentally measured, the author

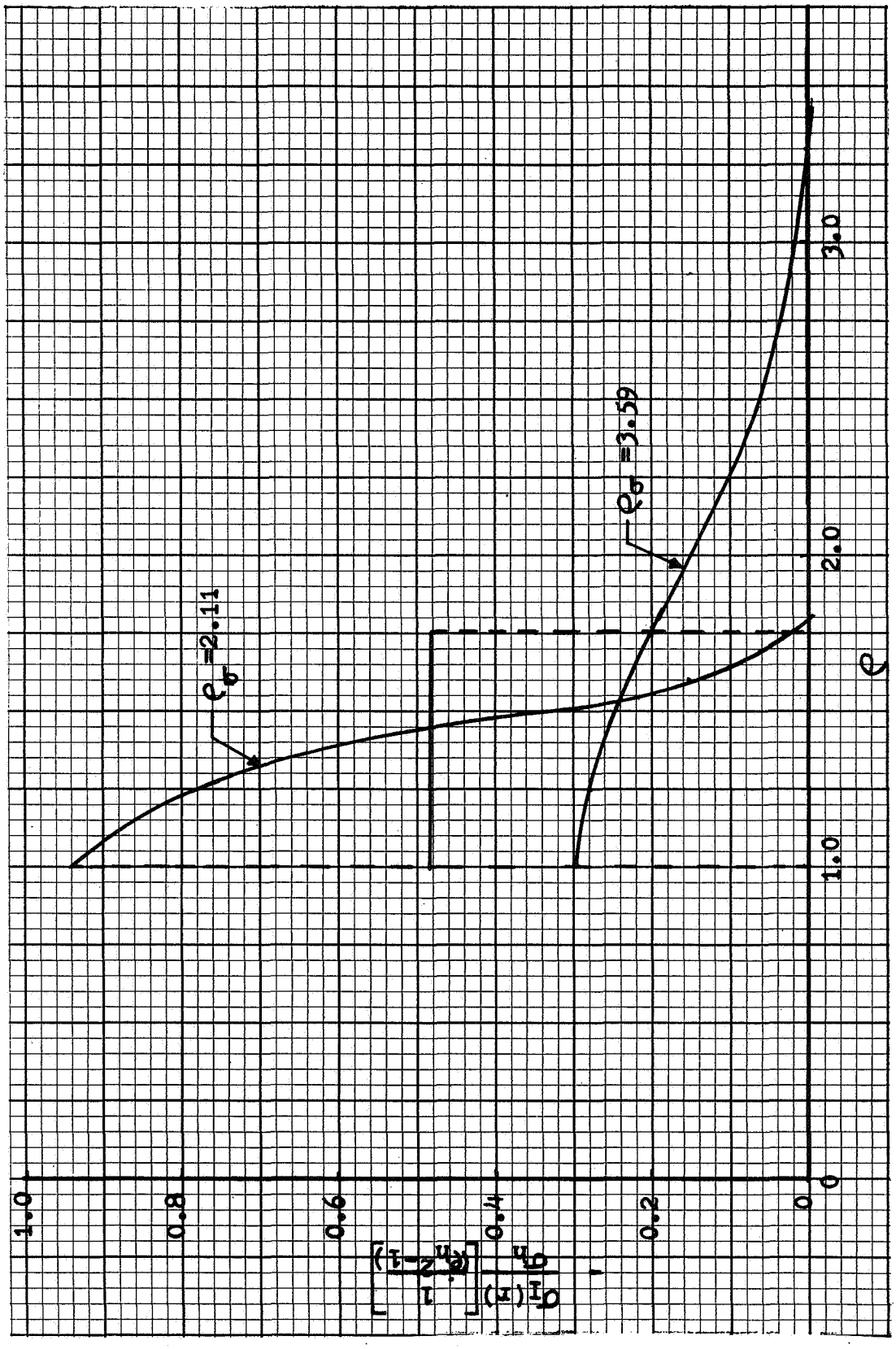

FIGURE II-10 INTERFACE STRESS DISTRIBUTION AS DETERMINED BY FERNLUND'S APPROXIMATE METHOD FOR TWO U.C.L.A. SPECIMENS

solved Lieb's basic (42) differential equation. Equations II-38 and II-39 were used for the interface stress instead of the equation (Figure II-8) used by Lieb. The two resulting lengthy equations for w, not given here, are available in reference 48. From these two equations, average values of interface gap thickness were obtained for the same five UCLA specimens mentioned previously. Equation II-30 was used to determine ρ_σ. For values of ρ_σ less than 2.35, Fernlund's approximate theory yielded negative deflections. In all cases the computed deflections were much smaller than the reported experimental values.

In both Lieb's and Fernlund's analyses, the assumption is made that the normal compressive stress under the fastener head is uniform. The two authors show good correlation between theory and experiment for idealized tests in which efforts were made to approach a uniform stress. However, either of their theoretical analyses when applied to plates fastened by round-head rivets, results in plate deflection values that are much too small. Intuitively, it seems unreasonable to expect uniform stress under a round-head bolt or rivet.

To investigate how the assumption of a different stress distribution would materially affect the form of equations II-26 and II-27, the author assumed an expression for $\sigma_h(r)$ and one for $\sigma_I(r)$ that is statically consistent with $\sigma_h(r)$. To avoid a blind guess for the distribution of σ_h, the physical picture of the joint was considered. Since the fastener head is rounded (Illustration II-3), the normal compressive stress was assumed to vary from zero at the edge of the head to a maximum at the shank. To obtain a stress distribution at the interface, the value of r_σ was assumed to be given by

$$r_\sigma = r_h + \eta b \qquad \text{(II-31)}$$

where η ranges from 1.3 to 1.7, depending upon the plate thickness. The following arbitrary criterion was used:

$$b = 0.031 \qquad \eta = 1.7$$

$$b = 0.062 \qquad \eta = 1.5$$

$$b = 0.133 \qquad \eta = 1.3$$

Along with this, $\sigma_h(r)$ and $\sigma_I(r)$ were postulated to be linear functions of r specified by

$$\sigma_h(r) = \sigma_{h_o}(1 - r/r_h)$$

$$\sigma_I(r) = \sigma_{I_o}(1 - r/r_\sigma) \ .$$

For static equilibrium, the total force due to σ_h must be equal to the total force due to σ_I. Thus, $\sigma_{I_o}/\sigma_{h_o} = r_h/r_\sigma$, or

$$\frac{\sigma_{h_o}}{\sigma_{I_o}} = 1 + \frac{\eta b}{r_h} \ . \qquad \text{(II-32)}$$

With these assumed stress distributions included, Lieb's basic differential equations were solved again. The following deflection equations were obtained:

$$w = \frac{\sigma_{I_o} r_\sigma^4}{16D}\left[\frac{1}{5} - \frac{1}{5}\frac{\sigma_{h_o}}{\sigma_{I_o}}\left(\frac{r_h}{r_\sigma}\right)^4\right]\left[\frac{(1-\mu)}{(1+\mu)}\left(\frac{r^2 - r_\sigma^2}{2R^2}\right) + \ln\left(\frac{r}{r_\sigma}\right)\right] \qquad \text{(II-33)}$$

for the free plate, and

$$w = \frac{\sigma_{I_o} r_\sigma^4}{16D}\left[\frac{1}{5} - \frac{1}{5}\frac{\sigma_{h_o}}{\sigma_{I_o}}\left(\frac{r_h}{r_\sigma}\right)^4\right]\left[\frac{r^2 - r_\sigma^2}{2R^2} + \ln\frac{r}{r_\sigma}\right] \qquad \text{(II-34)}$$

for the restrained plate.

The deflections for the five UCLA specimens were recalculated using equations II-33 and II-34. The values obtained for the average interface gap are given in the last column of Table II-2. From this table one can

see that considerable improvement in the experimental-theoretical correlation can be obtained if a different applied-stress distribution is assumed.

Note that the validity of the assumptions made for equations II-33 and II-34 has not been demonstrated here. The results serve only to show the importance of the $\sigma_h(r)$ distribution.

D. Problem Definition

From the preceding discussion it is clear that presently there is no adequate way to systematically predict the thermal conductance of bolted or riveted joints. The only available approach is experimentation. Much experimental information is needed and a comprehensive analysis must be performed in order to develop a reliable method of predicting the heat transfer across a bolted joint.

To predict the thermal conductance of a bolted joint, one must consider the various modes of heat transfer and define the area of the joint over which these modes are significant. As it was previously shown, radiation and convection across the interface gap usually can be neglected to simplify the problem. In such cases, the problem reduces essentially to determining the area of the contact zone, the stress distribution in the zone, and the width of the interstitial gap outside the contact zone.

The work described in the following chapters was an attempt to develop a practical analytical method and to furnish a base for the systematic development of a more comprehensive method. The primary objective was the development of an analytical technique which will adequately predict the thermal conductance of certain types of bolted joints and the

experimental verification of this technique. The experimental investigation of the normal stress distribution under boltheads, and the theoretical and experimental investigation of the deflection of bolted plates due to bolt loads were secondary objectives.

The work reported here was made up of the following tasks which are listed in the order that they are discussed in the following chapters.

(1) Experimental determination of the normal stress distribution under round- and flat-headed bolts.

(2) Development of an improved theoretical method to predict the deflection of joint members due to non-uniform fastener loads.

(3) Measurement of the stress distribution in the interface between two bolted plates and the area of apparent contact.

(4) Development of an analytical method to predict, from limited information, the thermal conductance in certain types of bolted joints.

(5) Measurement of the temperature distribution in two bolted joints to verify the analytical method.

CHAPTER III

EXPERIMENTAL INVESTIGATION OF NORMAL STRESS DISTRIBUTION UNDER BOLTHEADS

The effect of the normal stress distribution under a bolthead on the deflection of bolted plates was discussed in Chapter II. In analyzing the deflection of joint members due to the fastening stresses, both Lieb (42) and Fernlund (60) assumed a uniform stress under the fastener head. A literature search revealed no information concerning the actual pressure distribution under the head of a flat- (fillister) head or a round- (button) head bolt. An experimental program was undertaken to confirm or refute the assumption of a uniform stress under a flat-head bolt and obtain information on the pressure distribution under a round-head bolt.

The initial plan included an investigation of the pressure distribution under two 1-inch fillister-head bolts, two 3/8-inch round-head bolts, one 5/8-inch button-head bolt, and one 1-inch button-head bolt. All these are shown in Figure III-1 along with 1-inch and 5/8-inch nuts that were also to have been studied. Experimental difficulties prevented a detailed study of all but the 1-inch bolts shown, as originally fabricated, in Figures III-2 and III-3. All the bolts and nuts, were AISI C1020 steel. The experimental program consisted of two different methods of investigation. The first involved a study of the penetration of oil under the boltheads when the bolts were fastened to a plate and the assembly soaked in oil. The second part of the program involved the direct measurement of the pressure distribution under the boltheads. Both parts of the experimental program and the results obtained are discussed in the following paragraphs.

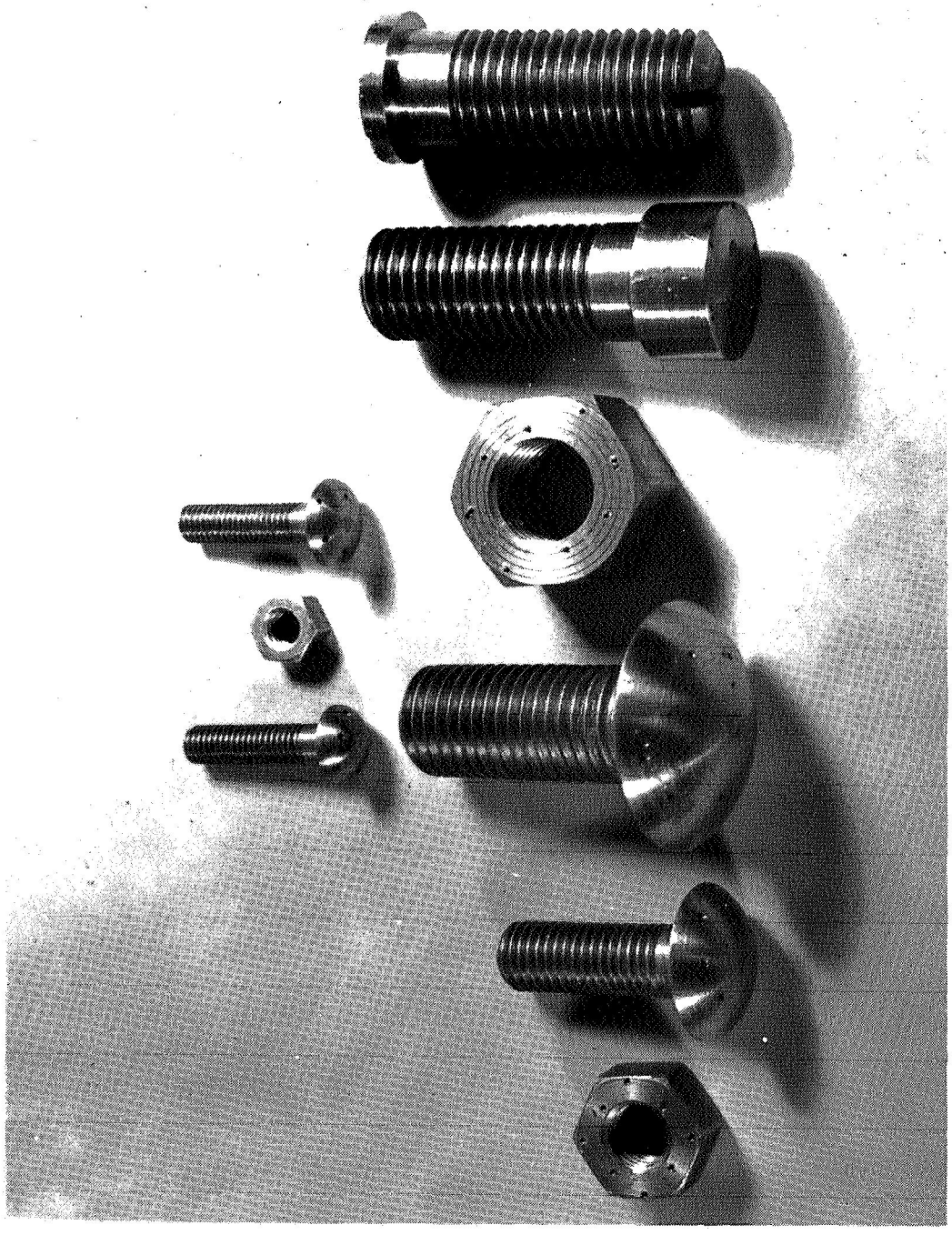

FIGURE III-1 1, 5/8, AND 3/8-INCH FASTENERS AS ORIGINALLY DESIGNED FOR STRESS STUDY

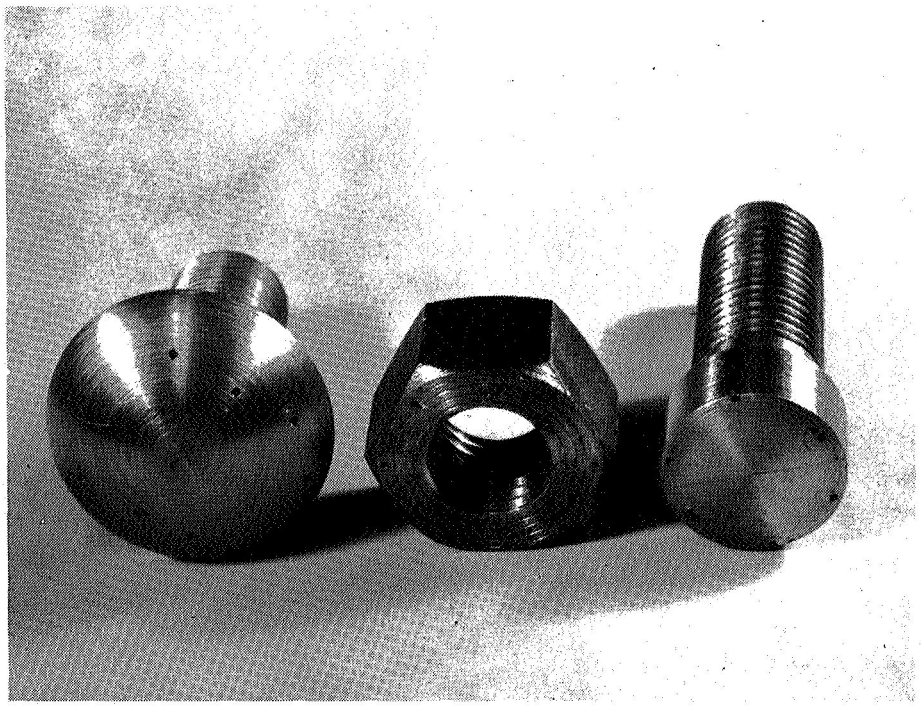

FIGURE III-2 1-INCH BUTTON-HEAD BOLT, NUT, AND FILLISTER HEAD BOLT.(NOTE HOLES)

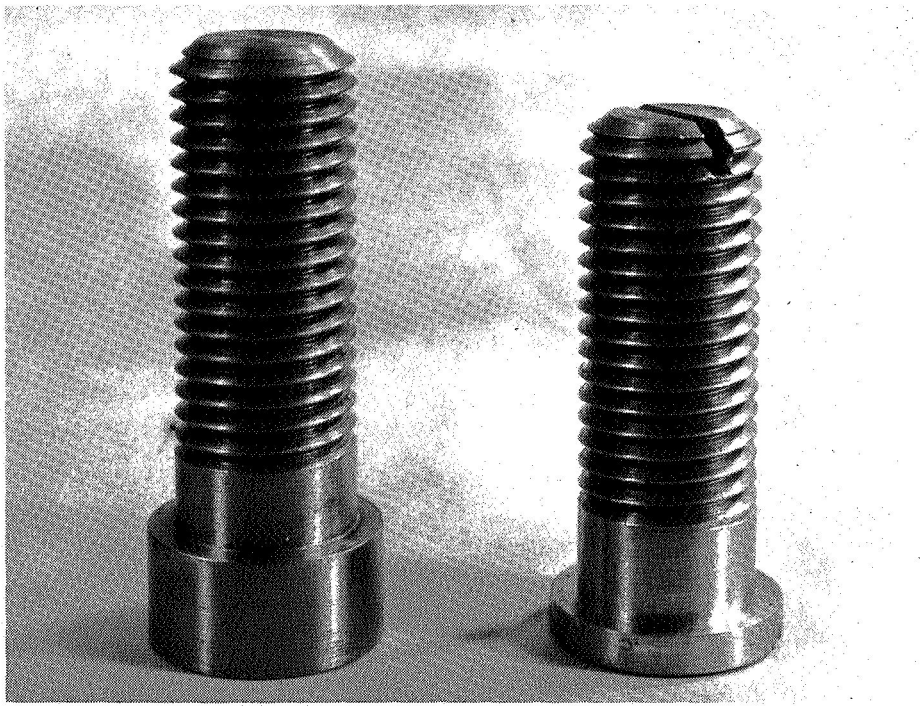

FIGURE III-3 1-INCH FILLISTER-HEAD BOLTS

A. Oil Penetration

In studying the interface stress distribution between bolted plates and the deflection of these plates, Fernlund (60), in a few tests, soaked a bolted joint in penetrating oil and observed the oil penetration distance between the plates as a function of time. He indicates that the results were inconclusive.

This use of penetrating oil to investigate the extent of interface stress was adopted for the present study to determine whether the normal stresses between boltheads and plates extended to the edges of the boltheads.

1) Oil Penetration Results:

The first tests involved a 1-inch button-head bolt fastened to either a 304 stainless steel or a 7075ST aluminum plate. Both plates were 0.625 inches thick (Figure III-4). The bolt was tightened with a Proto torque wrench within ± 3 percent of a given torque. The same wrench was used in all following experiments. After their assembly, the bolt, plate, and nut were placed in a bath of penetrating oil for a preset period of time. Care was taken to prevent the oil from entering the small injection holes that had been drilled in the bolthead.

After removal from the oil bath, the bolt was carefully loosened and removed from the plate for measuring the distance of oil penetration. This penetration could be seen on both the bolthead and the plate, but it was more easily measured on the bolthead.

A total of 64 tests on both an aluminum and a stainless steel plate were done with two different 1-inch button-head bolts. The fastening torque was varied from 40 foot-pounds to 150 foot-pounds (the maximum

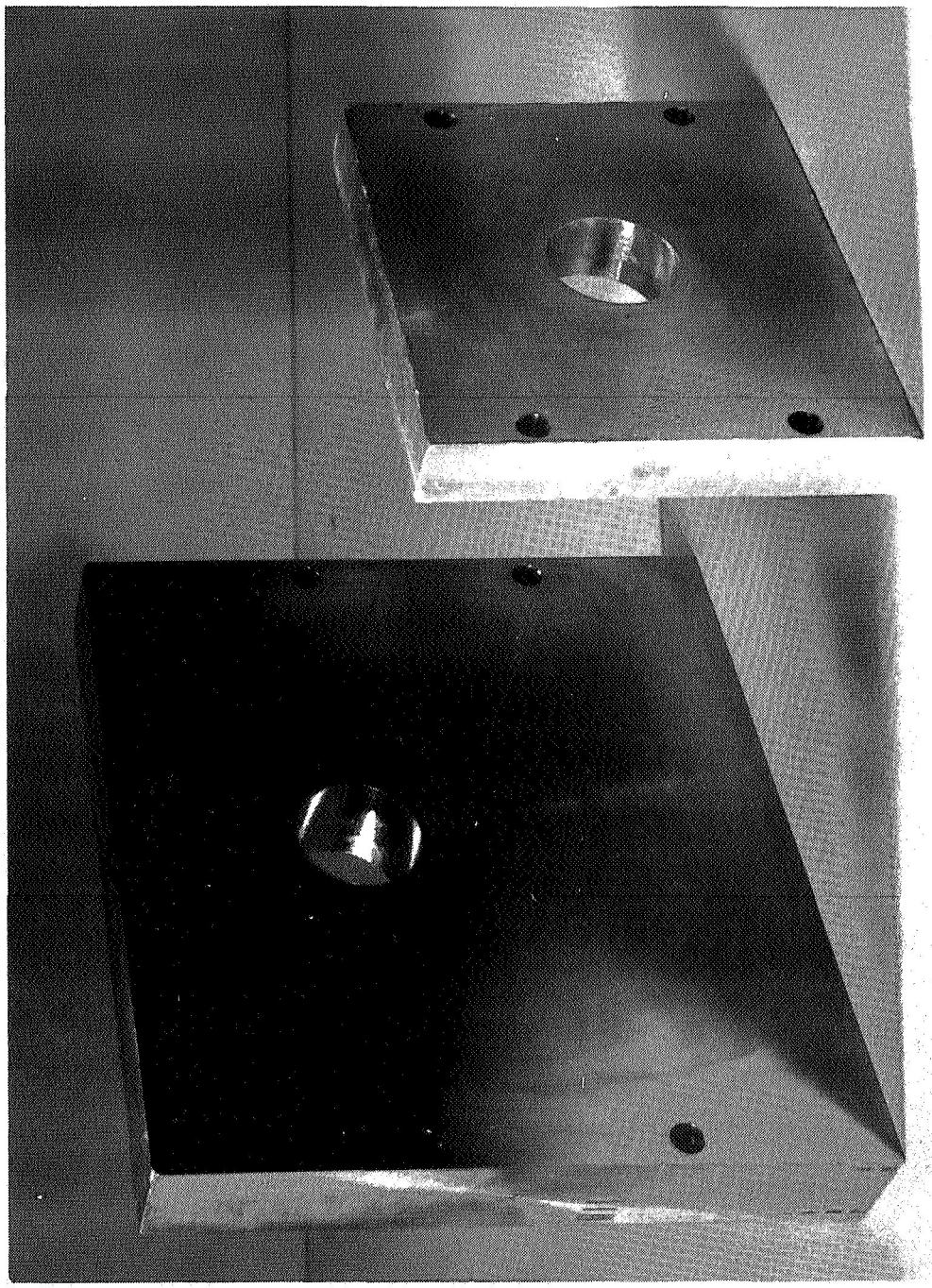

FIGURE III-4 STEEL AND ALUMINUM PLATES USED IN STUDY OF BOLTHEAD STRESS DISTRIBUTION

for the particular wrench); the soak time was varied from 10 seconds to 40 minutes. The results are plotted in Figure III-5.

It was concluded that the penetration distance was unaffected by the soak time and neither a material or torque effect was evident. Apparently, the boltheads were offering practically no resistance to penetration near their perimeter, but very great resistance 0.15 to 0.20 inches inside their perimeter. The normal stress apparently was low near the head perimeters and much higher 0.15-0.20 inches from the perimeters.

Similar tests with penetrating oil were carried out with two 1-inch fillister-head bolts (Figure III-3) with a 1-inch heavy-duty nut (Figure III-2) and a 5/8-inch button-head bolt (Figure III-1). The results are plotted in Figure III-6.

Again, the penetration distance did not vary with the soak time. Because no penetration was noted on the 1-inch, thick fillister-head bolt, the normal stress was apparently quite high at the head perimeter. The 5/8-inch button-head bolt allowed penetration to about 0.14 inches. This distance is 80 percent of the average (0.175 inches) found for the 1-inch diameter button-head bolt. One might surmise from linear scaling that the distance probably should be closer to 60 percent of the distance measured for the 1-inch bolt. The average penetration under the nut was very small, only 0.040 inches, and can be neglected for most nuts without appreciable error.

2) Oil Penetration Results with Gasket:

In obtaining the above data, the greatest difficulty was visual interpretation of the depth of radial oil penetration. Fernlund (60) suggested the blowing of lycopodium powder over the wetted surfaces to

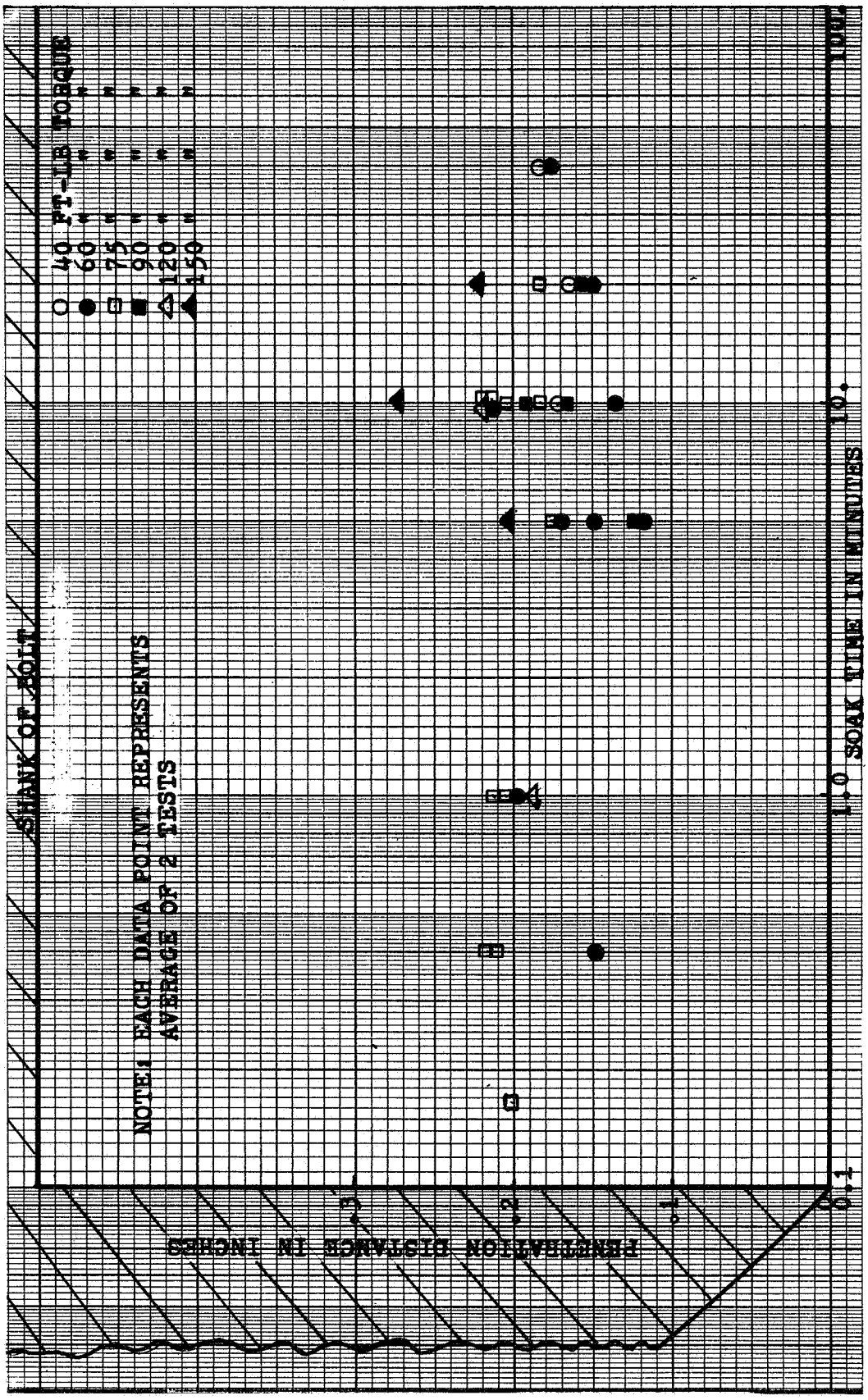

FIGURE III-5 PENETRATION OF OIL UNDER 1-INCH DIAMETER BUTTON-HEAD BOLT AS A FUNCTION OF TIME

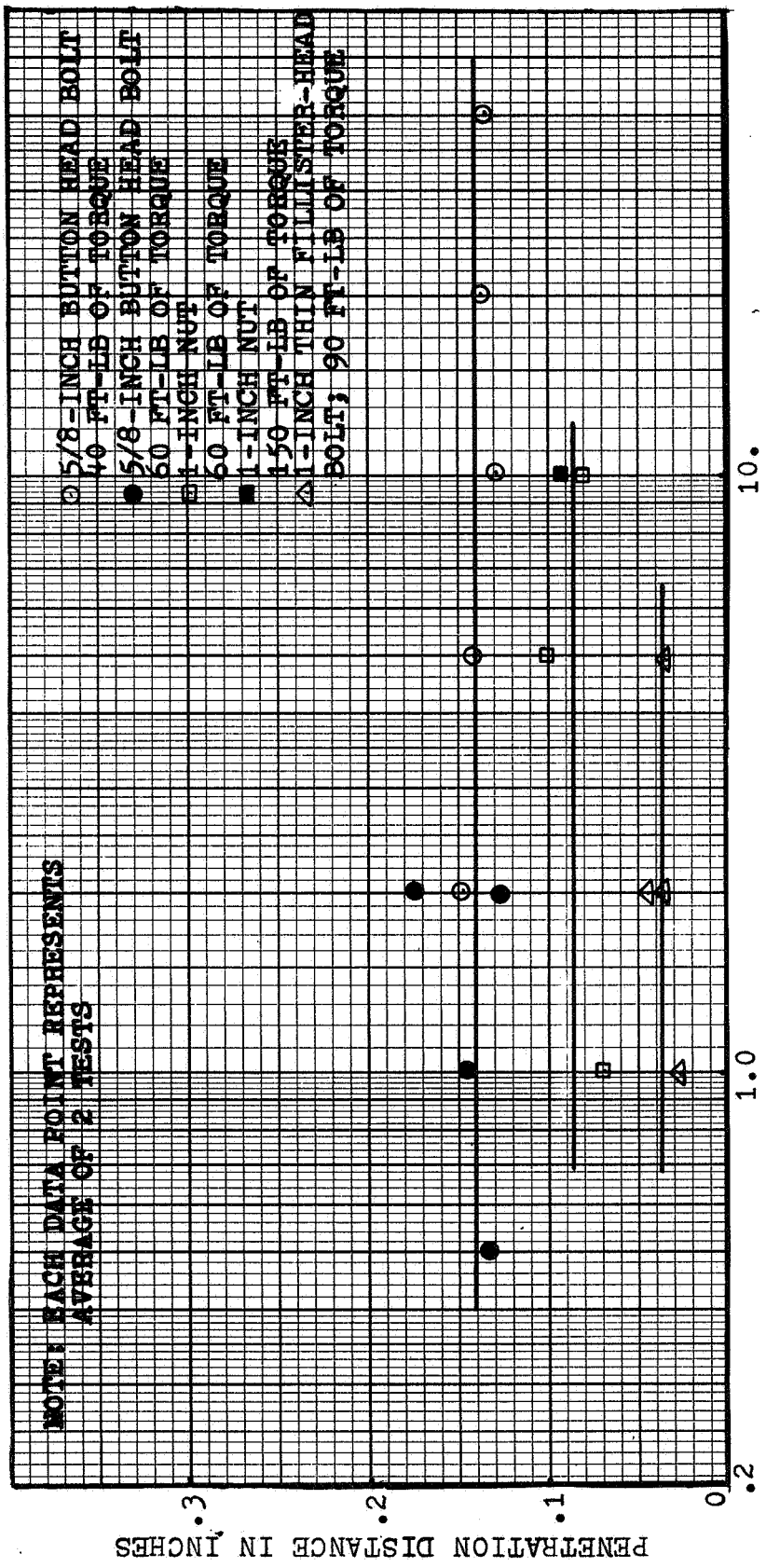

FIGURE III-6 PENETRATION OF OIL UNDER 1-INCH DIAMETER THIN FILLISTER-HEAD BOLT AND NUT AND 5/8-INCH DIAMETER BUTTON-HEAD BOLT

make the wetted region more visible. This procedure was tried but was not useful. To provide a more clearly-defined region of penetration, it was decided that a thin sheet of filter paper placed between the bolthead and the plate would not disturb the stress distribution appreciably. A foreseen drawback in the interpretation of the data as a function of soak time was eliminated by proper calibration of the filter paper.

Two brands of chemical filter paper were investigated to decide on the gasket material between the bolthead and the plate. One was Whatman (made in England); the other, Reeve Angel (made in the U.S.). Both brands come in multiple grades or types. From numerous tests, it was found that the Reeve Angel paper did not provide consistent results; the Whatman paper yielded good results. After further tests of several Whatman papers, Whatman No. 5 was chosen.

Initially, the tests with the filter paper were performed with penetrating oil, but a fluid of lower viscosity seemed desirable. Upon the recommendations of a representative from Mobil Oil, two types of diesel fuel were tried out. Esso Diesel 260 was chosen. Its specific gravity was 0.8493 and its viscosity, 3.39×10^{-7} reyns.

For calibrating the oil penetration rate, two methods were tried. In the first, with the paper gasket between the bolthead and plate, the assembly was made "hand tight" and placed in the diesel fuel for a predetermined period of time. However, even for periods of time less than five seconds, the gasket became completely soaked. This indicated an extremely rapid wetting of the gasket between the bolthead and the plate when unimpeded by pressure forces.

To establish a lower bound for the wetting time, a strip of the paper was suspended vertically above the fuel oil with a short length

immersed. The wetted height as a function of time was found to be readily duplicated. The conclusion was that if a region of very low normal stress existed near the perimeter of a bolthead, that region should exhibit a penetration-versus-time curve somewhere between the instant-wetting and free-suspension cases. The curve for penetration versus time plotted for the 1-inch button-head bolt did fall between the two limits; that for the 1-inch fillister-head bolt did not.

In 54 tests with a 1-inch button-head bolt torqued to a 5/8-inch plate (Whatman No. 5 filter paper gasket), the oil penetration as a function of soak time was measured for torques of 40, 60, 75, and 120 foot-pounds. From the results (shown in Figure III-7) it is obvious that a drastic change in penetration rate occurs at all torque values 0.15 to 0.25 inches in from the edge of the bolthead. The higher the torque, the nearer to the edge of the head the change seems to occur. In all cases, however, the break from the steep slope that is also characteristic of an unloaded bolthead-plate gasket occurs between 0.15 and 0.20 inches. This break agrees with the penetration data shown in Figure III-5. It also agrees with pressure measurements to be discussed later.

In every attempt to confirm the results in Figure III-6 on a 1-inch, thin fillister-head bolt, the gasket was completely wetted. Thus, no useful results were obtained.

However, for the 1-inch, thick fillister-head bolt with fastening torques of 40 and 75 foot-pounds, usable data was obtained. In Figure III-8, the initial slopes of the curves, at best no steeper than the slope for the free-suspension calibration, indicate that a pressure-free zone does not exist near the edge of this bolthead.

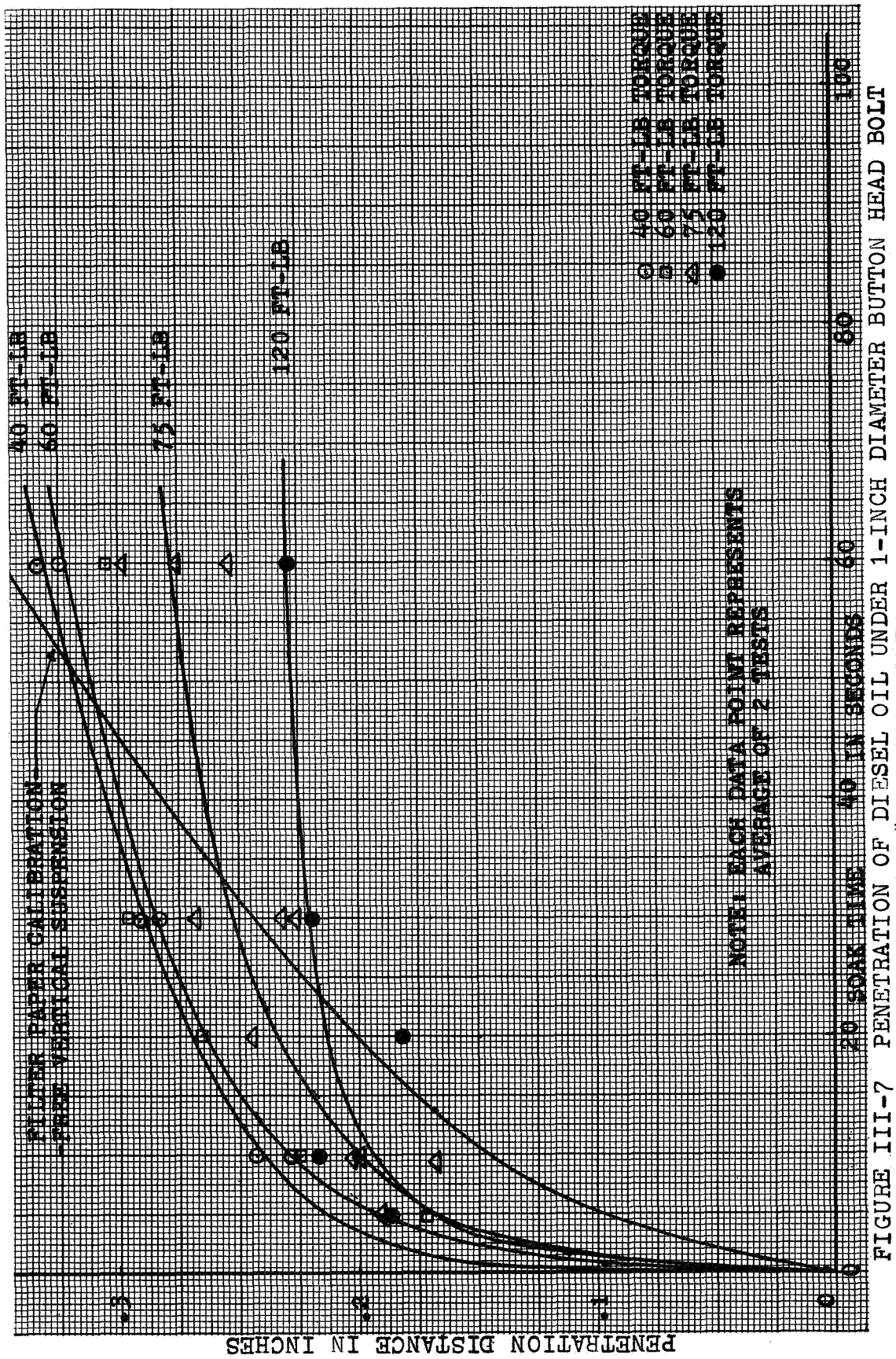

FIGURE III-7 PENETRATION OF DIESEL OIL UNDER 1-INCH DIAMETER BUTTON HEAD BOLT USING WHATMAN #5 FILTER PAPER

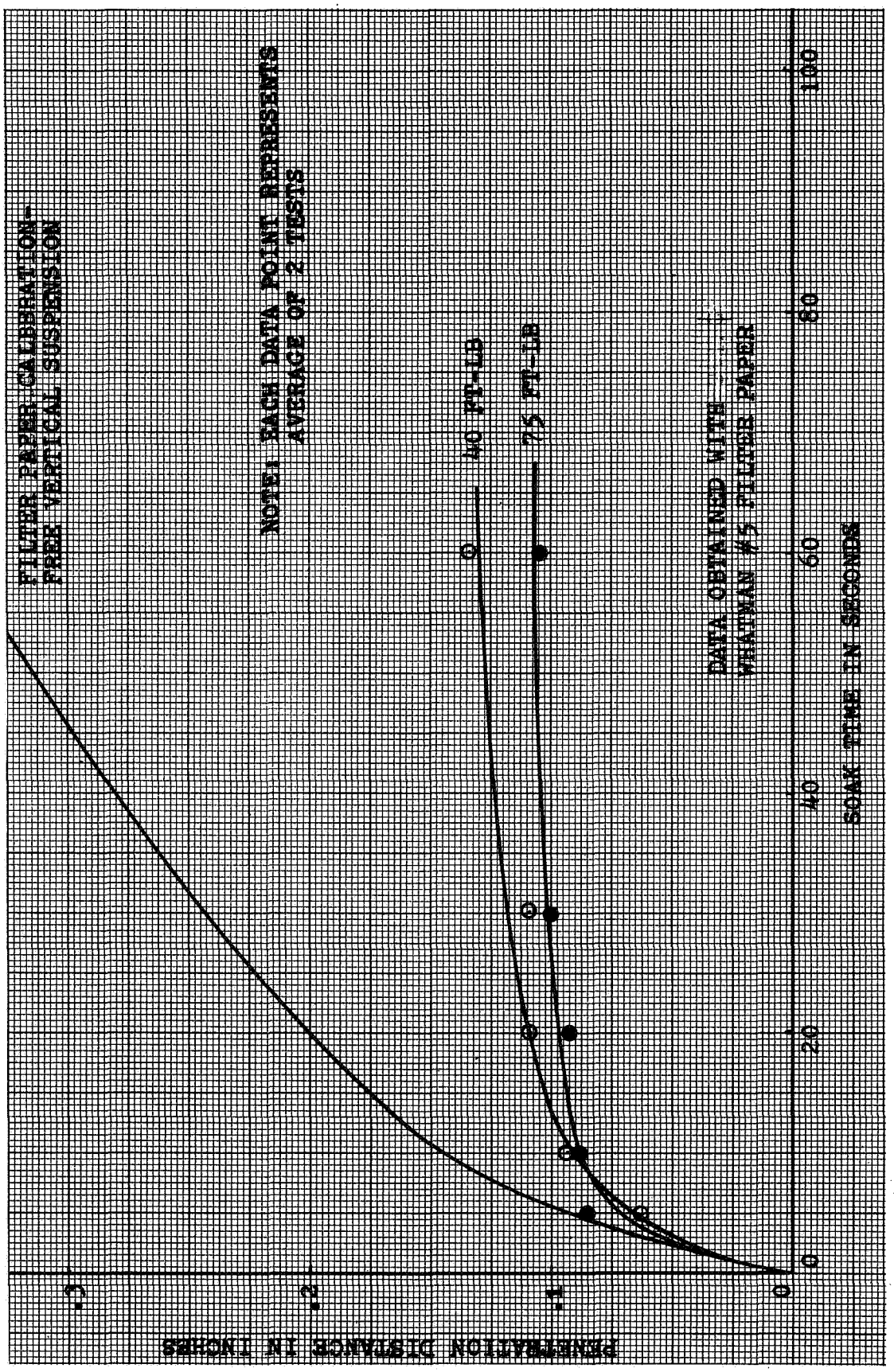

FIGURE III-8 PENETRATION OF DIESEL OIL UNDER 1-INCH DIAMETER THICK FILLISTER-HEAD BOLT

B. Pressure Measurements under Boltheads

The foregoing discussion has described the experiments to measure only the radial extent of the normal stresses under various types of boltheads. Because these tests do not give the actual pressures under the heads, quantitative measurements of the stress distribution become the next problem.

1) Initial Tests:

In 1961, Fernlund (60) described an experimental procedure that he used to measure the interface stress between thick bolted plates as a function of radial distance from the bolt shanks. He used an oil injector to inject oil into 0.050-inch diameter holes that had been drilled through one of the plates. The injection pressure at which oil was initially forced out between the plates was assumed equal to the local pressure at the injection hole. The results from this experimental procedure were shown by Fernlund to agree with his theoretical predictions within ± 7 percent.

Because no published attempt to measure the normal stress under a bolthead could be found, Fernlund's method for plates was adopted. It was anticipated that the pressure could be measured under two of the nuts and under all the boltheads shown in Figure III-1. A number of 0.015-inch diameter holes were drilled through the boltheads and the nuts. Each hole was concentrically tapped for a No. 0-80 thread. The thread was approximately 0.125 inches deep, to provide about 10 threads for attaching a male fitting. Cross sections of a typical hole and the mated pressure fitting are shown in Illustrations III-1 and III-2. The three original pressure fittings were brass. One of them is shown on the far right in Figure III-9.

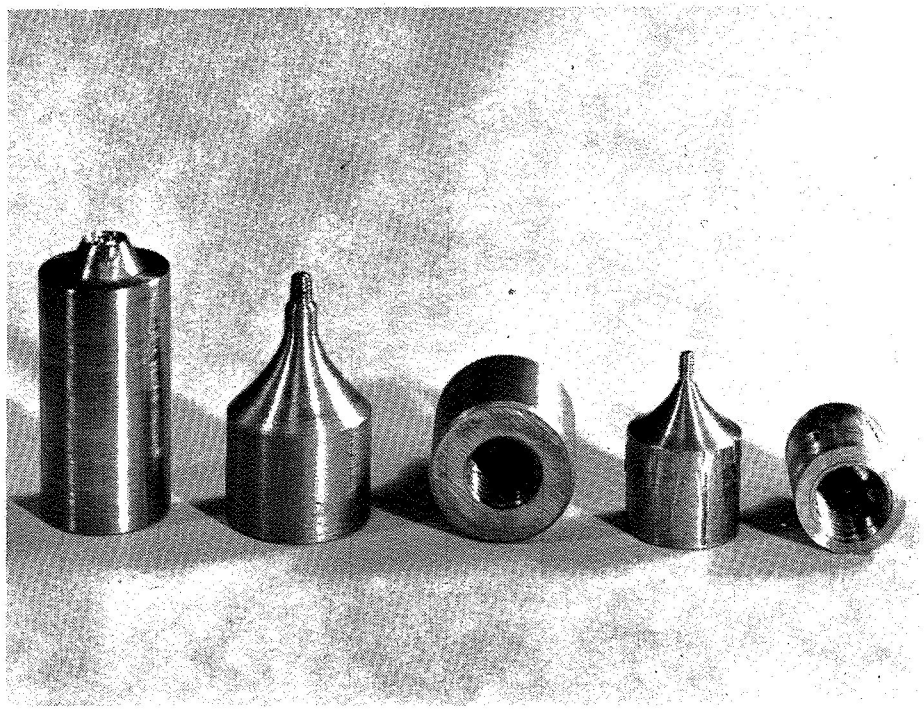

FIGURE III-9 GASKET CUTTER, IMPROVED PRESSURE FITTING, AND ORIGINAL FITTING.

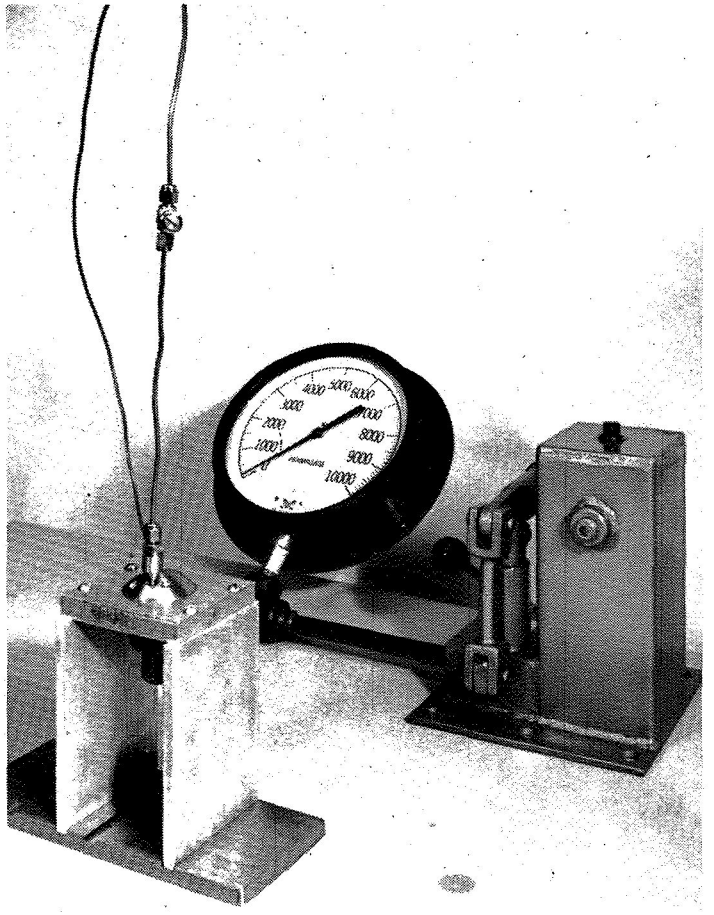

FIGURE III-10 EXPERIMENTAL SETUP FOR STUDY OF BOLTHEAD PRESSURE DISTRIBUTION

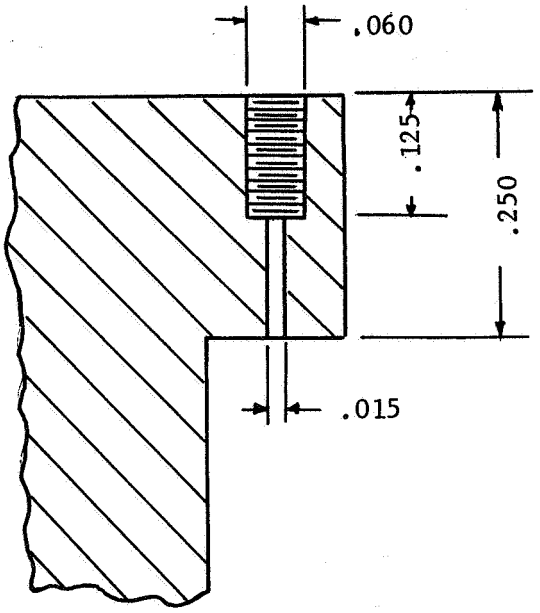

ILLUSTRATION III-1
Cross Section of Hole in
Thin Fillister-Head Bolt

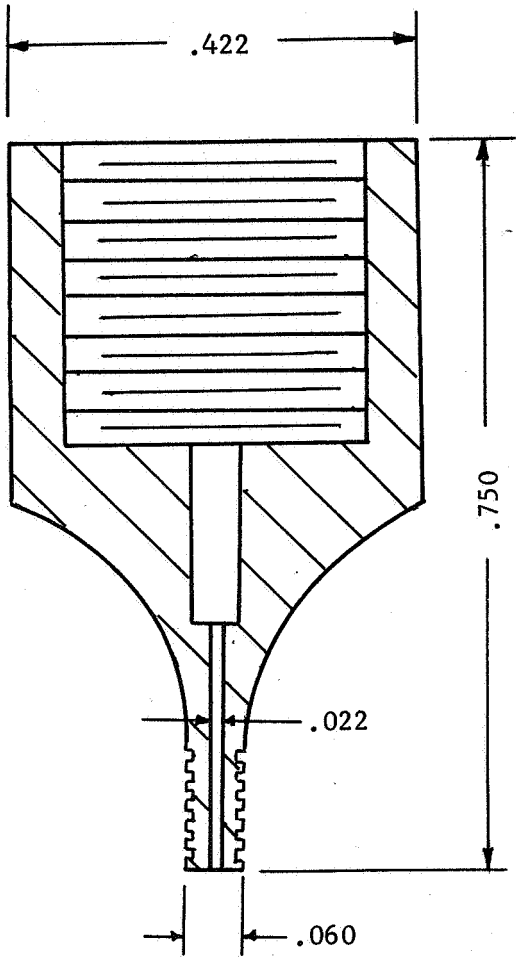

ILLUSTRATION III-2
Cross Section of Original
Pressure Fitting

In the first series of tests, the 1-inch, thin fillister-head bolt (Figure III-3), was used. The test setup is shown in Figure III-10 (a modified 1-inch button-head bolt is in place of the fillister-head bolt). The test fluid was penetrating oil. The bolt was tightened to 60 foot-pounds on the stainless steel plate of Figure III-4.

No oil flowed from under the bolthead at 2500 psi. An aluminum test plate was also tried with the same pressure, without result. (At 60 foot-pounds of torque, the oil had been expected to flow at about 1500 psi or

less.) Several attempts at both higher and lower torques led to the conclusion that either the compression in the bolthead closed the 0.015-inch holes or the penetrating oil was too viscous.

During the abortive attempts to inject oil into the first specimen, the three pressure fittings were ruined: two by the shearing off of the threaded tips; the third, by stripping of some of the threads on the tip after only a few assembly and disassembly operations. These fittings also leaked oil--a continual source of trouble.

In the design of the bolts and nuts with such small holes and oil injection fittings, the intention had been to keep the physical disturbances of the measurements at a minimum.

2) Redesign of Holes and Fittings:

After the initial lack of success the injection holes in the 1-inch bolts (Figures III-2 and III-3) were enlarged to 0.025 inches. A 2-64 threaded hole was tapped concentric with each hole. In addition, the hole was countersunk to accommodate a gasket and provide a pressure seal. A cross-section of this modified hole is shown in Illustration III-3. Four new pressure fittings, of AISI C1020 steel, were fabricated (center of Figure III-9, cross-section in Illustration III-4).

On the left in Figure III-9 is the gasket cutter, designed to cut small plastic rings which would seal the fitting when it was tightened in the tapped holes. To provide the needed clearance for the new, larger fittings the threaded hole was recessed on the 1-inch button-head bolt (Figure III-11). This modified button-head is also shown (attached to an aluminum plate in the test stand) in Figure III-12. No attempt was made to modify the 5/8-inch and 3/8-inch diameter bolts in this manner because of their smaller size.

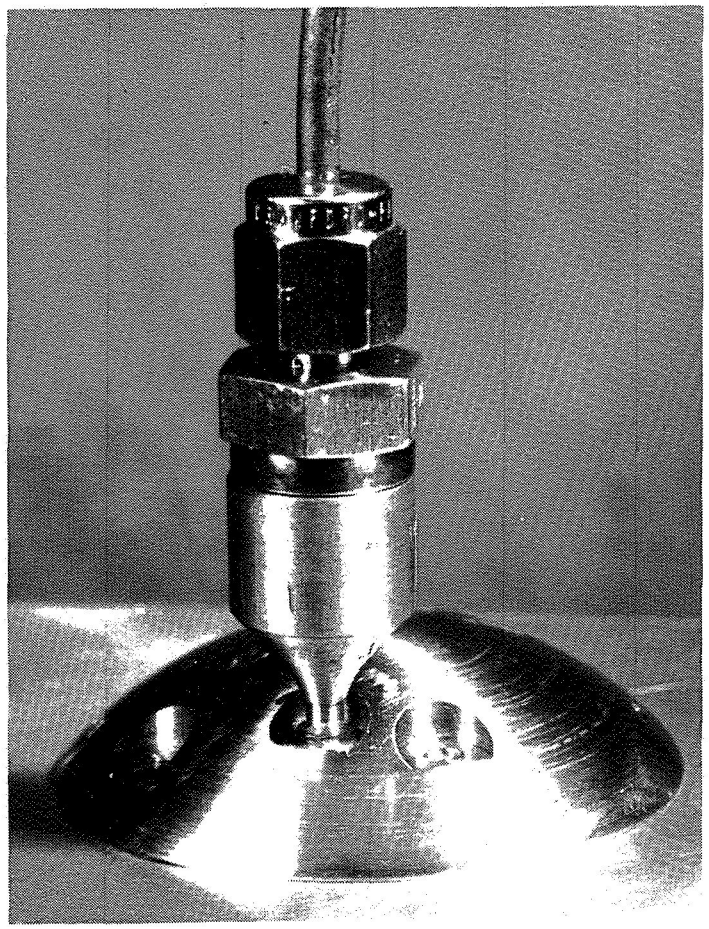

FIGURE III-11 MODIFIED 1-INCH BUTTON-HEAD BOLT WITH IMPROVED PRESSURE FITTING

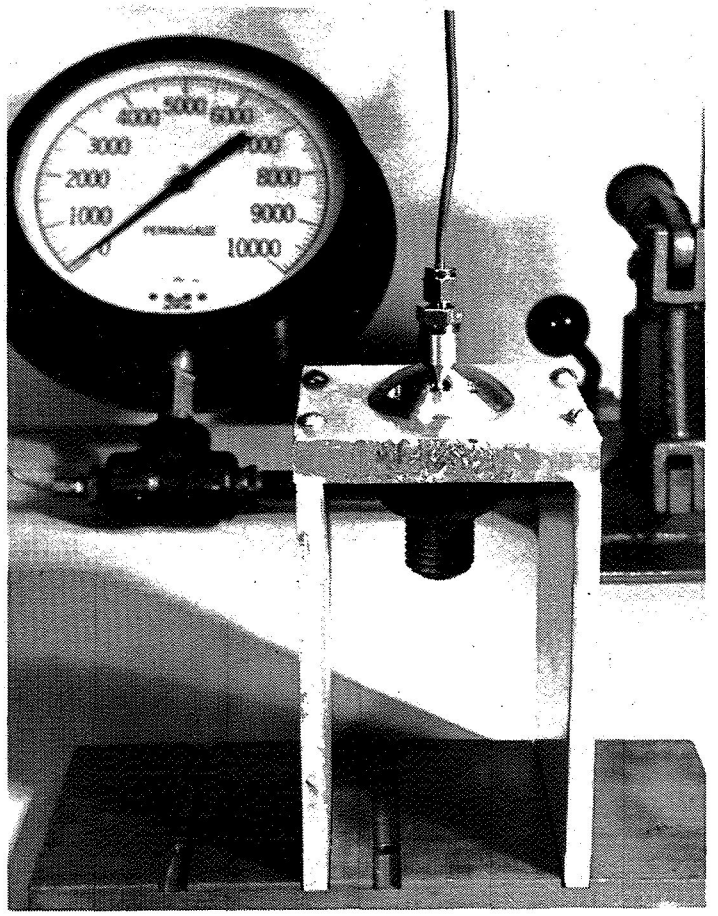

FIGURE III-12 MODIFIED 1-INCH BUTTON-HEAD BOLT AND ALUMINUM PLATE IN TEST STAND

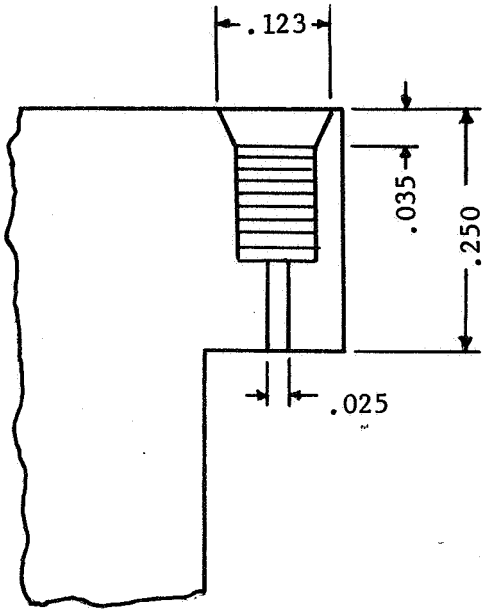

ILLUSTRATION III-3
Cross-Section of Modified Hole
in Thin Fillister-Head Bolt

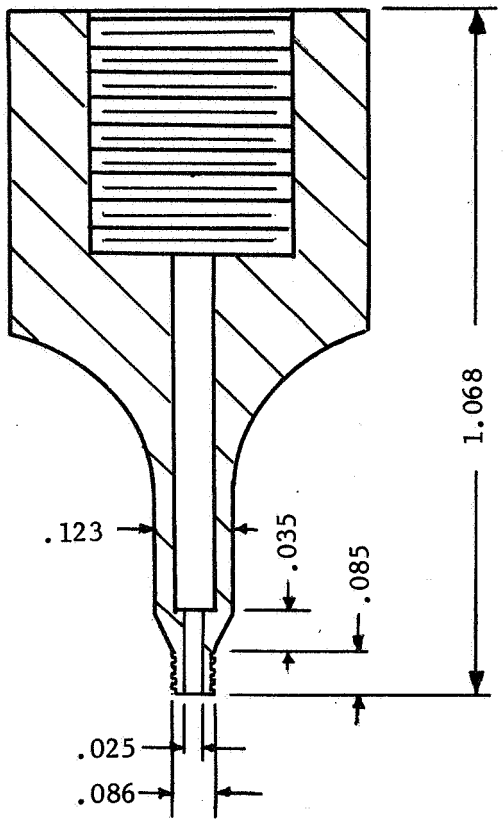

ILLUSTRATION III-4
Cross-Section of Improved
Pressure Fitting

In addition to these modifications, the injection fluid was changed from penetrating oil to the Esso Diesel 260, whose properties were given earlier and which approximates more closely the Velocite No. 6 oil used by Fernlund (60) in his study of interface pressures.

3) Thin Fillister-Head Bolt:

New pressure measurements were made on the thin fillister-head bolt with the enlarged holes, improved pressure fitting, and diesel oil. The pressure at which the oil began to flow between the bolt and the plate could now be determined with reasonable consistency. Four readings were

made and the results were then averaged. At high pressures, an attempt was made to observe the system pressure drop as a function of time, thus determining more closely when the oil began to flow. However, general system leakage made this too uncertain. The oil pressure-bolt torque curves for two of the four holes in the fillister head are shown in Figure III-13.

Holes #1 and #3, which had originally been drilled very near the edge of the bolthead, could not be enlarged and countersunk to accommodate the pressure seal. Consequently, without the new threads and seal, pressure measurements were not taken.

In Figure III-13, the curve labeled "Average Stress Based on Total Area" represents the normal stress that would be calculated if the stress is assumed to be uniformly distributed under the head. The average stress would be simply the total axial force in the shank divided by total area under the head. The axial forces, as a function of fastening torque, were estimated with data given on page 36 of reference 64.

Also plotted in Figure III-13 is the curve labeled "Average Stress Based on Reduced Area," which represents the average stress on a ring with an inside radius of 0.50 inches and an outside radius of 0.62 inches. The reduction in outside radius from 0.65 to 0.62 inches is based on the lower limit of the results from the oil penetration studies plotted in Figure III-6. From Figure III-13, it is apparent that the measured pressures are only 63 percent (at 40 foot-pounds) and 70 percent (at 30 foot-pounds) of the average "reduced area" stress. In reference 64 it is pointed out that this is not unusual and that one might obtain values for axial bolt tensions as much as 50 percent below the average values given there for specially prepared specimens.

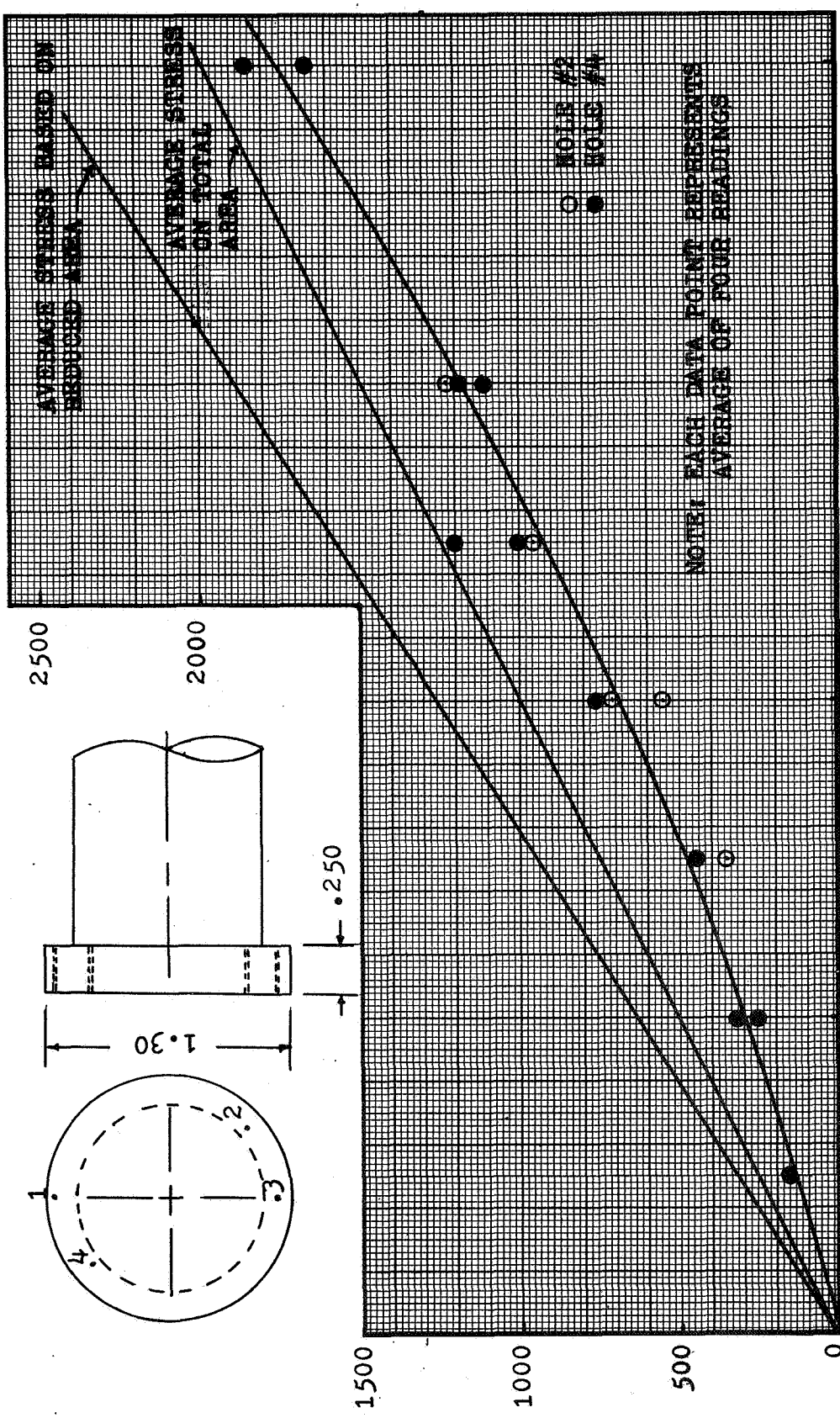

FIGURE III-13 PRESSURE MEASUREMENTS WITH DIESEL OIL UNDER THIN FILLISTER-HEAD BOLT AS A FUNCTION OF TORQUE

The pressures given in Figure III-13 have been replotted in Figure III-14 as a function of radial distance--with fastening torque a parameter. Evident from this figure is that the unmodified holes #1 and #3, which were located respectively 0.075 and 0.11 inches from the shank, would have provided valuable readings. However, it is known from the oil penetration data that the pressure must drop to zero approximately 0.03 inches in from the edge of the bolthead.

The pressure measurements, oil penetration results, and Figure 7 of reference 65 were next combined for plotting the curves in Figure III-14. These represent an approximation of the actual normal stress distribution under the thin fillister-head bolt.

4) Thick Fillister-Head Bolt:

Pressure measurements were also made under the head of the 1-inch, thick fillister-head bolt with the same techniques. In Figure III-15 the pressures are shown as a function of fastening torque. For torques of 30 foot-pounds or less, the pressures agreed with the average stresses calculated with values of axial force taken from reference 64. The entire area under the bolthead was assumed to be stressed--an assumption consistent with the results from the oil penetration study.

The high pressure readings at torques above 40 foot-pounds are unexplainable.

This same pressure data has been replotted in Figure III-16 as a function of radial distance, with fastening torque as a parameter. As they were for the thin fillister-head, all the measurements were necessarily confined to the middle of the bolthead ring area. Because the head did not separate from the plate, the assumption is that the normal

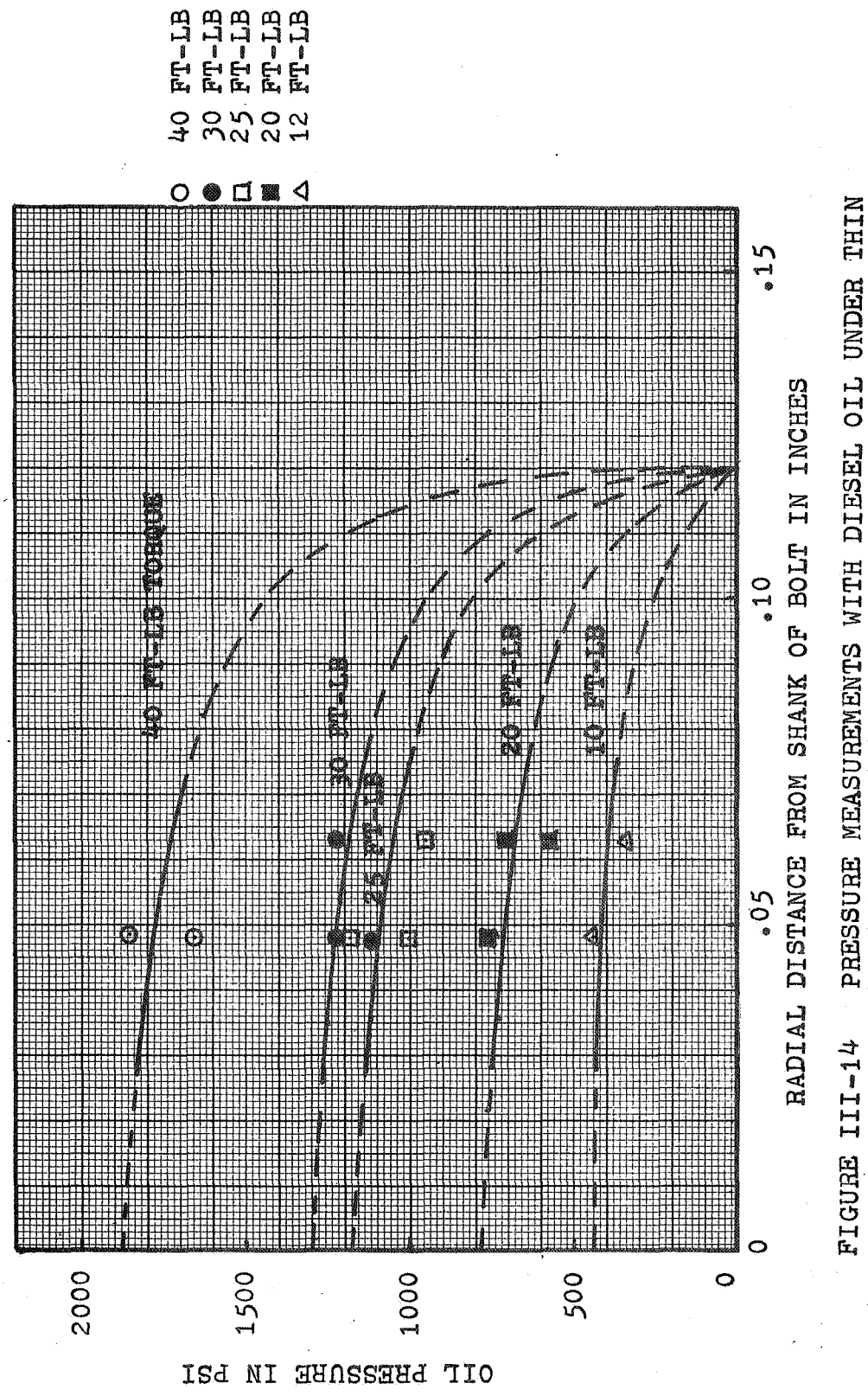

FIGURE III-14 PRESSURE MEASUREMENTS WITH DIESEL OIL UNDER THIN FILLISTER-HEAD BOLT AS A FUNCTION OF RADIAL POSITION

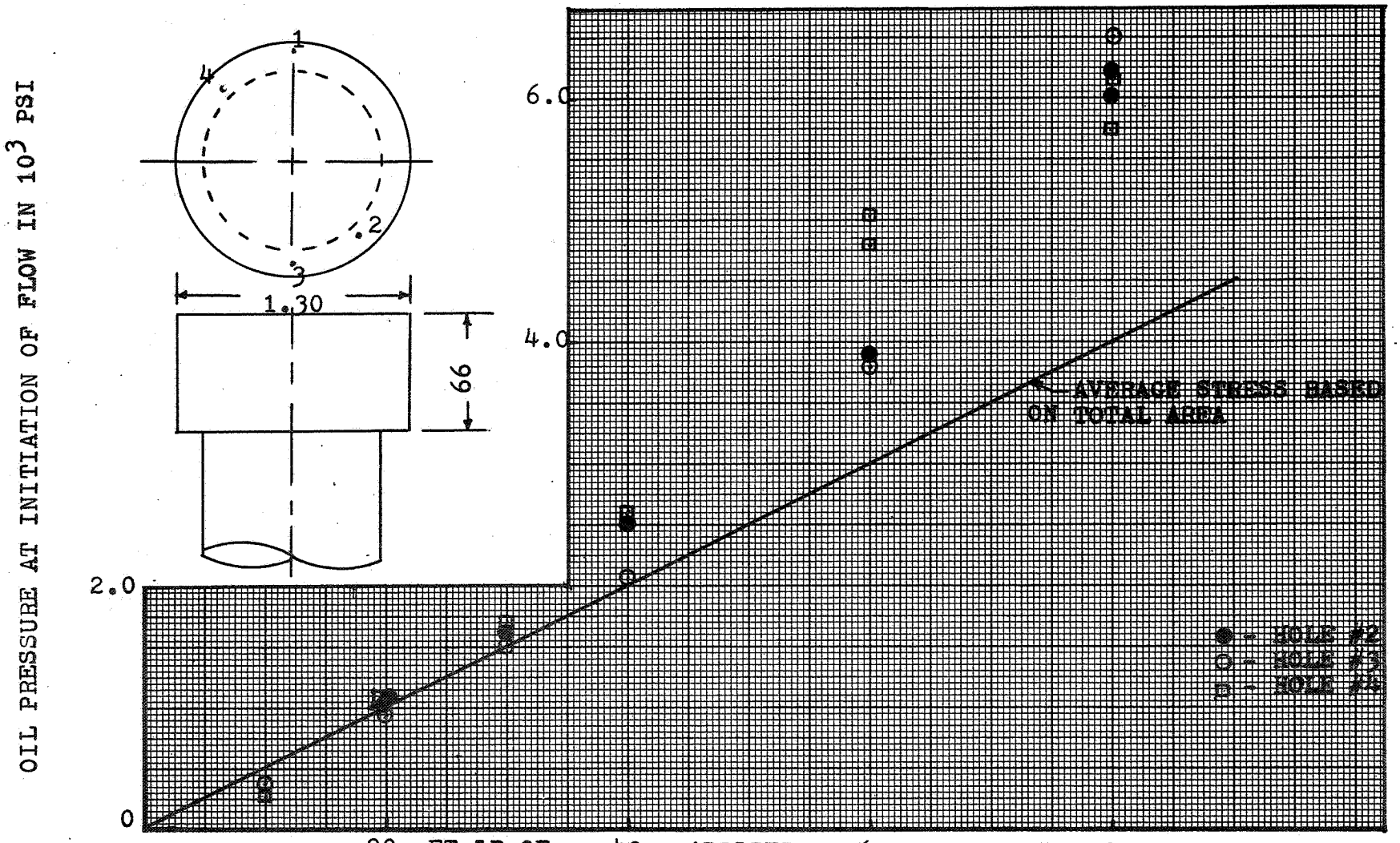

FIGURE III-15 PRESSURE MEASUREMENTS WITH DIESEL OIL UNDER THICK FILLISTER-HEAD BOLT AS A FUNCTION OF TORQUE

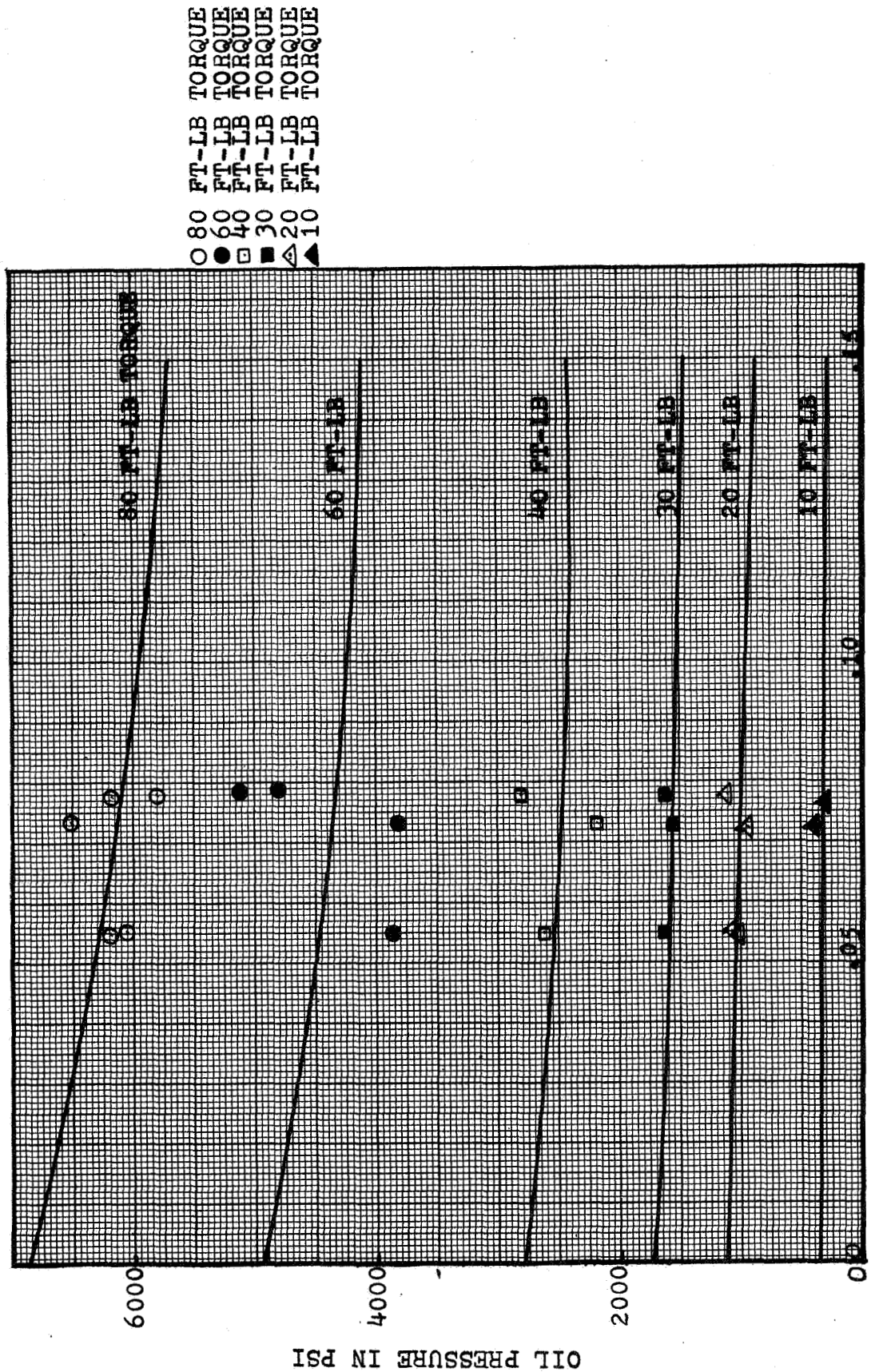

FIGURE III-16 PRESSURE MEASUREMENTS AS A FUNCTI[illegible] UNDER THICK FILLISTER-HEAD BOLT

stress was significantly high at the edge of the bolthead. This assumption, along with Figure 7 of reference 65, was used to obtain the curves shown in Figure III-16.

5) Button-Head Bolt:

In contrast to the pressures obtained from the fillister-head bolts, readings were taken for six radial distances under the 1-inch modified button-head bolt. The pressures are plotted as a function of torque in Figure III-17 and of radial distance, with torque as a parameter, in Figure III-18. From Figure III-18 it is clear that the normal stress is dependent on the radial distance from the shank. Two curves for average stress are shown. One is based on the total ring area; the other, on a ring of 0.34 inches outside radius.

The selection of 0.34 inches as the radial distance at zero stress is based on both the oil penetration results previously discussed and the curves of Figure III-18, which indicates that between 0.20 and 0.30 inches from the shank the normal stress drops rapidly. The average distance of 0.34 inches, selected for the radial position where the normal stress becomes zero, is in agreement with the pressure data for torques ranging from 10 to 100 foot-pounds.

Also plotted in Figure III-18 are the average stress values computed with the assumption of uniform pressure on the entire ring area. The ratios of the areas under the measured-pressure curves to the area under the average-stress curves were then computed and plotted in Figure III-19. The total bolt load determined from the pressure measurements varies from 37 to 56 percent of that computed assuming a uniformly-distributed normal stress. In reference 64, a torquing efficiency (percent of impressed torque converted to compressive load) of 50 percent was mentioned as a

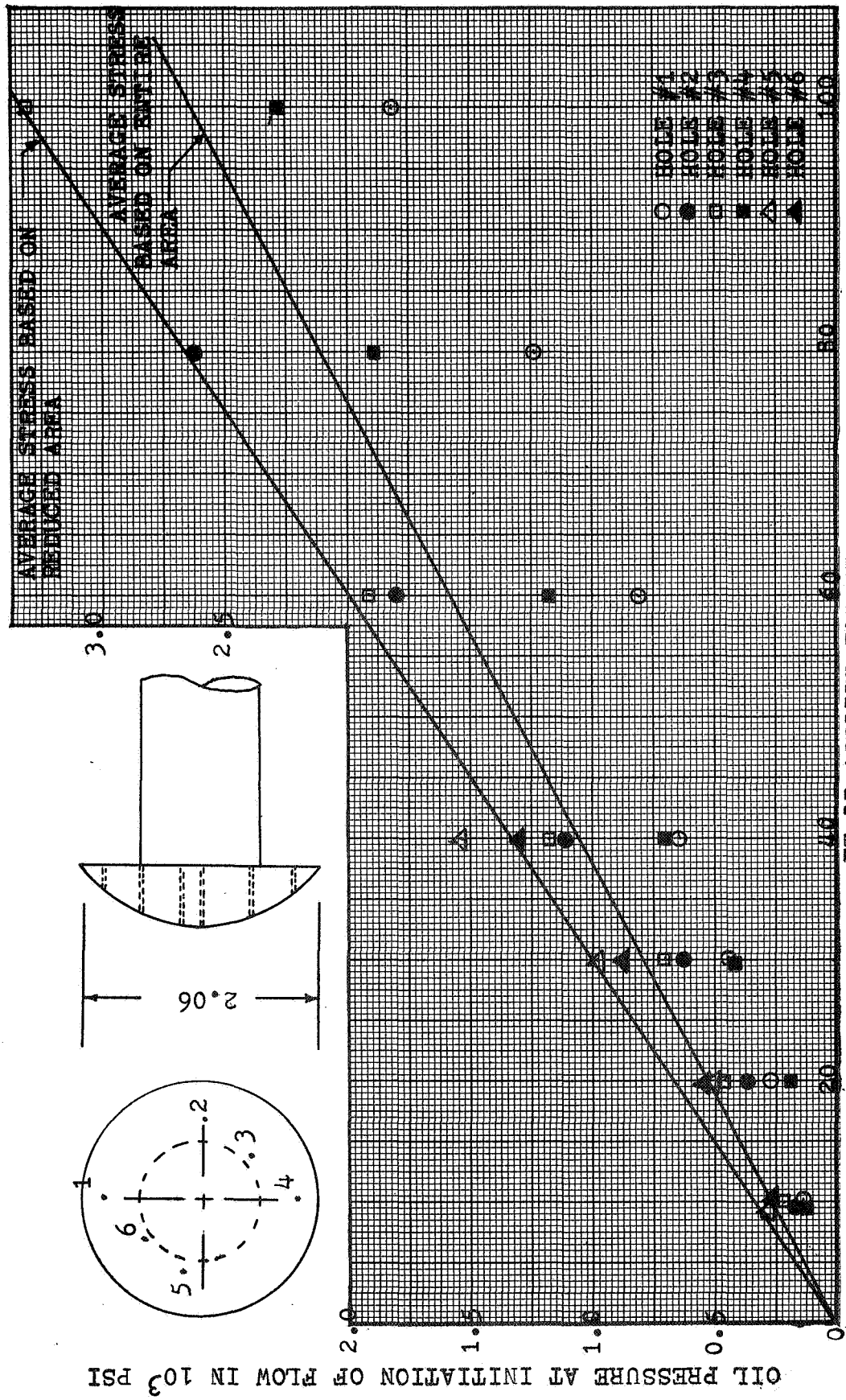

FIGURE III-17 PRESSURE MEASUREMENTS WITH DIESEL OIL UNDER 1-INCH DIAMETER BUTTON-HEAD BOLT AS A FUNCTION OF TORQUE

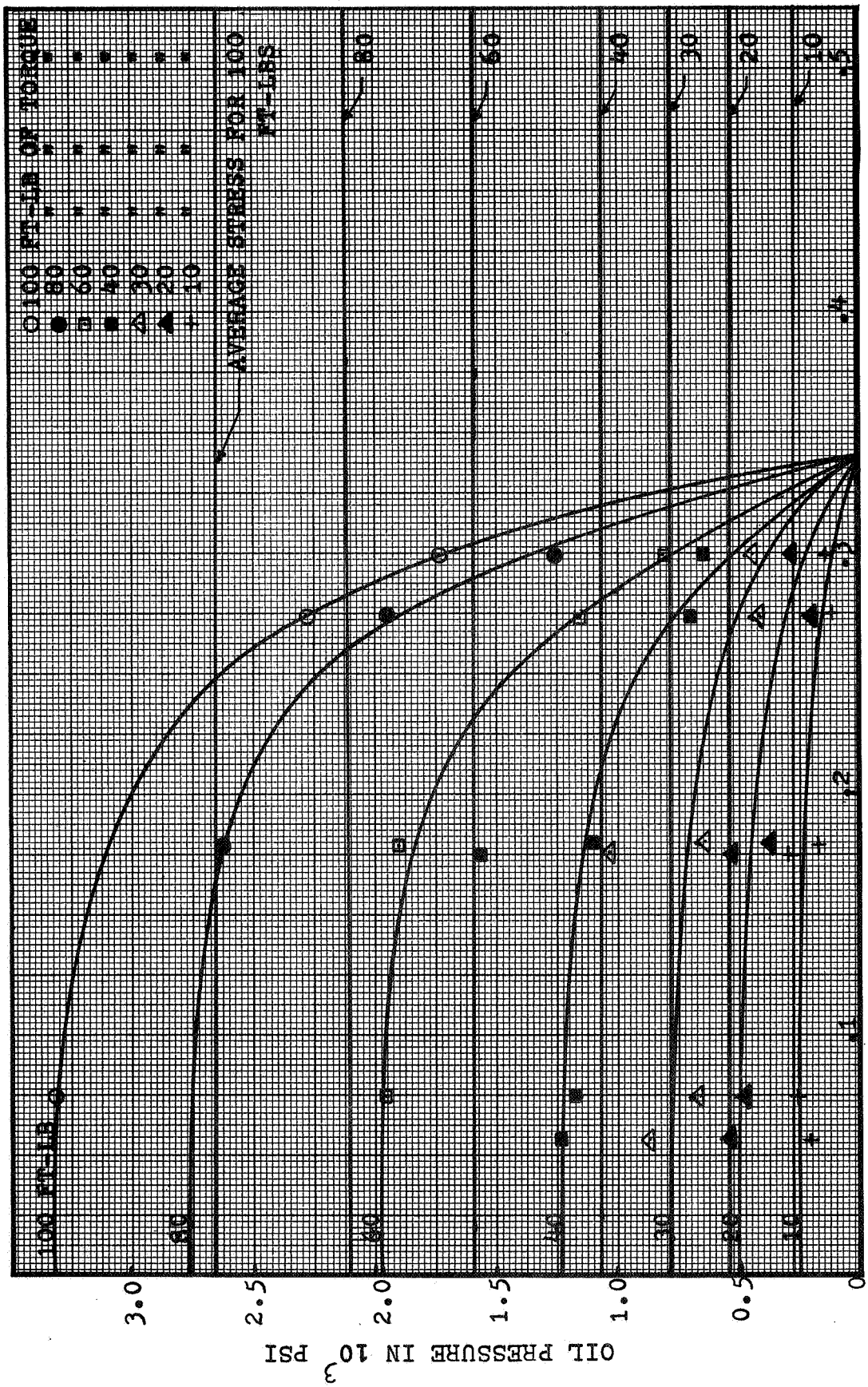

FIGURE III-18 PRESSURE MEASUREMENTS AS A FUNCTION OF r FOR THE 1-INCH BUTTON-HEAD BOLT

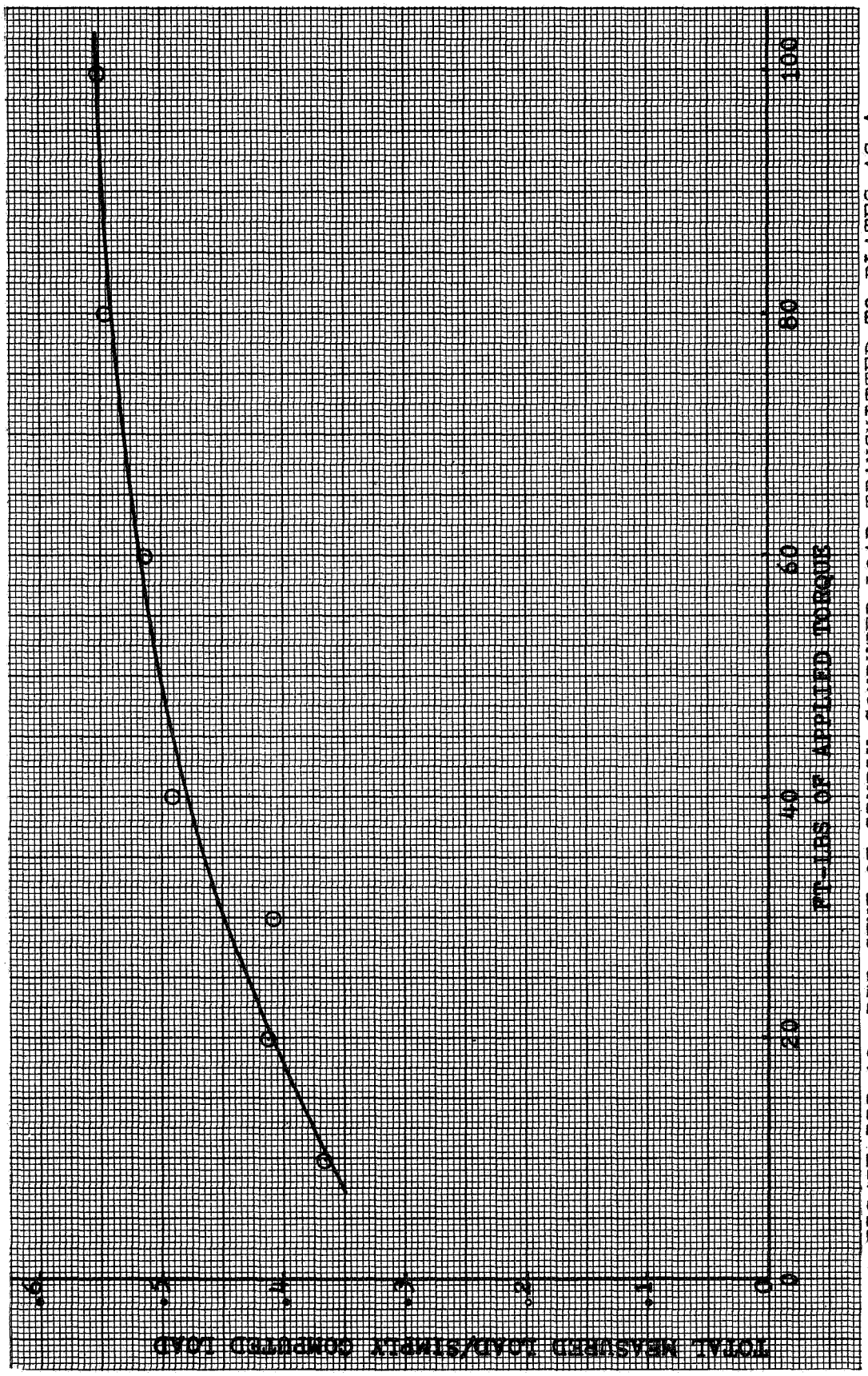

FIGURE III-19 PER CENT OF SIMPLY COMPUTED LOAD TRANSMITTED TO PLATES AS A FUNCTION OF APPLIED TORQUE

possible value. For torques above 50 foot-pounds, efficiencies of at least 50 percent were found. It appears, however, that at lower torques the bolt is not so efficient.

In a further analysis of the data for the button-head bolt, the maximum normal stresses were taken from Figure III-18 and plotted as a function of torque in Figure III-20. For comparison, the average normal stresses (uniform distribution) for total and reduced ring areas are plotted in the same figure. Note that the curve for the maximum pressure is coincident with the average-stress curve (total ring area) for torques less than 30 foot-pounds and is nearly coincident with the average-stress curve (reduced area) for higher torques. Figures III-18 and III-20 show, then, that the normal stress under a button-head bolt becomes more non-uniform as the torque is increased.

C. Effect of Bolthead Stress Distribution on Plate Deflection

From the experimental results just discussed, it is apparent that in some cases the distribution of normal stress under a bolthead will be non-uniform. Since the problem under consideration is not the bolthead stress distribution itself, but rather the effect of such distribution on the deflection of bolted plates, a parametric analysis of the latter problem was performed with a digital program discussed in the next chapter.

No attempt was made to describe the plate interface stress distribution. Only the normal stress under the bolthead was considered. Because the interface stress will adjust itself to changes in the bolthead stress distribution and thereby reduce the effect of varying the bolthead stress,

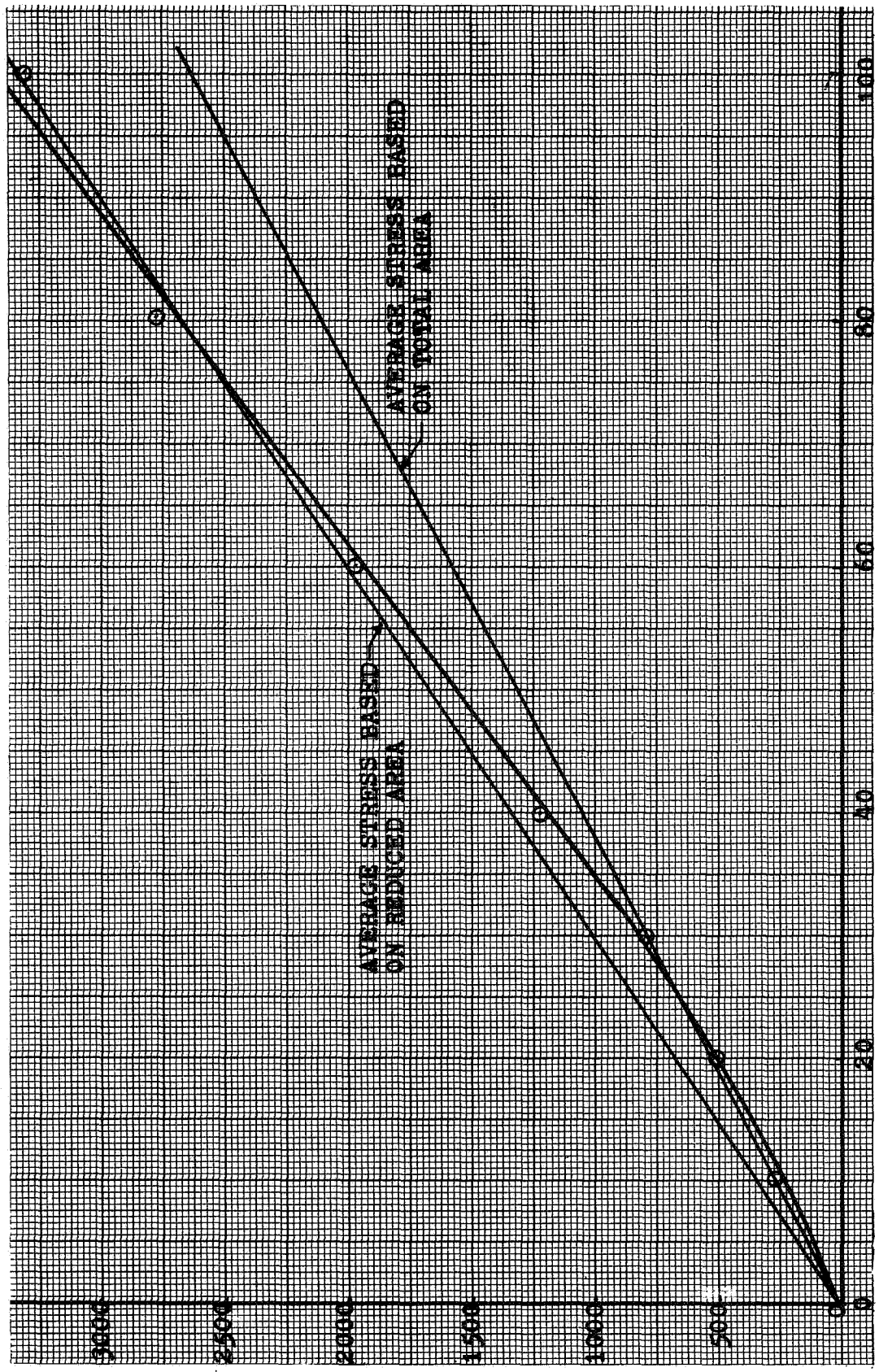

FIGURE III-20 MAXIMUM NORMAL STRESS UNDER 1-INCH DIAMETER BUTTON-HEAD BOLT

the parametric analysis was intended only to place an upper limit to the effect of non-uniform bolthead stress on the deflection of bolted plates.

This analysis considered a symmetrically-loaded 10-inch circular aluminum plate with a 1-inch hole in its center. Plate thicknesses of 0.125, 0.250, and 0.500 inches and six different stress distributions (Illustration III-5) were considered. Each stress distribution represents the same total load.

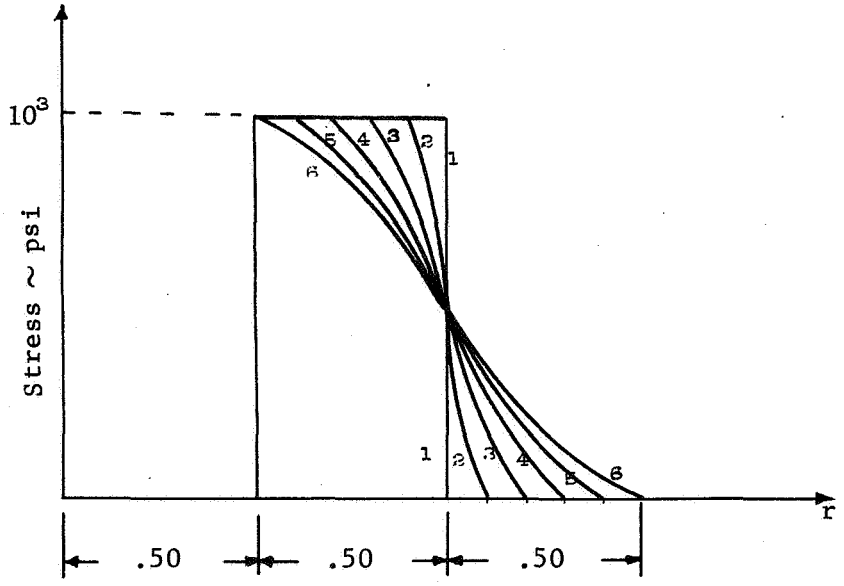

ILLUSTRATION III-5 Load Distributions Considered in Parametric Study

The computer results for the 0.125-inch plate with free and constrained edges are shown in Figures III-21 and III-22, respectively. The constrained-edge case represents a section of a joint between two bolts. For cases 2 through 6 (non-uniform stress), the edge deflections were normalized by dividing them by the edge deflection for case 1 (uniform stress). The results are shown in Figure III-23, which is valid for any thin plate.

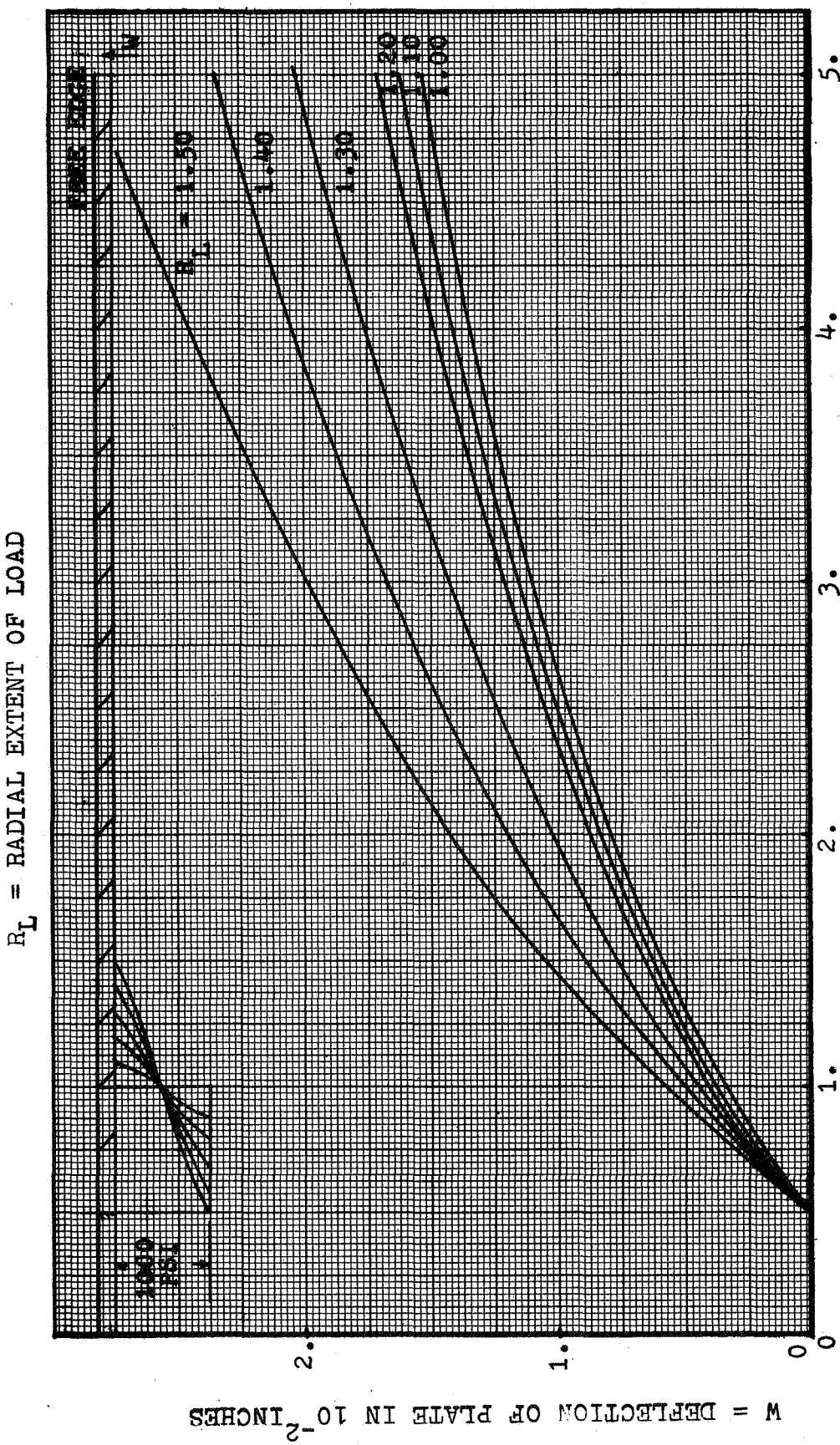

FIGURE III-21 EFFECT OF LOAD DISTRIBUTION ON DEFLECTION OF .125 INCH THICK ALUMINUM CIRCULAR PLATE - FREE EDGE

FIGURE III-22 EFFECT OF LOAD DISTRIBUTION ON DEFLECTION OF .125 INCH THICK ALUMINUM CIRCULAR PLATE - CONSTRAINED EDGE

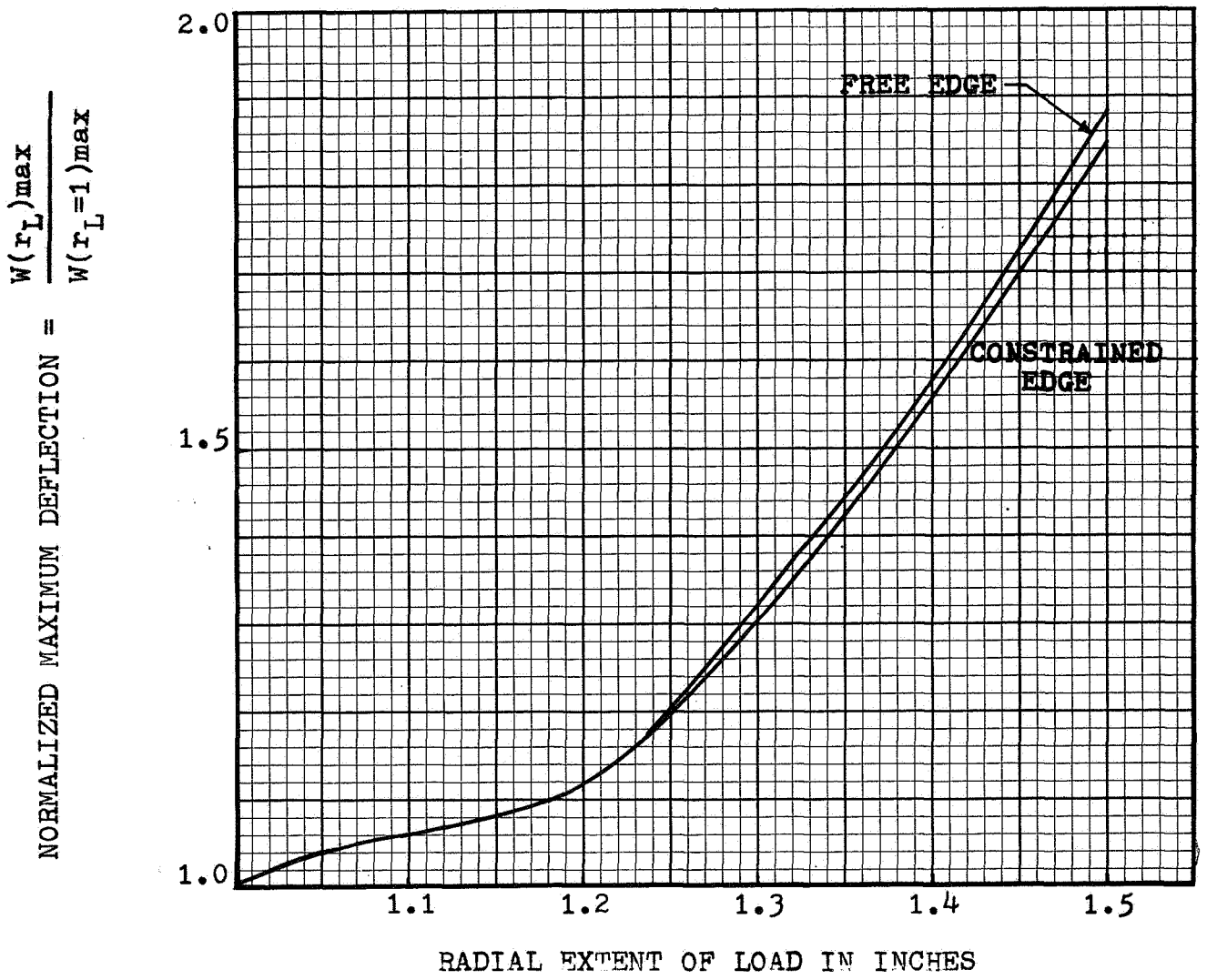

FIGURE III-23 NORMALIZED MAXIMUM DEFLECTION AS A FUNCTION OF RADIAL EXTENT OF LOAD

From Figure III-23 it can be seen that if the radial extent of the load (measured from the bolt center) is within 20 percent of that obtained assuming a uniform load, the error produced by assuming a uniform distribution is less than 18 percent. Thus, in the case of the thin fillister-head bolt, where the actual radial extent was found to be about 0.62 rather than 0.65 inches (Figure III-14) the maximum error in assuming 0.65 would be only about 5 percent if the total actual load were precisely known. Even in the case of the button-head bolt where the radial extent of the load was found to be about 0.84 inches instead of 1.03 inches the maximum error in assuming 1.03 inches instead of 0.84 inches would be only about 20 percent. Clearly, it is more important to know the actual total load transmitted to the plate than the precise distribution of normal stress under the bolthead.

CHAPTER IV

INTERFACE STRESS DISTRIBUTION AND PLATE DEFLECTION

The determination of the heat transfer across the interface between two bolted or riveted plates requires a knowledge of the area(s) of plate contact, the pressure distribution in those area(s), and the width of the gap outside the contact area(s).

To date, the effort of Lindh and his coworkers (42) at UCLA is the only known systematic attack on this problem. Their study, which was primarily an investigation of gap thickness or plate deflections, was confined to riveted specimens and consisted of both tests and theoretical analyses. The experiments involved measurements of rivet shank stresses and the gap between riveted plates with plate thicknesses ranging from 0.031 to 0.133 inches.

The theoretical work, done by Lieb (42), has already been discussed at some length in Chapter II. He briefly discussed the interface stress distribution in the contact zone around a bolt, but only to the extent necessary to demonstrate how he had applied Sneddon's (61) results in the analysis.

Sneddon (61) and Fernlund (60) were primarily concerned with the interface stress distribution. The discussion in Chapter II was limited to Fernlund's efforts because they were an extension of the analyses by Sneddon. Also mentioned in Chapter II were results obtained by Coker and Filon (62) and Aron and Colombo (63) for the radial extent of the interface stress distribution.

From the previous discussion it is apparent that an analytic method to describe plate deflection is needed which accounts for the bolt hole

in the plate and the non-uniform stress distributions, both under the bolthead and between the plates. Such a method has been developed in this study for thin plates. It would have greater value if it could be extended to thick plates in which shear stresses have important effects. However, to analyze plate deflections, good definitions of the bolthead and interface stress distributions are needed. In this chapter, a theoretical analysis developed for the plate deflection and an experimental study of both the interface stress distribution and plate deflection are presented.

A. Analysis of Plate Deflection

In most structural joints, rectangular symmetry exists in the general features of the joint. However, in the area immediately adjacent to the individual fasteners, circular symmetry exists; the stress distributions under the fastener head and between the plates approach perfect circular symmetry around the shank. As a result, an exact analysis of the deflection of bolted rectangular plates requires rectangular plate equations with appropriate boundary conditions and circularly symmetrical loading. This formidable problem would probably require a finite-difference approach for a solution. Instead of such a solution, a joint with circular symmetry was assumed, because over most of a real rectangular joint this condition of symmetry is approached.

First, a comparison was made between the deflection of simply-supported circular and rectangular plates subject to a concentrated load at the center. This was accomplished with equations given by Timoshenko and Woinowsky-Krieger (66). The maximum deflection of a circular

aluminum plate was 7 percent more than that of a square aluminum plate. For square steel plates, the difference was 11 percent.

Because real joints are usually rectangular, instead of square, there is some error, but if the rectangular joint is nearly square, the errors introduced by assuming circular symmetry are small in comparison to the errors caused by the uncertainties in the applied loads. The small gain in exactness that would be obtained does not justify the added complexities in the solution of the rectangular plate problem at this time.

1) Theoretical Approach:

For the assumption of circular symmetry, the general partial differential equation governing the deflection in the case of axial symmetry is given by Timoshenko and Goodier (67) in polar form as

$$\left(\frac{\partial^2}{\partial r^2} + \frac{2}{r}\frac{\partial}{\partial r} + \frac{1}{r^2}\,\mathrm{ctn}\,\theta\,\frac{\partial}{\partial\theta} + \frac{1}{r^2}\frac{\partial^2}{\partial\theta^2}\right)\left(\frac{\partial^2\Phi}{\partial r^2} + \frac{2}{r}\frac{\partial\Phi}{\partial r} + \frac{1}{r^2}\,\mathrm{ctn}\,\theta\,\frac{\partial\Phi}{\partial\theta} + \frac{1}{r^2}\frac{\partial^2\Phi}{\partial\theta^2}\right) = 0 \qquad \text{(IV-1)}$$

where θ is the angle measured from the z axis to the radial position and Φ is the stress function. The determination of Φ is simplified by noting that solutions to equation IV-1 are also solutions to

$$\frac{\partial^2\Phi}{\partial r^2} + \frac{2}{r}\frac{\partial\Phi}{\partial r} + \frac{1}{r^2}\,\mathrm{ctn}\,\theta\,\frac{\partial\Phi}{\partial\theta} + \frac{1}{r^2}\frac{\partial^2\Phi}{\partial\theta^2} = 0\ . \qquad \text{(IV-2)}$$

Timoshenko and Goodier also illustrate how expressions for Φ can be obtained for certain simple problems involving small deflections by superposition. In general, expressions for Φ are obtained as polynomials of order 0 to n and solutions are obtained by judicious combinations of these expressions. The same authors give expressions for Φ only to a

fifth-order polynomial, but they state that bending of circular plates by nonuniformly-distributed loads can be investigated by taking polynomials of seventh order and higher. In addition, they state that the solutions to equation IV-2 for circular plates with holes at the center must be of a different form than the polynomial expressions given by them.

Following the general method given in reference 67, polynomial expressions were developed for Φ from order -1 to -10. For the case of a plate with a hole in the center, polynomial expressions containing positive exponents did not satisfy the differential equation. Numerous attempts were made to combine the negative order polynomials to obtain a stress function which would satisfy the boundary conditions, but none was found.

Since an exact solution for the deflection of a circular plate with a non-uniform load, symmetrically distributed about a center hole, could not be found, an alternate approach was taken. Chapter III of reference 66 contains the equations which describe the small deflection of thin circular plates. The question arises: What is meant by small deflections and thin plates? Wahl and Lobo (68) state that for a deflection to be considered small, it should be less than 1/2 the plate thickness, and that for a plate to be considered thin its thickness should be less than 1/3 the plate radius if its edges are free, and less than 1/6 the radius if its edges are fixed. With these criteria, most structural joints fit into the category of thin plates experiencing small deflections.

In reference 66, Timoshenko and Woinowsky-Krieger give the differential equation for the deflection of a thin circular plate, symmetrically loaded, as

$$r \frac{d}{dr}\left[\frac{1}{r}\frac{d}{dr}\left(r\frac{dw}{dr}\right)\right] = \frac{1}{D}\int_0^r \sigma(r)dr \ . \qquad \text{(IV-3)}$$

This equation cannot be applied directly to a bolted plate because the plate is not loaded continuously over its entire area. Illustration IV-1(b) shows such a case--an isolated plate that is loaded non-uniformly on both the top and bottom surfaces. The top loading extends to r_h and the bottom, to r_σ.

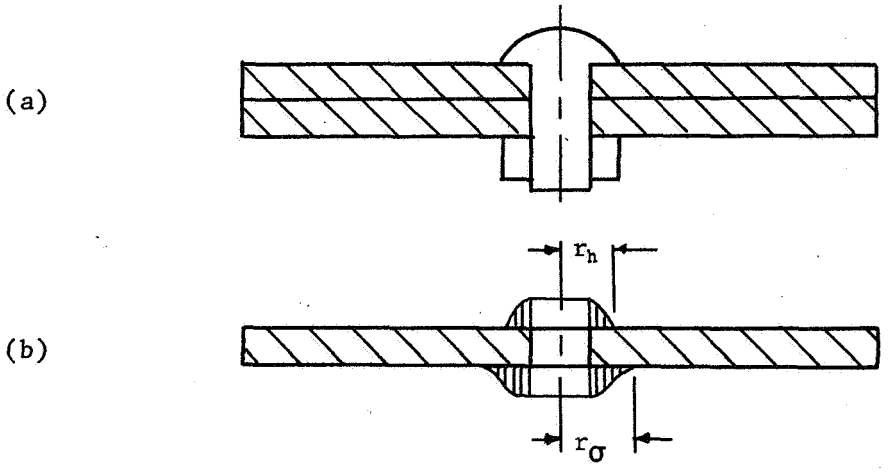

ILLUSTRATION IV-1 Loading of a Circular Bolted Plate

Equations describing the deflection of the circular plate shown in Illustration IV-1(b) were developed in this study by first applying the principles of superposition and then splitting the solution into two separate, concentric rings whose end conditions match. (Illustration IV-2.) In the development of the deflection equations, the outer radius of the inner (loaded) ring was designated r_L --to represent either r_h or

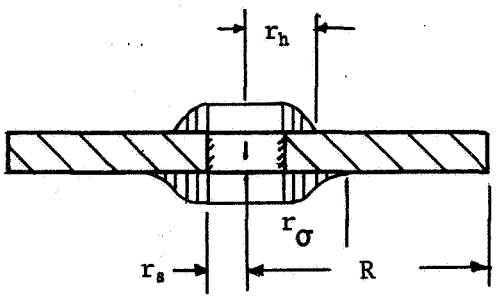

Method of Superposition Yields

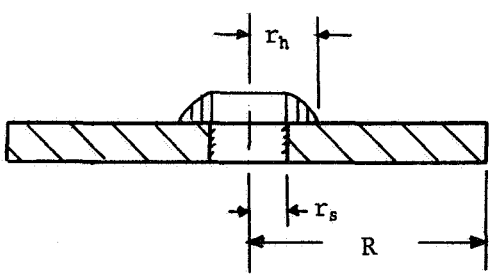

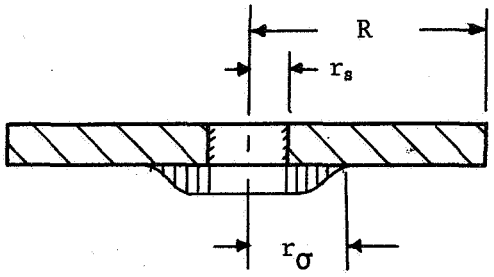

Splitting into Two Concentric Rings Gives

(1)

(2)

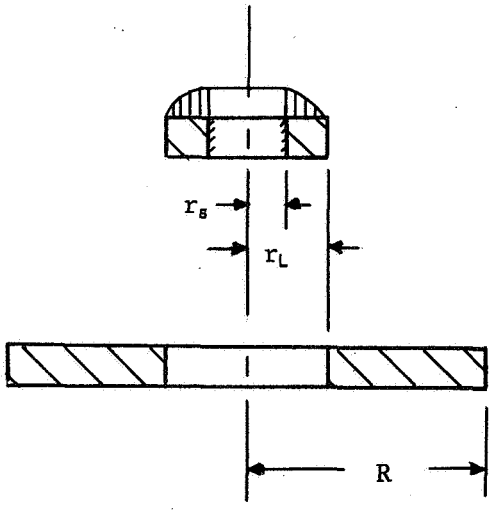

At $r=r_L$:

$$w_1 = w_2$$

$$\frac{dw_1}{dr} = \frac{dw_2}{dr}$$

$$\frac{d^2w_1}{dr^2} = \frac{d^2w_2}{dr^2}$$

ILLUSTRATION IV-2 Method of Solution of Plate Deflection

r_σ. The inner radius was designated r_s, the radius of the bolt shank. For the boundary conditions at the outer edge of the outer ring, two different cases were considered. In one case, the edge was considered free; in the other, the slope of the edge was set equal to zero, to represent the region between two adjacent bolts.

To keep the analysis general, the load density $\sigma(r)$ was represented as a polynomial of unspecified order:

$$\sigma(r) = \sum_{i=0}^{n} A_i r^i \quad . \tag{IV-4}$$

To solve equation IV-3 for the two rings, the following boundary conditions were applied:

$$(1)\ w_1 = 0 \text{ at } r = r_s$$

$$(2)\ \frac{dw_1}{dr} = 0 \text{ at } r = r_s$$

$$(3)\ \frac{d^2w_1}{dr^2} = \frac{d^2w_2}{dr^2} \text{ at } r = r_L$$

$$(4)\ w_2 = w_1 \text{ at } r = r_L \tag{IV-5}$$

$$(5)\ \frac{dw_2}{dr} = \frac{dw_1}{dr} \text{ at } r = r_L$$

$$(6a)\ \frac{d^2w_2}{dr^2} + \frac{\mu}{r}\frac{dw_2}{dr} = 0 \text{ at } r = R \text{ (Plate with free ends)}$$

$$(6b)\ \frac{dw_2}{dr} = 0 \text{ at } r = R \text{ (Plate with ends of zero slope)}$$

The solutions to equation IV-3 for the deflection of ring 2 (the region of interest), with the stress distribution on ring 1 given by equation IV-4 and the boundary conditions given by equations IV-5 were obtained and are given below. For the ring with a free outer edge,

$$w_2 = w_L + S_L r_L \left\{ \ln \rho + \frac{\rho^2 - (1 + 2 \ln \rho)}{2\left[\frac{(1+\mu)}{(1-\mu)} \rho_R^2 + 1\right]} \right\} \qquad \text{(IV-6)}$$

where

$$w_L = \left\{ S_5 + S_6 + \left[\frac{1 - \bar{\rho}_s (1 - 2 \ln \bar{\rho}_s)}{2(1 + \bar{\rho}_s^2)} \right] [S_1 + S_2 + \alpha S_L] \right\} r_L \qquad \text{(IV-7)}$$

and

$$S_L = \frac{S_3 + S_4 + (S_1 + S_2)\beta}{(1 - \alpha\beta)} \, . \qquad \text{(IV-8)}$$

For the ring with outer edge of zero slope (constrained edge) the solution was:

$$w_2 = w_L + S_L r_L \left[\ln \bar{\rho} - \frac{\bar{\rho}^2 - (1 + 2 \ln \bar{\rho})}{2(\bar{\rho}_R^2 - 1)} \right] \qquad \text{(IV-9)}$$

where

$$w_L = \left\{ S_5 + S_6 + \left[\frac{1 - \bar{\rho}_s^2 (1 - 2 \ln \bar{\rho}_s)}{2(1 + \bar{\rho}_s^2)} \right] [S_1 + S_2 - \gamma S_L] \right\} r_L \qquad \text{(IV-10)}$$

and

$$S_L = \frac{S_3 + S_4 + (S_1 + S_2)\beta}{1 + \gamma\beta} \, . \qquad \text{(IV-11)}$$

The parameters in equations IV-6 through IV-11 are:

$$\begin{aligned} \alpha &= \left[1 - \frac{(1+\mu)}{(1-\mu)} \bar{\rho}_R^2 \right] \left[1 + \frac{(1+\mu)}{(1-\mu)} \bar{\rho}_R^2 \right]^{-1} \\ \beta &= (1 - \bar{\rho}_s^2)/(1 + \bar{\rho}_s^2) \\ \gamma &= (\bar{\rho}_R^2 + 1)/(\bar{\rho}_R^2 - 1) \end{aligned} \qquad \text{(IV-12)}$$

$$\bar{\rho} = \frac{r}{r_L}, \quad \bar{\rho}_R = \frac{R}{r_L}, \quad \text{and} \quad \bar{\rho}_s = \frac{r_s}{r_L} \, .$$

The S's in equations IV-7, IV-8, IV-10, and IV-11 are:

$$S_1 = \frac{1}{D} \sum_{i=0}^{n} \frac{A_i (i + 3)}{(i + 2)^2 (i + 4)} r_L^{(i+3)} [1 + \bar{\rho}_s^{(i+4)}]$$

$$S_2 = \frac{1}{D}\sum_{i=0}^{n} \frac{A_i}{4(i+2)} r_L^{(i+3)} [\bar{\rho}_s^2(1 - 2 \ln r_s) - (1 + 2 \ln r_L)]$$

$$S_3 = -\frac{1}{D}\sum_{i=0}^{n} \frac{A_i}{(i+2)^2(i+4)} r_L^{(i+3)} [1 - \bar{\rho}_s^{(i+4)}]$$

$$S_4 = \frac{1}{D}\sum_{i=0}^{n} \frac{A_i}{4(i+2)} r_L^{(i+3)} [\bar{\rho}_s^2(1 - 2 \ln r_s) - (1 - 2 \ln r_L)]$$

$$S_5 = -\frac{1}{D}\sum_{i=0}^{n} \frac{A_i}{(i+2)^2(i+4)^2} r_L^{(i+3)} \{1 - \bar{\rho}_s^{(i+4)} [1 - (i + 4) \ln \bar{\rho}_s]\}$$

$$S_6 = -\frac{1}{D}\sum_{i=0}^{n} \frac{A_i}{4(i+2)} r_L^{(i+3)} \{(1 - \ln r_L) + \bar{\rho}_s^2[(1 - 2 \ln r_s) \ln \bar{\rho}_s - (1 - \ln r_s)]\} . \qquad \text{(IV-13)}$$

The flexural rigidity of the plate, D, is given by

$$D = \frac{Eb^3}{12(1 - \mu^2)} . \qquad \text{(IV-14)}$$

2) Applications and Comparisons:

Equations IV-6 through IV-14 were programmed for digital solution to facilitate their use. This program is given in Appendix A. Several comparisons were made between deflections predicted by this program and those given in other sources. For an initial check on the program's validity, several simple cases involving uniform loading were considered. The solutions to these, the work of Wahl and Lobo (68), are given by Timoshenko and Woinowsky-Krieger (66).

The results, listed in Table IV-1, involve plates with both free and constrained edges and four different ratios of plate-hole radii.

Table IV-1

COMPUTER PROGRAM RESULTS COMPARED WITH REFERENCE 66

Plate Radius / Hole Radius	Coefficient k_1 of Equation (76) from Reference 66			
	Free Edges		Constrained Edges	
	Reference 66	Computer Program	Reference 66	Computer Program
5	0.564	0.563	0.234	0.233
4	0.448	0.447	0.179	0.178
3	0.293	0.284	0.110	0.108
2	0.0938	0.0821	0.0329	0.0326

Table IV-1 shows excellent agreement for all radii ratios for plates with constrained outer edge and for radii ratios 5 and 4 only, for plates with free outer edge. In the free edge case, for the smaller plate-hole ratios, the results from the computer analysis do not agree too well with the published solutions; there is no explanation for this discrepancy other than the possibility that Wahl and Lobo may have applied a shear stress correction not discussed in their paper, and not applied in the present analysis. However, these differences are in cases outside our interest; our concern is for bolted plates with large values of the radii ratios. For example, a ratio of 3 would mean a joint fastened by 1/4-inch bolts at 1 1/2-inch spacing.

The deflections predicted by the computer program were also compared with those predicted by Lieb's equations (42), which have been given earlier as equations II-26 and II-27. These comparisons are shown in Figures IV-1 and IV-2, the curves of which are for the plate geometries and loadings shown in Illustrations IV-3 and IV-4. In both cases, σ_h

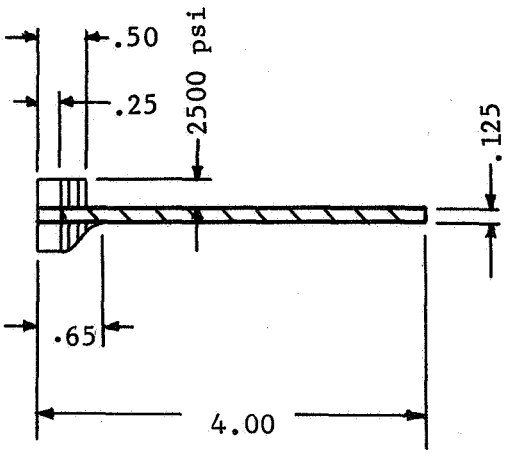

ILLUSTRATION IV-3
Plate Geometry and Loading
for Figure IV-1

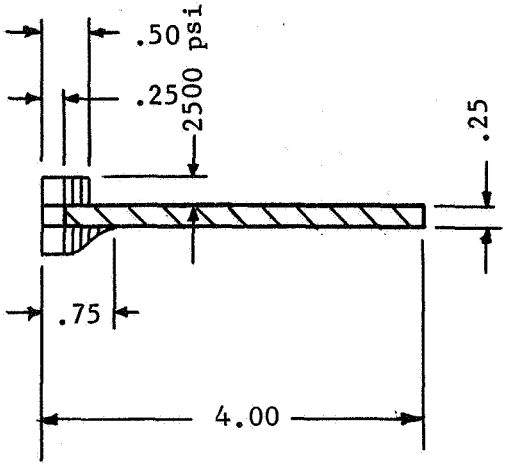

ILLUSTRATION IV-4
Plate Geometry and Loading
for Figure IV-2

was assumed to be constant with r (uniform ring load); σ_1 varies as given by Lieb (42) on page 50 of his report.

In Figure IV-1, for the case of $r_h/b = 2$, it is seen that the deflections from equations IV-6 and IV-9 are slightly smaller than those from equations II-26 and II-27. However, in Figure IV-2, one can see that IV-6 and IV-9 yield substantially larger deflections than those obtained from equations II-26 and II-27.

In his development of equations II-26 and II-27, Lieb ignored the hole in the plate. However, the large differences between deflections predicted by his equations and those of this study are primarily due more to the manner of handling the interface stress distribution σ_I. In Lieb's analysis, the curves given for σ_I on page 50 of reference 42 (which are from Sneddon) were not fitted with a polynomial expression (as in this study); they were approximated by the expression $\sigma_I = \sigma_{I_o}\left[1 - \left(\frac{r}{r_\sigma}\right)^m\right]$. The value of m is given in Figure II-6. A considerable discrepancy exists between $\sigma_I(r)$ given by this approximation and

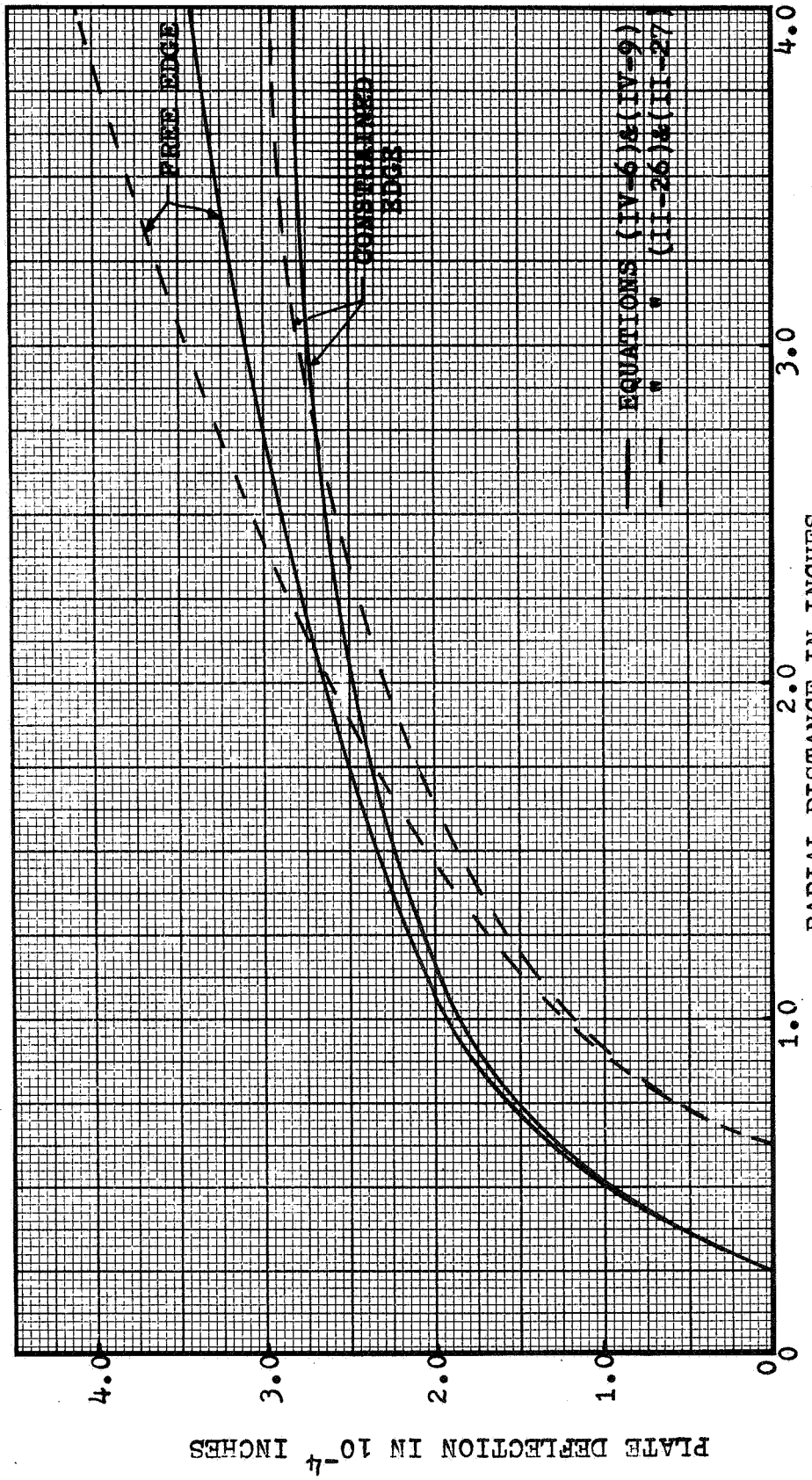

FIGURE IV-1 COMPARISON OF PLATE DEFLECTIONS PREDICTED BY LIEB'S EQUATIONS WITH THOSE GIVEN BY EQUATIONS (IV-6) & (IV-9) FOR $r_h/b = 2$

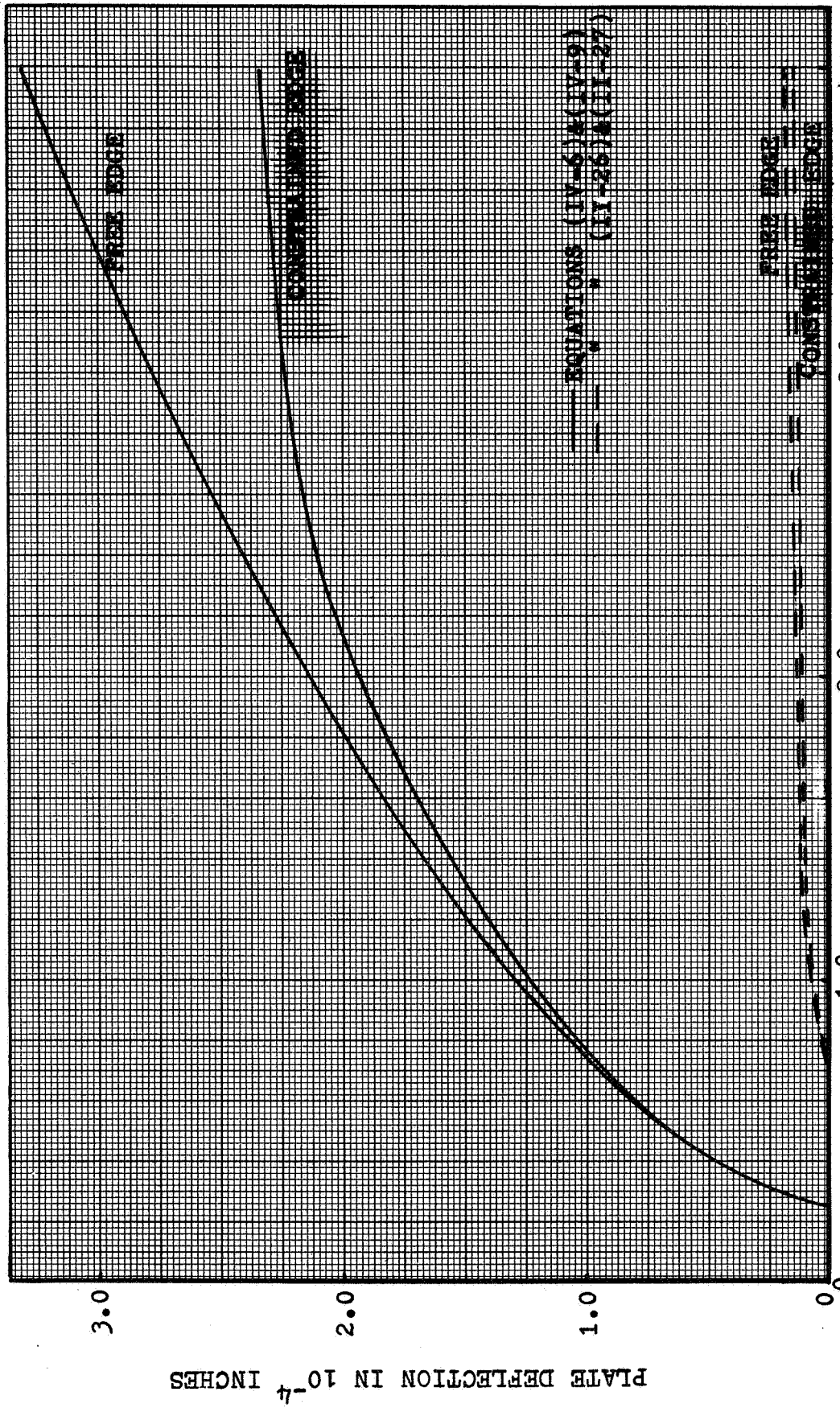

FIGURE IV-2 COMPARISON OF PLATE DEFLECTIONS PREDICTED BY LIEB'S EQUATIONS WITH THOSE GIVEN BY EQUATIONS (IV-6) & (IV-9) FOR $r_h/b = 1$

Sneddon's curves for the region near r_σ. The strong dependence of plate deflection on r_σ is discussed in the next paragraph.

3) Predicting Plate Deflections:

Comparisons between circular plate deflections predicted by equations IV-6 and IV-9 and experimental measurements were desired in addition to the comparisons previously discussed. Plate deflections and values of r_σ obtained from experimental studies will be discussed in Section B of this chapter.

To provide insight concerning the dependence of plate deflection on r_σ, a parametric investigation was made with the computer program of Appendix A. Two aluminum plates were studied; one was 8 inches in diameter and 0.072 inches thick; the other, 9.5 inches in diameter and 0.125 inches thick. Both plates had a center hole of 0.625 inches diameter. They were assumed to be uniformly loaded on the top surface (ring loading) between radii of 0.313 and 0.500 inches and non-uniformly loaded on the bottom surface between radii of 0.313 inches and r_σ. The value of r_σ, the bottom load, was varied from 0.53 to 0.700 inches. In all cases, the total bottom surface load was made equal to the top surface load. The bottom load distributions for the five values of r_σ considered are shown in Figure IV-3 along with the top load distribution, r_h. The results obtained for the two plates are shown in Figures IV-4 and IV-5.

In both figures, it is apparent that without accurate knowledge of the location of r_σ, determination of the correct plate deflection is impossible. This is even more evident in Figure IV-6, where the maximum deflection of the 8-inch $\times$ 0.125-inch plate is plotted as a function of r_σ. Further discussion of this point will be included later in relation to the adequacy of the experimental data for r_σ.

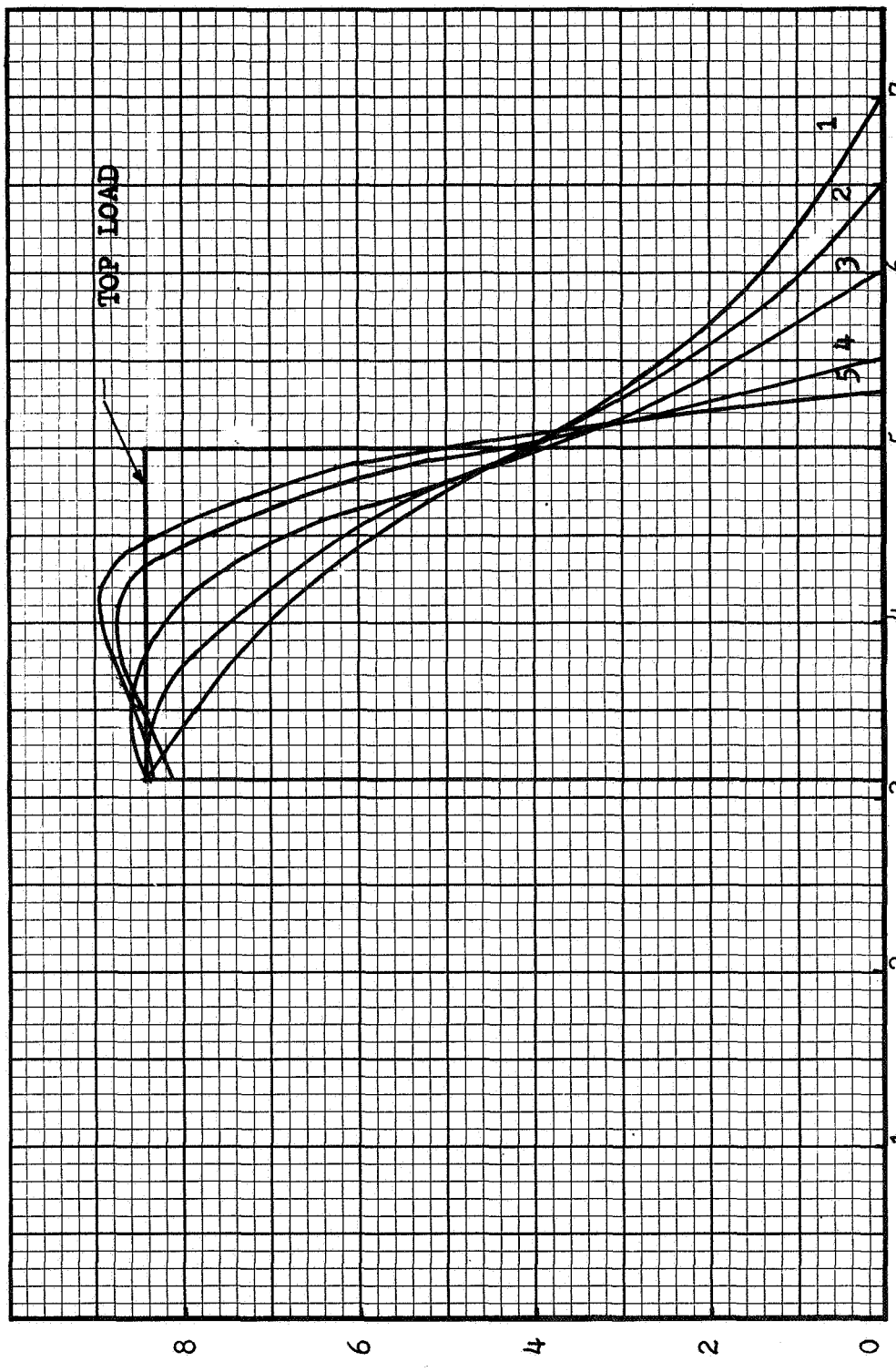

FIGURE IV-3 BOTTOM LOAD DISTRIBUTIONS FOR THE FIVE CASES OF FIGURES IV-4 AND IV-5

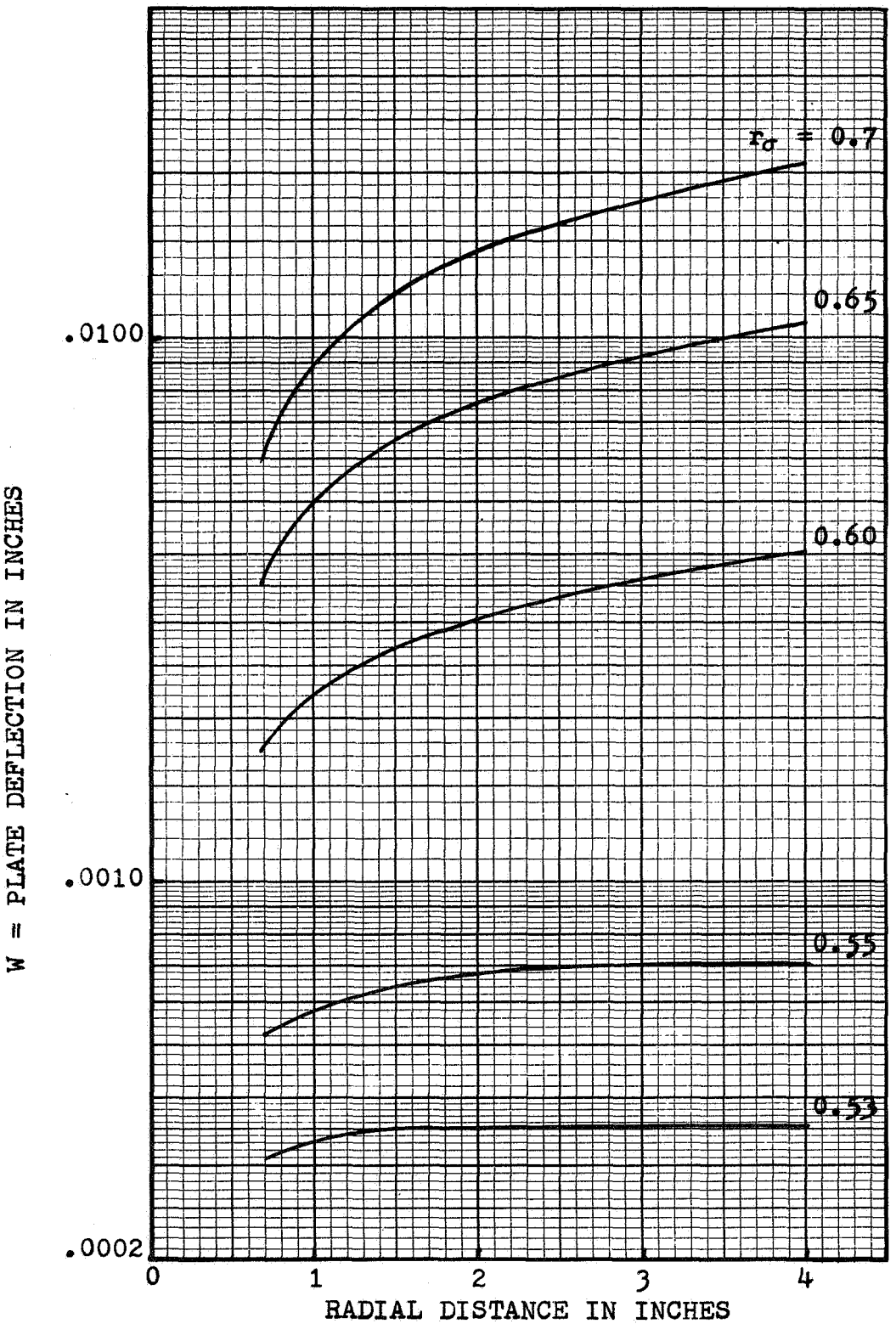

FIGURE IV-4 DEFLECTION OF 8" x .072" CIRCULAR ALUMINUM PLATE AS A FUNCTION OF BOTTOM LOAD DISTRIBUTION

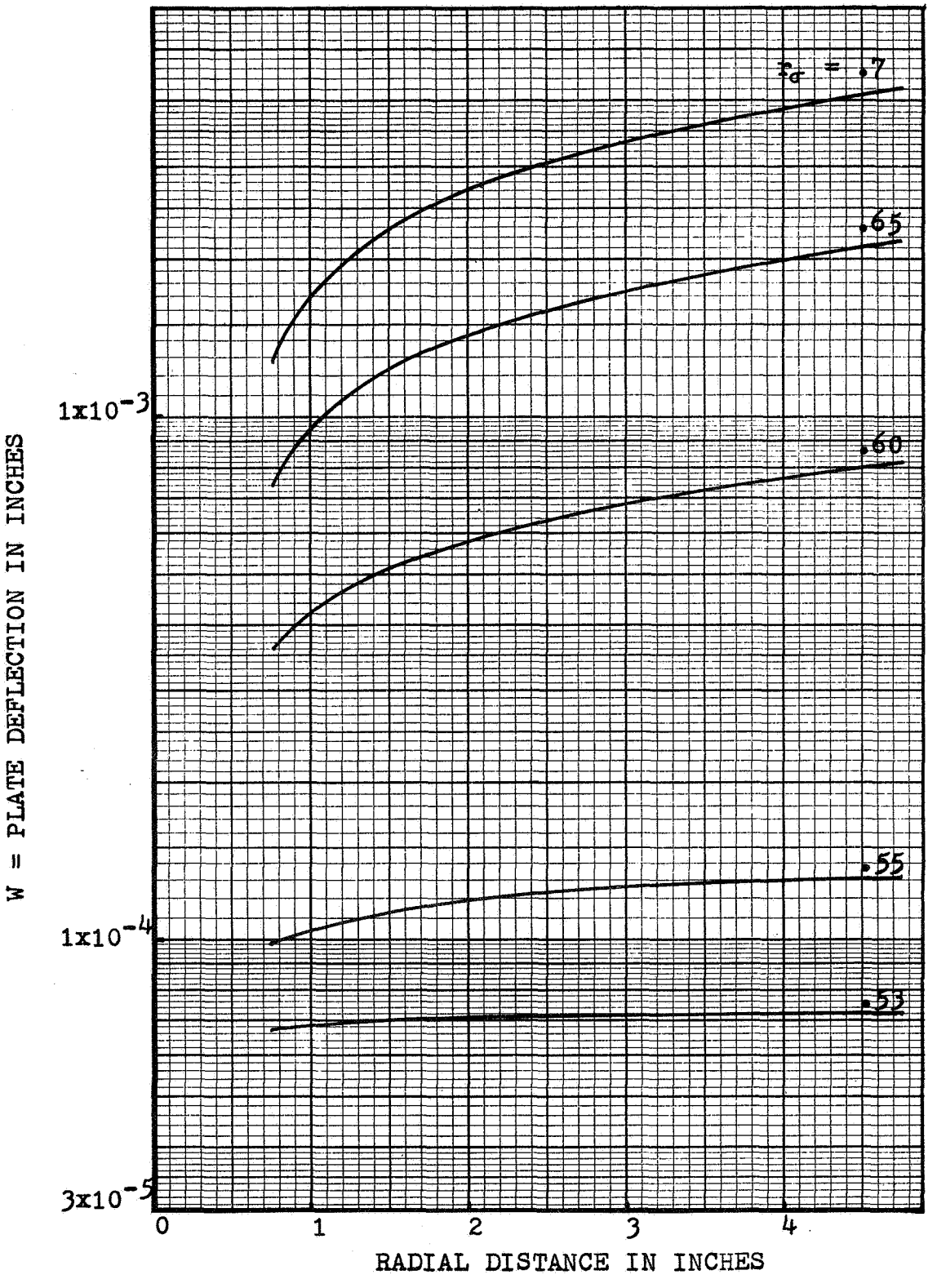

FIGURE IV-5 DEFLECTION OF 9.5" x .125" CIRCULAR ALUMINUM PLATE AS A FUNCTION OF BOTTOM LOAD DISTRIBUTION

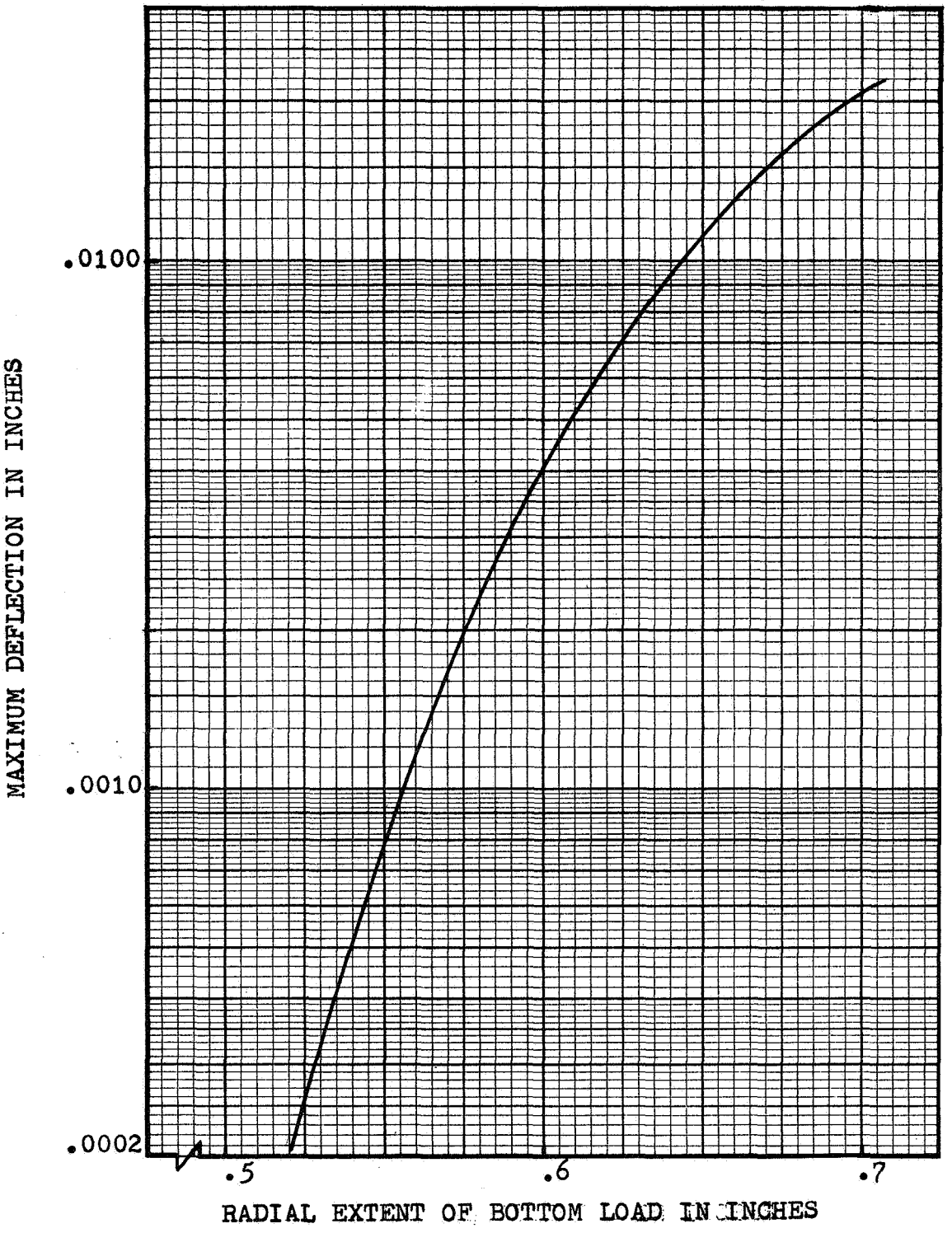

FIGURE IV-6 MAXIMUM DEFLECTION OF 8" x .072" CIRCULAR PLATE AS A FUNCTION OF RADIAL EXTENT OF BOTTOM LOAD

B. Experimental Study of Interface Stress Distributions

Very little information on the magnitude and extent of the normal stress distribution between bolted plates is available. The only reported experimental data is that from Fernlund (60) who tested only one joint. The only theoretical results are from Fernlund and Sneddon (61). In the light of the previous discussion (Section A) on the importance or r_σ, one should recall from Chapter II that the magnitude of r_σ as a function of plate thickness and bolthead radius is very poorly defined. To fill some of the gaps in the present knowledge about r_σ, and to provide a value of r_σ for correlating the plate deflection theory with experiments, a testing program was set up. This program included: (1) measurements of the radial extent of the interface stress; (2) an attempt to measure the distribution of the interface stress in several joints; and (3) direct measurement of the interface gap between bolted plates, both circular and square.

1) Oil Penetration Measurements:

The diesel oil-filter paper technique described in Chapter III (for finding the radial extent of the normal stresses under boltheads) was also used to determine the radial extent of the interface stress, r_σ, in two circular joints and one lap joint. One circular joint is shown in Figure IV-7; the lap joint, in Figure IV-8. (The grid shown on the lap joint was used for interface gap measurements that will be discussed later.)

The results from oil penetration tests in the circular joints are shown in Figures IV-9 and IV-10.

Figure IV-9 concerns two 9.5-inch × 0.158-inch circular aluminum plates that were clamped by a 5/8-inch button-head bolt and hexagonal

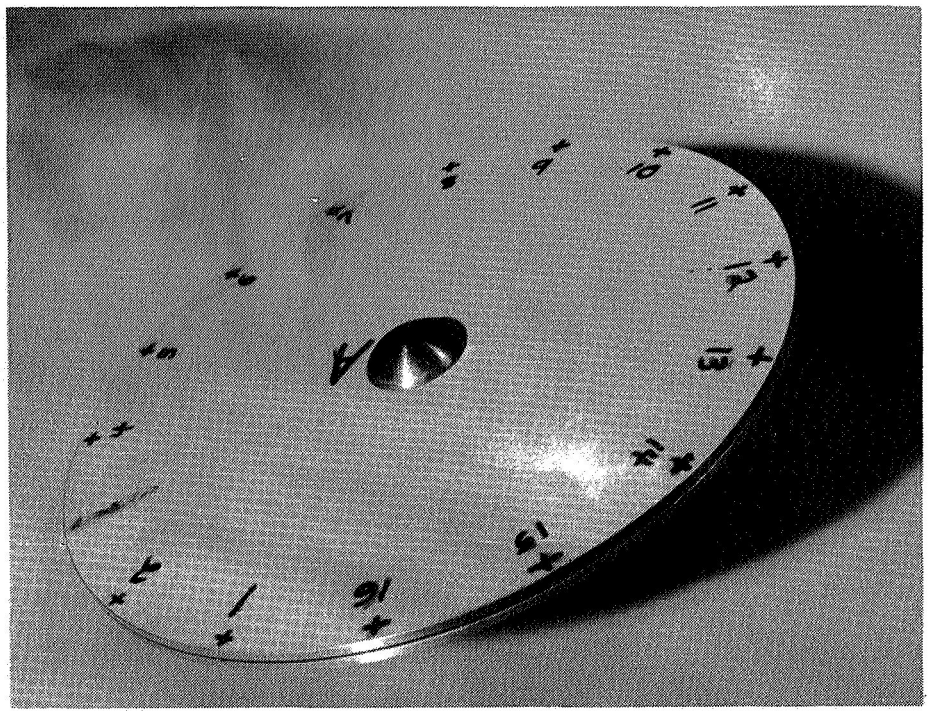

FIGURE IV-7 9.5-INCH DIAMETER ALUMINUM JOINT USED IN PLATE DEFLECTION STUDY

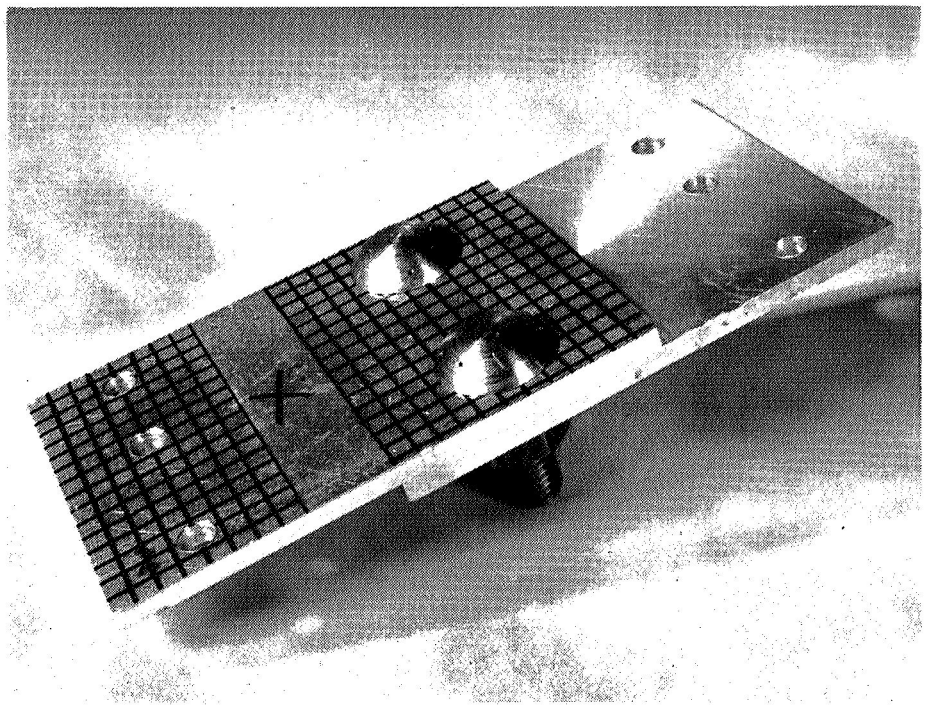

FIGURE IV-8 4"x2" ALUMINUM JOINT USED IN PLATE DEFLECTION STUDY

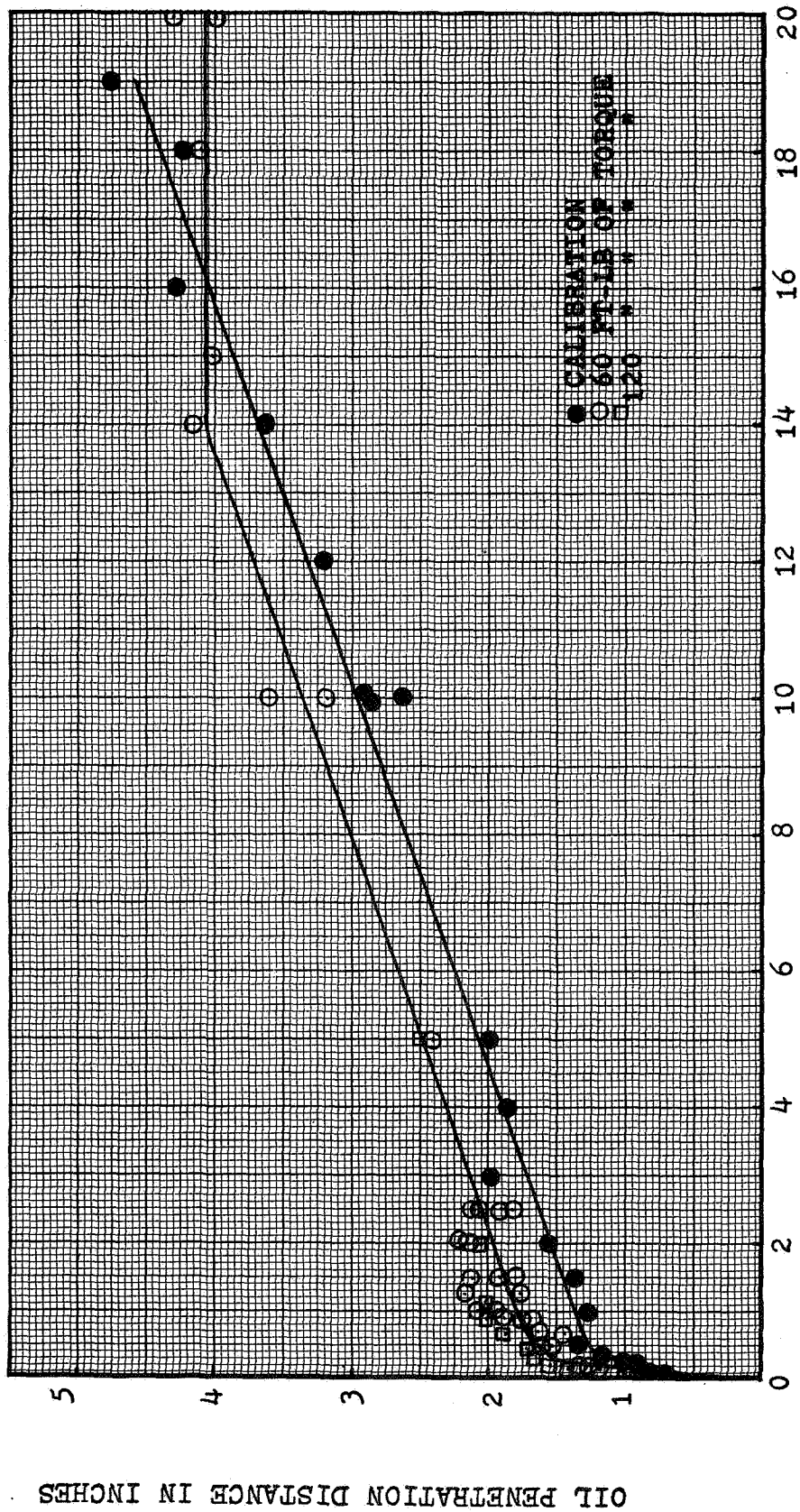

FIGURE IV-9 DIESEL OIL PENETRATION BETWEEN 9.5" x .158" ALUMINUM PLATES FASTENED BY 5/8" DIAMETER BOLT - WHATMAN #1 FILTER PAPER

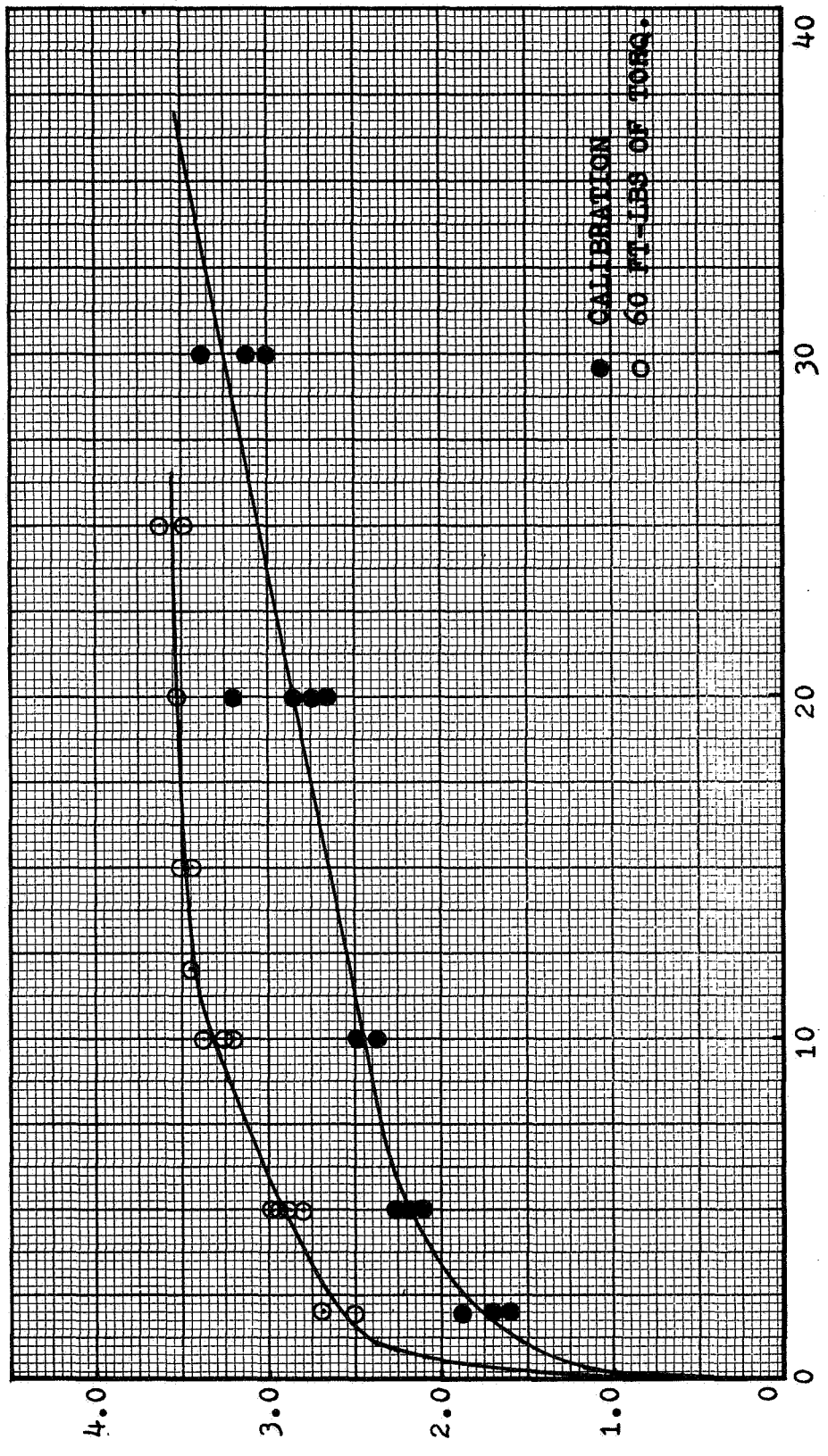

FIGURE IV - 10 DIESEL OIL PENETRATION BETWEEN 8" X .072" ALUMINUM PLATES FASTENED BY 5/8" DIAMETER BOLT - WHATMAN #30 FILTER PAPER

nut without washers. The bolt is also shown separately in Figure III-1. Although the radius of the bolthead was 0.650 inches, the earlier study of the 1-inch button-head bolt led to the approximation that the radial extent of the normal stress under the head of the 5/8-inch bolt should be about 0.53 inches. The bearing area of the hexagonal nut was also assumed to extend to a radius of 0.53 inches.

Oil penetration readings obtained at 60 and 120 foot-pounds torque exhibited no torque effect within the accuracy of the measurements. The curve drawn through the data for 60 foot-pounds has a sharp break about 4.05 inches in from the outer edge of the plate, but the calibration curve, obtained with the bolt and nut finger-tight only, does not have a similar break. From the value of 4.05 for the break point, 0.70 inches is obtained for r_σ. This distance will be compared to other data later.

Figure IV-10 shows the results for a joint consisting of two 8-inch × 0.072-inch round aluminum plates fastened by a 5/8-inch hexagonal-head bolt and hexagonal nut without washers. The circular loaded regions on both bolt and nut were 1.00 inches in diameter. Between 3.4 and 3.5 inches in from the outer edge of the joint, the curve drawn through the data for 60 foot-pounds torque exhibits a sharp break which is not evident in the calibration curve. (The calibration curve, again, represents data taken with the bolt and nut fastened finger-tight.) If 3.45 inches is taken as the break point in the curve, then r_σ is 0.55 inches. The significance of this value will be discussed later.

There is one noticeable difference between Figures IV-9 and IV-10. The abscissa in Figure IV-9 is dimensioned in minutes; that in Figure IV-10, in seconds. For Figure IV-9, an oil penetration distance of 3.5 inches was obtained in 10 minutes, but for Figure IV-10, the same

distance was reached in only 15 seconds. The longer times in Figure IV-9 were obtained with Whatman No. 1 filter paper before the supply of this paper grade was exhausted. The data in Figure IV-10 was obtained with the coarser Whatman No. 30 filter paper. In studies of this nature, both grades of filter paper have advantages although the results obtained with the No. 1 grade are considered more accurate.

The oil penetration data obtained for the lap joint (Figure IV-8) is shown in Figure IV-11. The plates were fastened with two of the 5/8-inch diameter button-head bolts and hexagonal nuts previously described. Fastening torques of 40, 75, and 120 foot-pounds were applied but any possible torque effect is obscured by the scatter in the experimental data. Whatman No. 5 filter paper was used here. The calibration was done with the bolts and nuts fastened hand-tight.

A break point between 0.50 and 0.60 inches from the joint edge was found in this instance. If a value of 0.55 is assumed, then r_σ is 0.95 inches. This value will also be discussed later.

2) Oil Pressure Measurements:

Oil-pressure measurements were made with two aluminum joints and one stainless steel joint to obtain a more definitive value of r_σ for lap joints and make quantitative measurements of the interface stress distributions. The technique was similar to that used to study bolthead stresses (Chapter III). One of the steel and one of the aluminum plates are shown in Figure IV-12. The results are presented in Figures IV-13, IV-14, and IV-15.

From Figures IV-13 and IV-14 it is apparent that the interface stress drops to zero about 1.00 to 1.05 inches from the bolt center. This compares closely with the 0.95 inches obtained during oil penetration

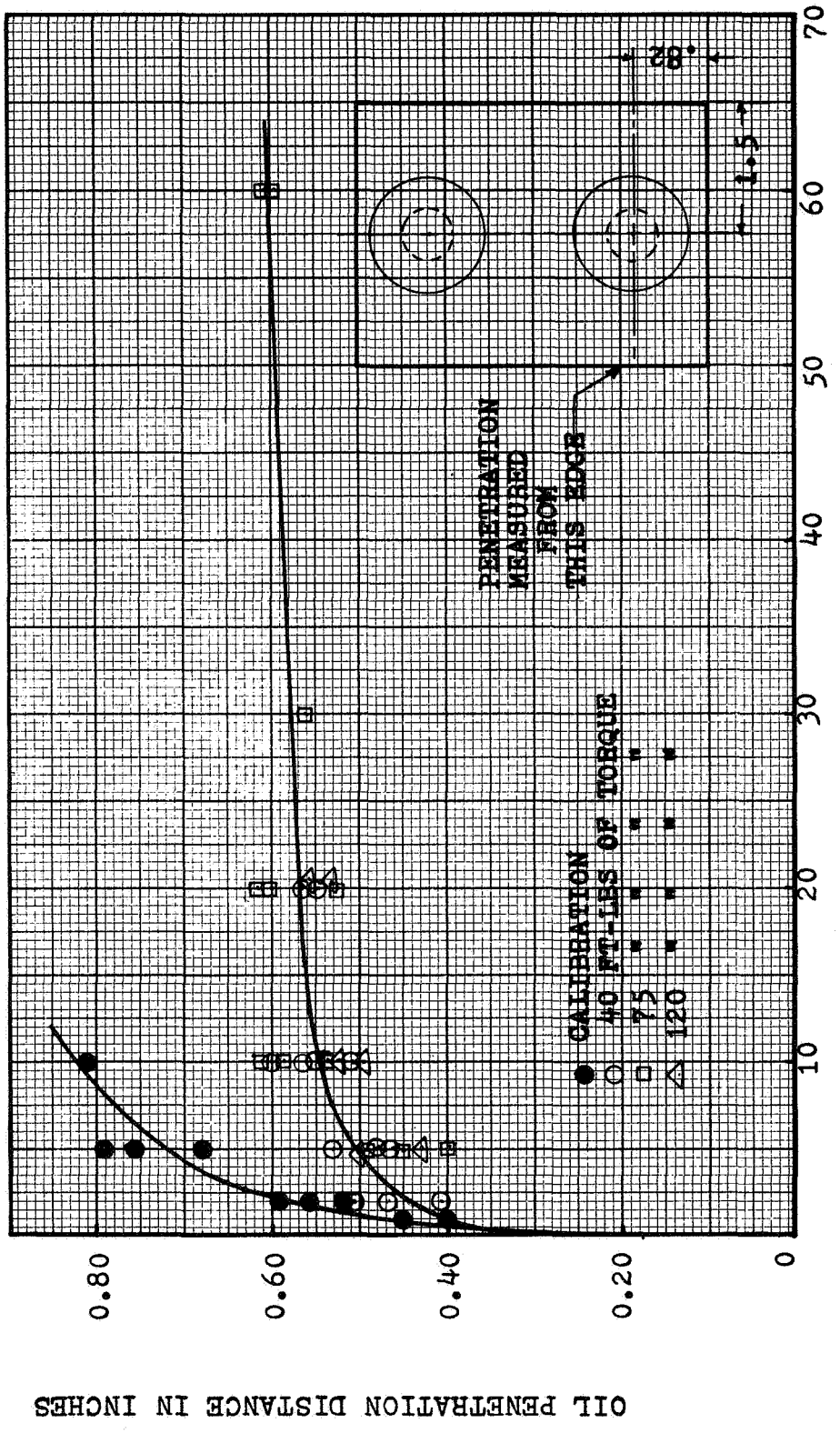

FIGURE IV-11 DIESEL OIL PENETRATION BETWEEN 1/4" ALUMINUM PLATES FASTENED BY 5/8" DIAMETER BOLTS - WHATMAN #5 FILTER PAPER

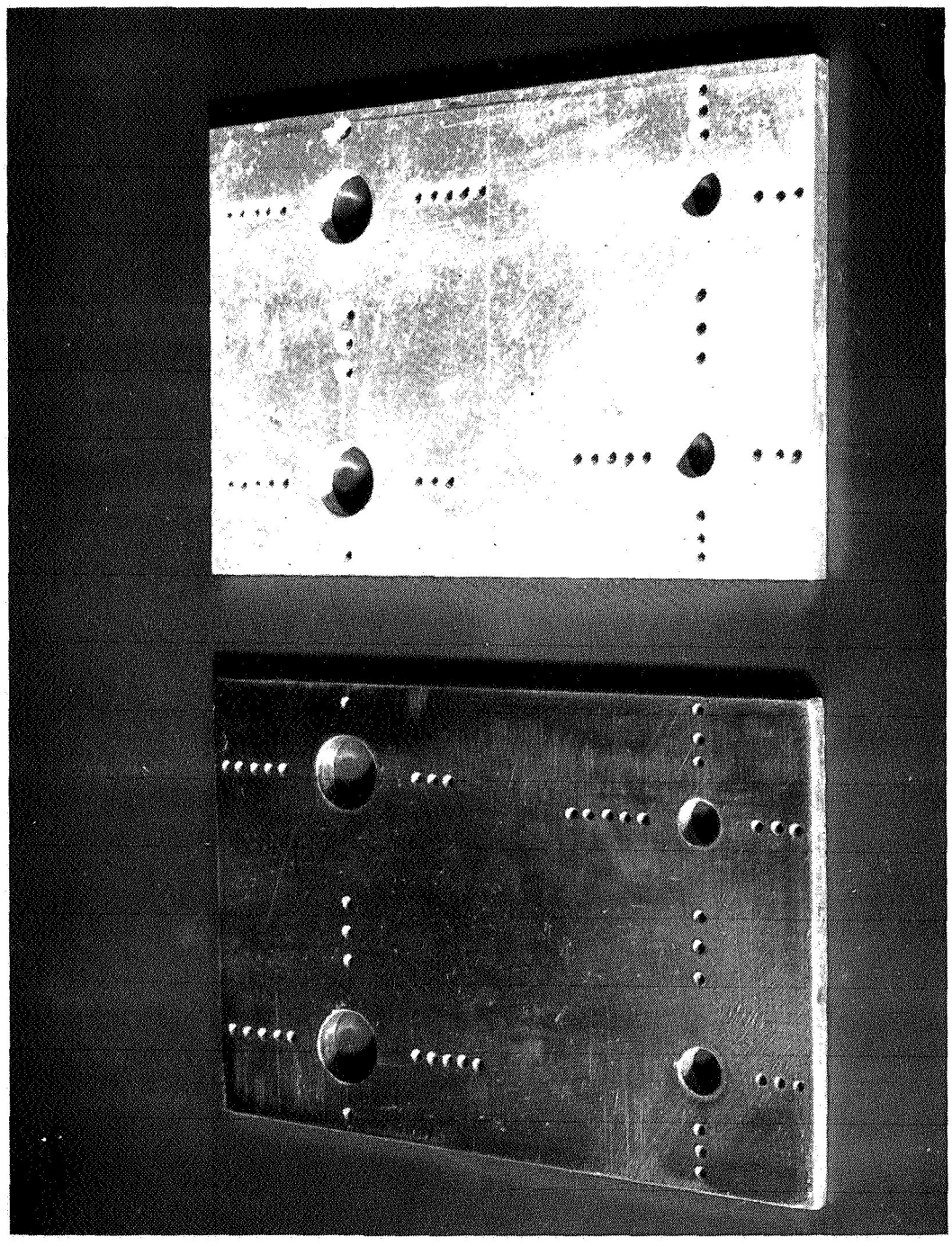

FIGURE IV-12 TOP VIEW OF 4"×8"×1/4" PLATES USED TO STUDY INTERFACE STRESSES

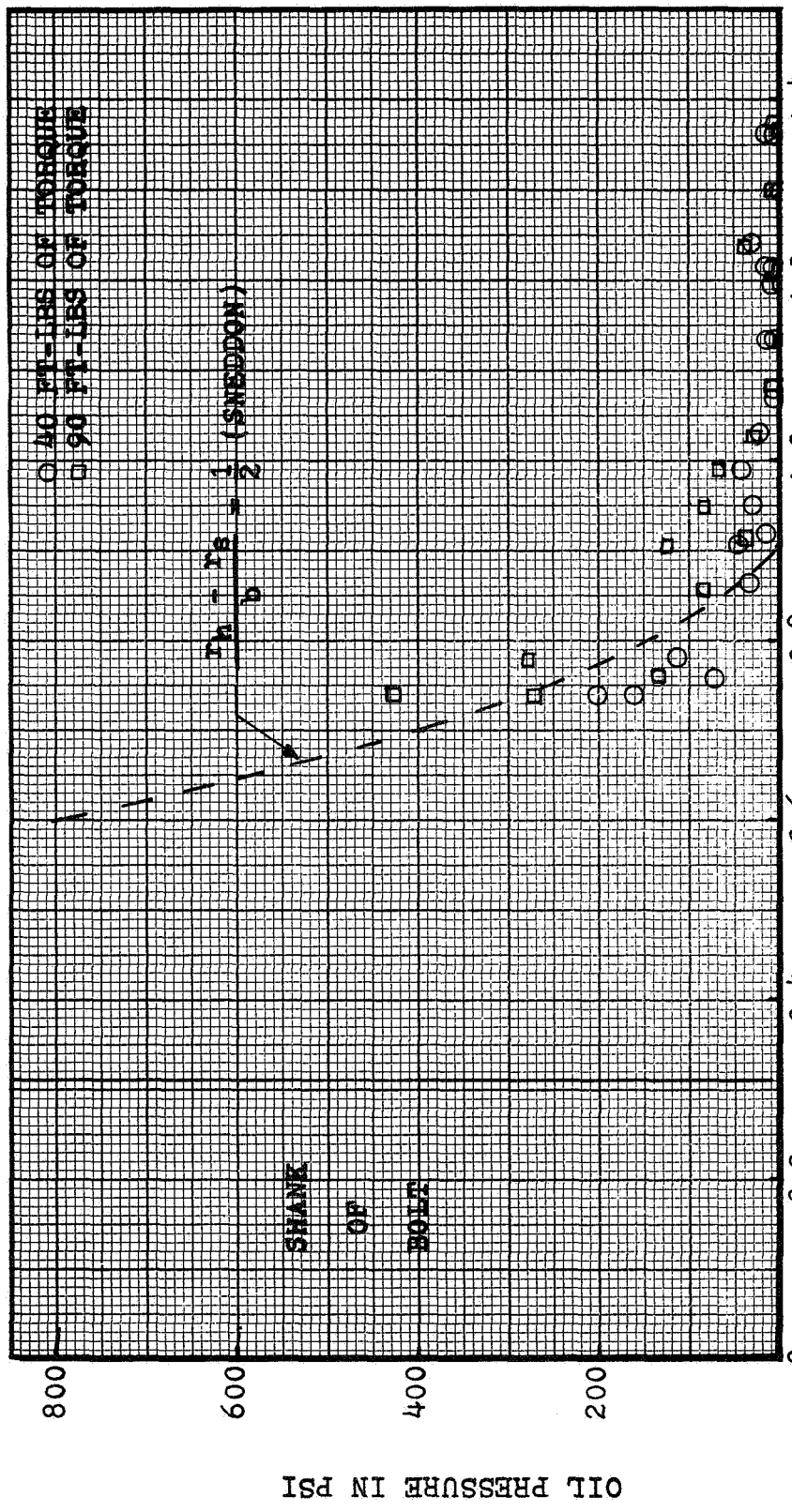

FIGURE IV-13 OIL PRESSURE MEASUREMENTS BETWEEN 1/4" STEEL PLATES FASTENED BY 5/8" DIAMETER BOLTS

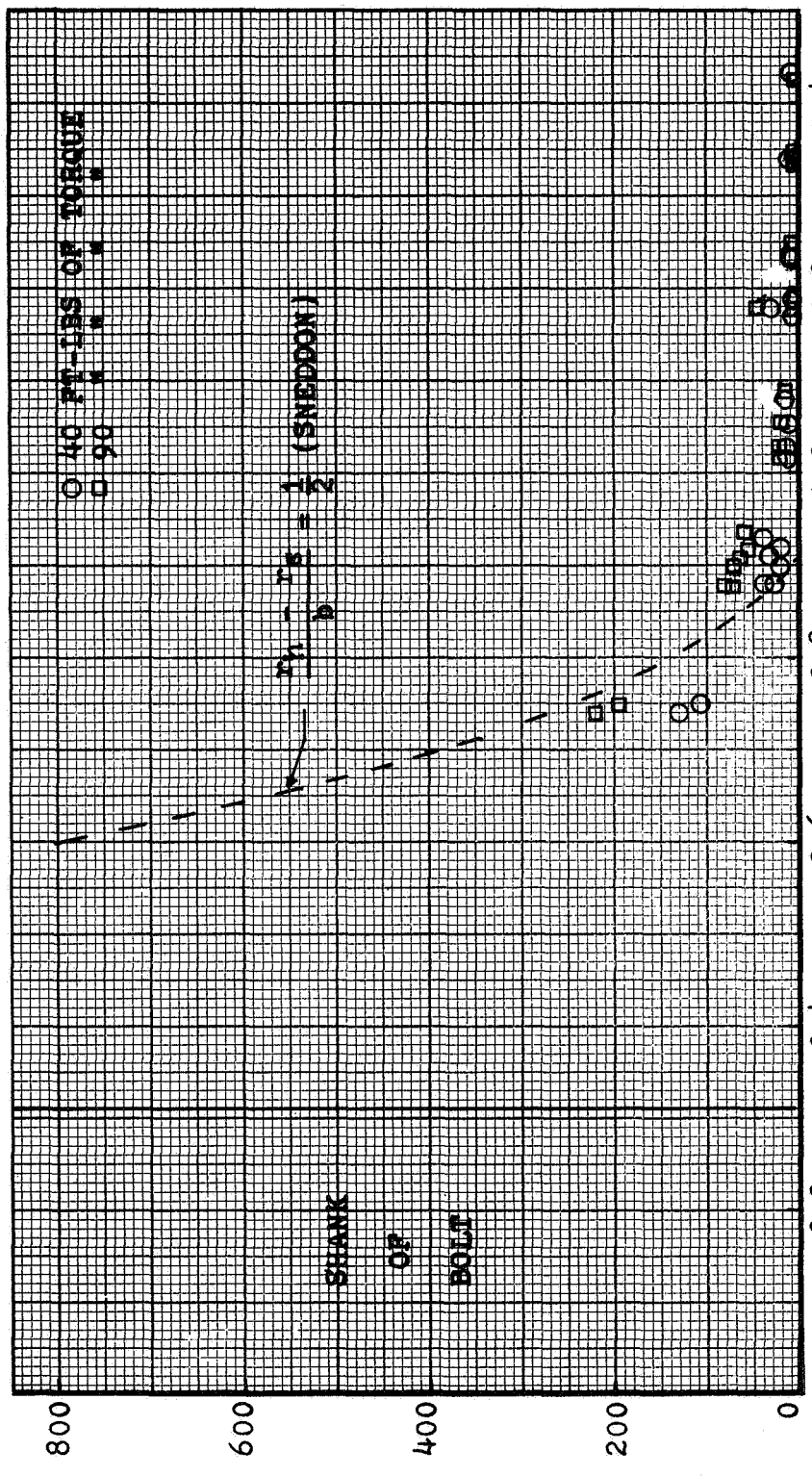

FIGURE IV-14 OIL PRESSURE MEASUREMENTS BETWEEN 1/4" ALUMINUM PLATES FASTENED BY 5/8" DIAMETER BOLTS

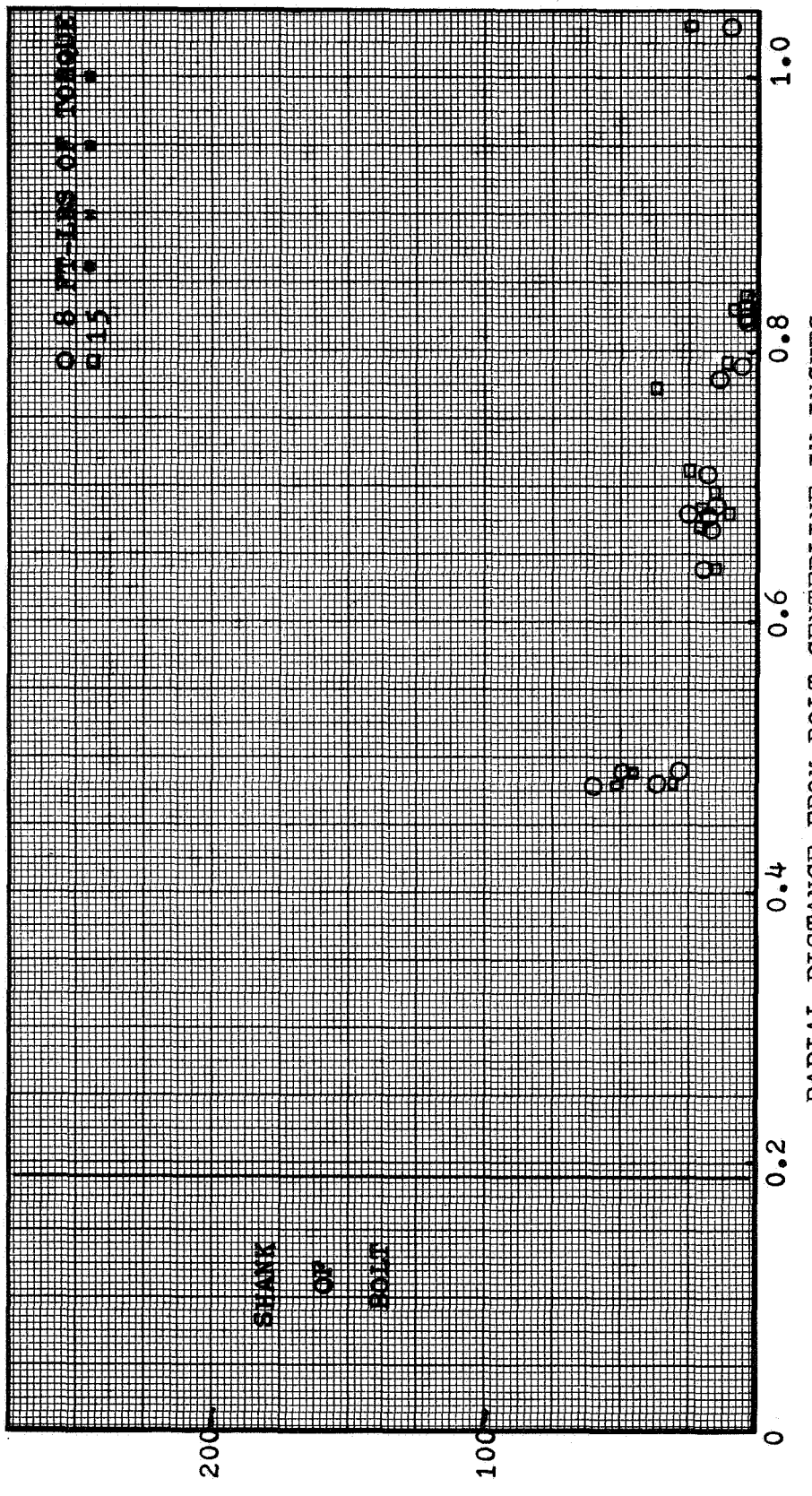

FIGURE IV-15 OIL PRESSURE MEASUREMENTS BETWEEN 1/4" ALUMINUM PLATES FASTENED BY 3/8" DIAMETER BOLTS

measurements. Apparently, the measurements were made only in the region where the interface stress drops off. The pressure could not be measured any closer to the bolthead due to interference of the bolthead with the pressure fitting.

The dashed line in both figures is the stress distribution calculated from Sneddon's approximation for the case in which $(r_h - r_s)/b = 1/2$. For that case Sneddon gave a value of 3.0 to the ratio $\left(\frac{r_\sigma - r_s}{r_h - r_s}\right)$. For the joints in question, the value of $(r_h - r_s)/b$ was 0.89. The ratio $\left(\frac{r_\sigma - r_s}{r_h - r_s}\right)$ fell between 3.10 and 3.32. Thus, Sneddon's curve should indicate only the general nature of the stress distribution. The experimental data, despite the considerable scatter, follow the general trend of the theoretical curve.

Figure IV-15 was plotted from measurements on the 1/4-inch aluminum plates joined by two 3/8-inch button-head bolts with hexagonal nuts. Here, because of the data obtained for the 1-inch button-head bolt, the radial extent of the loads under the boltheads was taken to be 0.32 inches (0.07 inches inside the bolthead perimeter). With this as the value of r_h and $r_\sigma = 0.8$ (from the pressure data), the ratio $(r_h - r_s)/b$ is 0.528 and the ratio $\left(\frac{r_\sigma - r_s}{r_h - r_s}\right)$ is 3.88. Again, this ratio is higher than that predicted by Sneddon's approximation.

At this point a summary of the newly obtained r_σ values, compared with values predicted by the theories of Sneddon and Fernlund and measured by others would be very helpful. Table IV-2 and Figure IV-16 provide such a summary and a comparison.

A χ^2 test was performed using the new r_σ data to determine how well the curve based on Sneddon's theory fits this data. It was found that the fit was good with a probability of 90 percent ($\chi^2_{0.10}$). However,

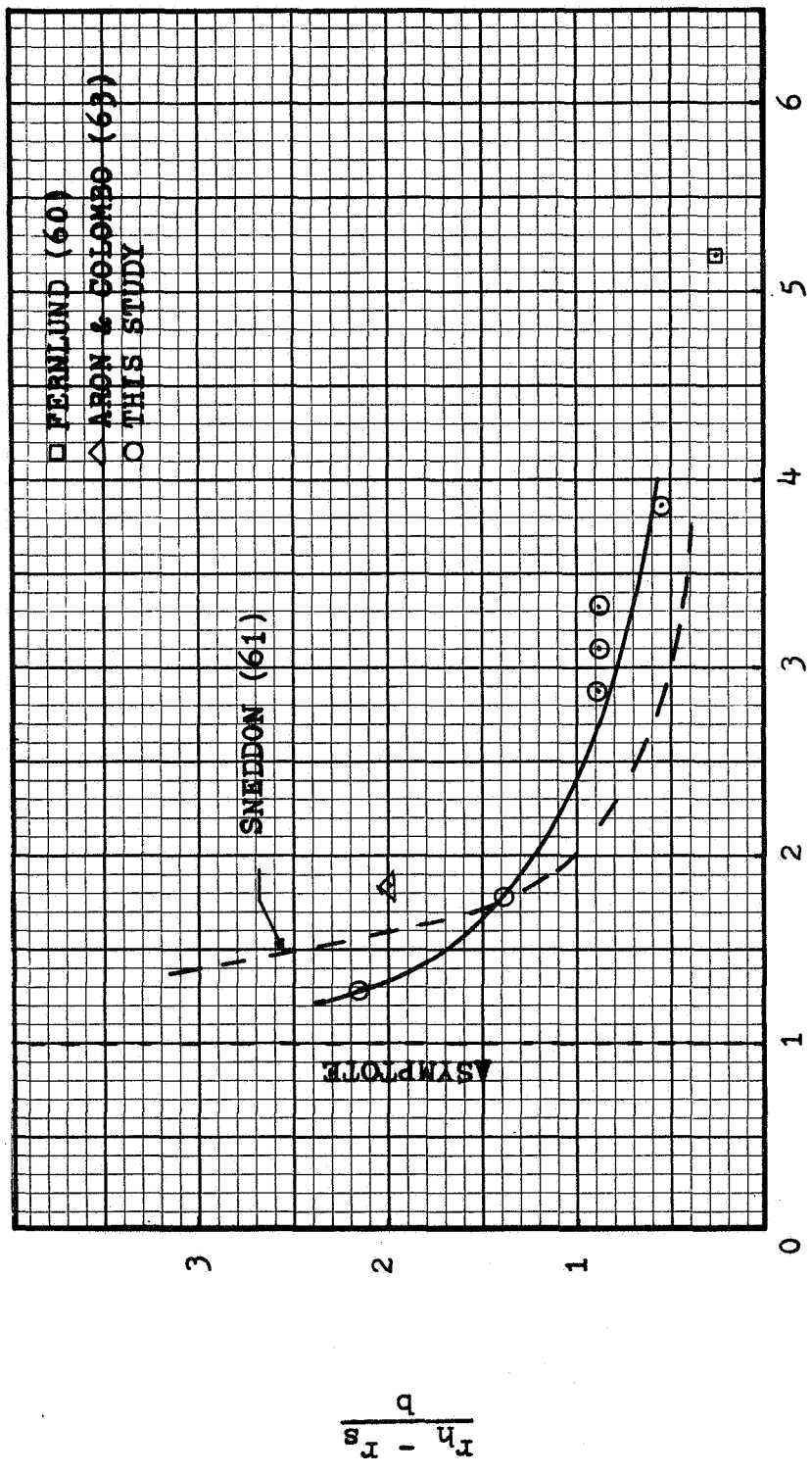

FIGURE IV-16 COMPARISON OF MEASURED VALUES OF r_σ WITH RESULTS OF PREVIOUS STUDIES

Table IV-2

VALUES OF r_σ AS DETERMINED BY VARIOUS INVESTIGATORS

$\frac{r_h - r_s}{b}$	$\frac{r_\sigma - r_s}{r_h - r_s}$	Type of Data	Source
0.5	3.0	Theoretical	Sneddon (61)
1.	2.0	Theoretical	Sneddon (61)
2.	1.6	Theoretical	Sneddon (61)
3.	1.4	Theoretical	Sneddon (61)
∞	1.0	Theoretical	Sneddon (61)
0.25	5.6	Theor. & Oil Press.	Fernlund (60)
2.00	1.83	Photoelastic	Aron & Colombo (63)
0.53	3.88	Oil Pressure	This Study
0.89	3.32	Oil Pressure	This Study
0.89	3.10	Oil Pressure	This Study
0.89	2.88	Oil Penetration	This Study
1.38	1.78	Oil Penetration	This Study
2.62	1.27	Oil Penetration	This Study

better agreement is needed between theory and experiment. Because predictions of the plate deflection are extremely sensitive to the values of r_σ, more experimental information is needed as well as further theoretical investigation.

C. Plate Deflection Measurements

As previously mentioned, direct measurements to check the plate deflection analysis were planned. Numerous attempts were made to measure joint gap thicknesses before a successful method was found.

The UCLA report (42) describes several techniques that had been used to measure the gap between riveted plates. In one method, the individual plate thicknesses, before riveting, and the thickness of the riveted joint, after riveting, were measured with a micrometer. Another method

required thickness measurements of a gelatin film formed in the interface after the joint had been assembled in a hot gelatin bath, removed from the bath, and allowed to cool. After the joint was disassembled, the gelatin film was removed and measured. In the report by Lindh et al. (42), it is stated that the gelatin film method was not very useful, but that direct measurement with a micrometer was successful.

Because direct micrometer measurement seemed easier, the UCLA method was tried first, but without the measurement of the individual plate thicknesses before assembly. Instead, the total joint thickness was measured for initial readings with the joint bolted finger-tight. However, in the several joints tried, the micrometer contact pressure closed any existing gap between the plates (due to warping). Thus, an accurate base for measuring gap thickness or plate deflection was impossible and no worthwhile data could be obtained. It is not known how the UCLA experimenters overcame this problem.

The gelatin film method, tried next, also was unsuccessful. Even after remaining in a refrigerator for three days, the gelatin between the plates was still soft when the plates were separated. The gelatin film hardened on the separated plates only when they were left in the refrigerator for one day. The results from the film hardened in this manner indicated, however, that local changes in film thickness took place during the hardening process.

Plate deflections were finally obtained with a modified direct-measurement technique for an 8-inch circular joint and an 8-inch square joint. In both cases, the plates were 0.072-inch thick aluminum alloy fastened with a 5/8-inch hex-head bolt and nut. (This is the same combination that was used to obtain the oil penetration data of Figure IV-10.)

After the plates had been assembled and the bolt had been torqued to the desired tension, the joint was placed in a hot gelatin bath and allowed to come to thermal equilibrium. The joint was then removed, immediately placed in a refrigerator, and allowed to cool. After 24 hours, the joint was taken from the refrigerator. The gelatin film on the outside of the plates was quickly removed and the joint then returned to the refrigerator for about an hour to prevent softening of the solid gelatin in the interface gap near the edges.

The joint was periodically returned to the refrigerator between measurement sessions to prevent gelatin softening. The results from this method are plotted in Figure IV-17. Each point is the average of eight measurements at the perimeter of the 8-inch plates. Each gap thickness plotted here was determined by subtracting the joint thickness at 10 foot-pounds of torque from that measured at higher torques. (A 10 foot-pounds torque as a reference was found to yield more repeatable initial data then unmeasured hand-tightening.)

Also shown in Figure IV-17 for comparison are gap thicknesses determined by the computer program previously mentioned. Gap thicknesses were computed with assumed r_σ values of 0.53, 0.54, and 0.55. Obviously, a small error in the r_σ value will greatly affect any possible correlation of computed and measured gaps.

From the oil penetration data of Figure IV-10, any value for r_σ between 0.53 and 0.57 inches would be reasonable, as well as the mean, 0.55 inches, previously suggested. A value of 0.54 inches, however, is more in agreement with the experimental data of Figure IV-16. The curve in Figure IV-16 based on Sneddon's theory yields a value for r_σ of 0.600, which is obviously too high.

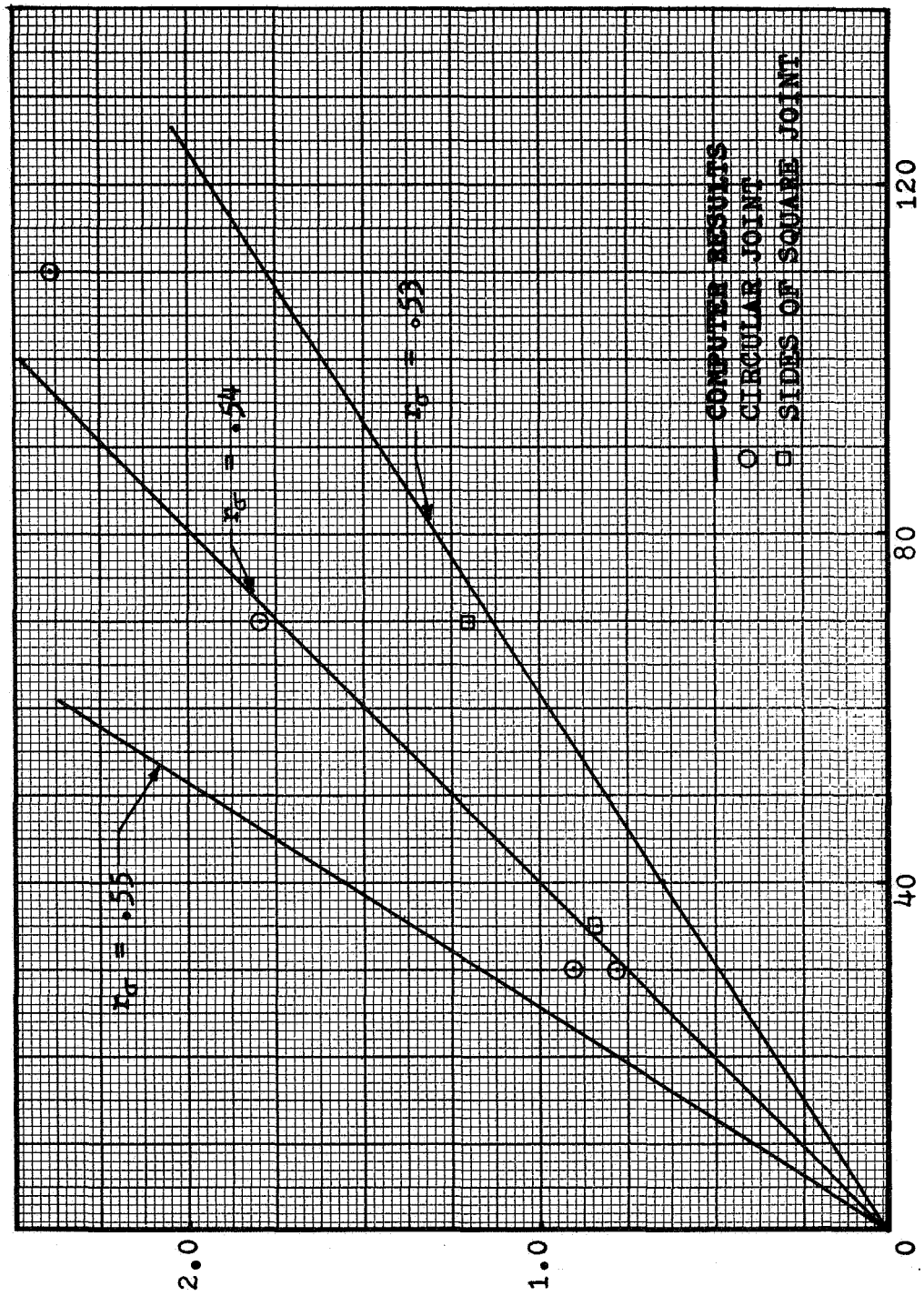

FIGURE IV-17 COMPARISON OF EXPERIMENTAL VALUES OF GAP THICKNESS FOR 8" X .072" ALUMINUM JOINT WITH THEORETICAL PREDICTIONS

It should be noted that the data for the square plate fell lower (below the circular plate data) than anticipated from the theory. However, the application of circular plate theory to a square plate evidently produces deflections with acceptable accuracy, considering that the value of r_σ is not known so accurately itself.

In the computation of the gap thicknesses shown in Figure IV-17 it was necessary to determine the interface stress distribution. The method used to do this is discussed in the next section.

D. Calculation of the Interface Stress Distribution

Earlier, it was mentioned that very little information had been found regarding the stress distribution in the joint interface. In fact, the theoretical work of Sneddon and Fernlund and the one experiment of Fernlund furnish all the data available at this writing. The attempt (described earlier in this chapter) to obtain complete experimental data for thin plates was unsuccessful because of the proximity of r_σ to the edge of the bolthead. An approximation for the interface stress distribution is therefore necessary to determine plate deflections.

Fernlund (60) has demonstrated a simplified approach for obtaining interface stresses in thick plates when both the total bolthead load and r_σ are known. The stress is described by a fourth-order polynomial whose coefficients are determined from four assumed boundary conditions and the known constraints. Assuming the slope of the stress curve to be horizontal at $r = r_s$ and at $r = r_\sigma$ and the stress function and its second derivative with respect to r to be equal to zero at $r = r_\sigma$, Fernlund showed that the resulting stress distribution closely approximated the exact solution for the case he considered.

In the numerical example to which Fernlund applied his simplified method, $b = 2r_s$, thus making $(r_\sigma - r_h)$ more than four times as large as $(r_h - r_s)$. Such is not the case for thin plates.

For the 8-inch × 0.072-inch aluminum joint just discussed, $(r_h - r_s) = 0.188$ inches and $(r_\sigma - r_h)$ varied from 0.03 to 0.05 inches. Interface stress distributions were calculated for the two cases of $(r_\sigma - r_h) = 0.03$ and 0.05 ($r_\sigma = 0.53$ and 0.55) by Fernlund's simplified method as well as by an approximate one better suited to thin plates. The results are shown in Figure IV-18.

This approximate method, developed in this study, assumes that the interface stress distribution is identical to the bolthead stress distribution between $r = r_s$ and $r = (2r_h - r_\sigma)$. Between $r = (2r_h - r_\sigma)$ and $r = r_\sigma$, the distribution is modified to satisfy static equilibrium.

To obtain a further comparison between Fernlund's simplified method and the approximate method, plate deflections were calculated using the stress distributions of Figure IV-18. The stresses obtained with Fernlund's simplified method caused plate deflections 1-4 × 10^3 larger than those produced by the stresses obtained with the approximate method. Since the deflection calculated with the stresses from the approximate method using $r_\sigma = 0.53$ and 0.55 agrees at worst with measured plate deflections within 80 percent, it is clear then Fernlund's simplified method is not adequate for thin plates.

In the next chapter Fernlund's simplified method will be applied to a case on the borderline between thick and thin plates where it was found to be adequate.

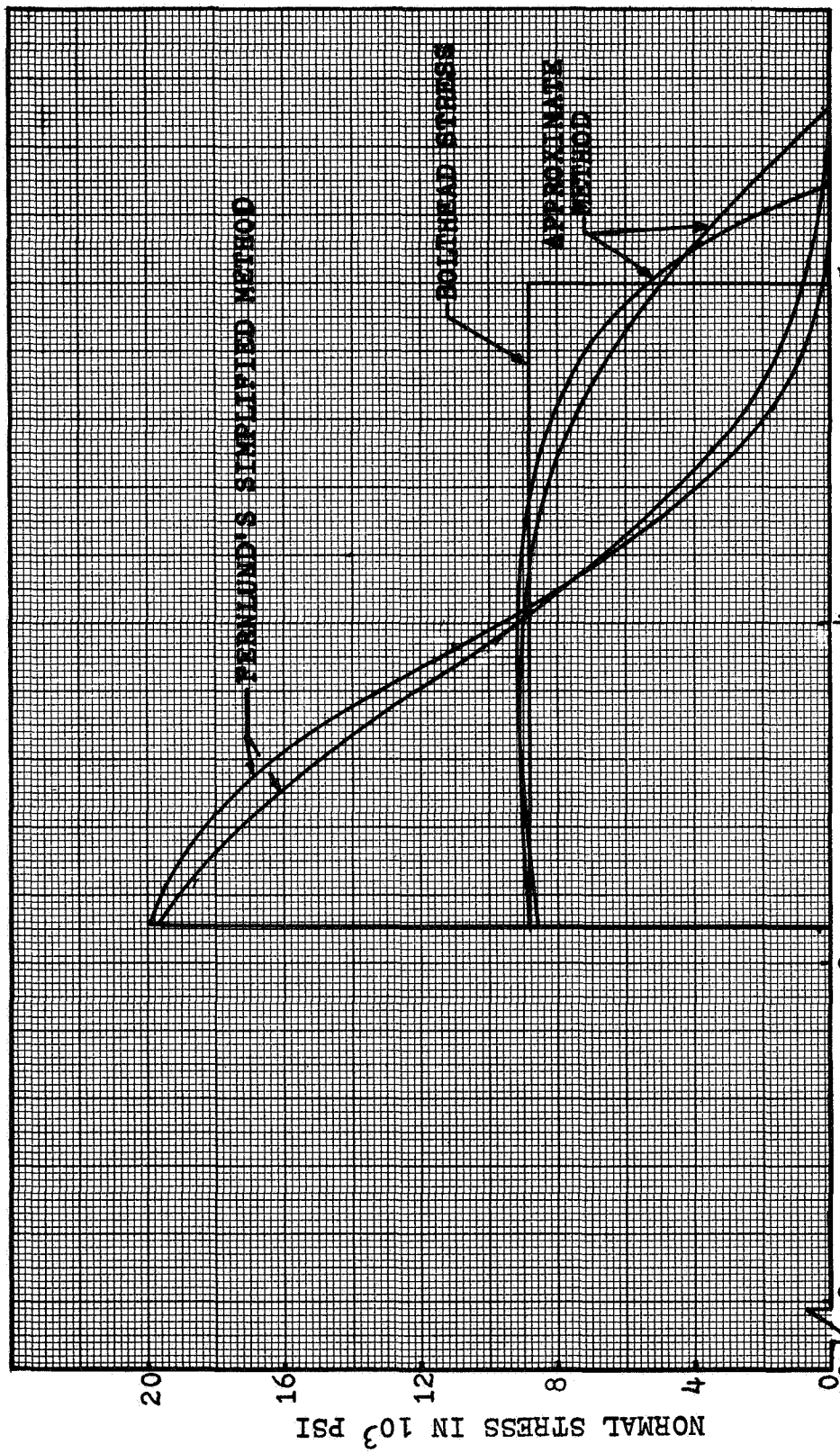

FIGURE IV-18 INTERFACE STRESSES FOR 8"x.072" ALUMINUM JOINT AS GIVEN BY APPROXIMATE METHOD AND FERNLUND'S SIMPLIFIED METHOD

CHAPTER V

JOINT INTERFACE THERMAL CONDUCTANCE

In Chapter II, attention was centered on the major difficulties in predicting the thermal conductance of a joint interface, after a brief discussion had been given on the nature of heat transfer across bolted joints. Experimental and theoretical investigations to provide additional information on the interface stress distribution and the width of the interface gap, were described in Chapters III and IV.

The results of these investigations will now be used in an analysis of the interface thermal conductance of two bolted joints. First, the entire heat transfer problem and the general approach to its solution will be reviewed and then the specific details of the solution will be outlined. An experimental investigation of the temperature distribution in two bolted joints will be described and the results reported. A finite-difference heat transfer analysis incorporating theoretically determined values of the interface conductance will then be described. Finally, the experimental and the computed values of the interface temperature gradients will be compared.

A. Mathematical Model of Joint Heat Transfer

A mathematical model of a typical, simple bolted joint was formulated in order to arrive at a technique that would adequately describe the interfacial heat transfer. The actual joint considered is sketched in Illustration V-1. Because the interfacial heat transfer is of primary interest (and not the entire joint) the bolts were eliminated to give the simplified model shown in Illustration V-2. Due to symmetry, the model can be further refined (Illustration V-3).

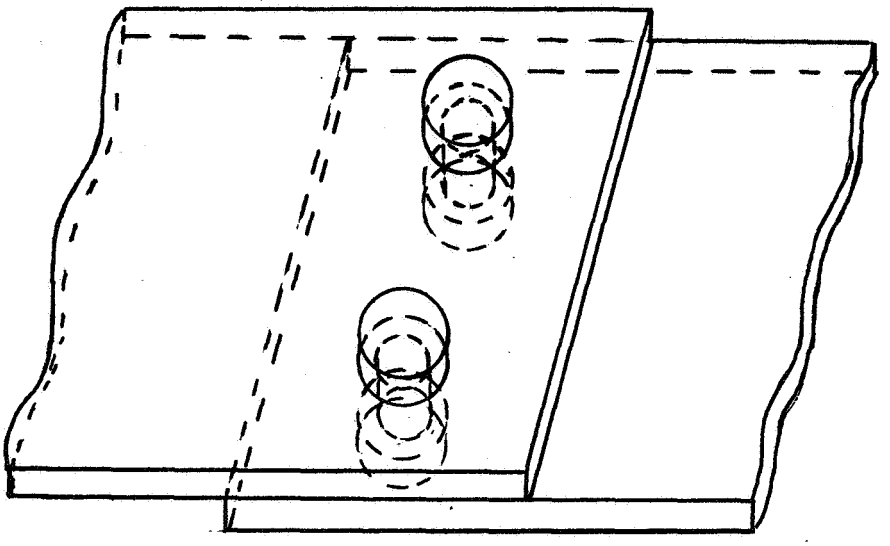

Illustration V-1 Lap Joint Under Investigation

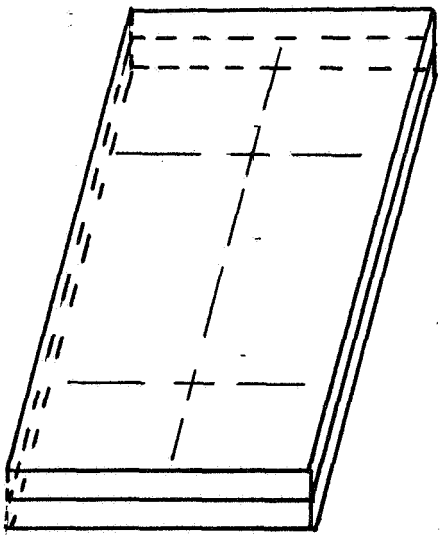

Illustration V-2
Simplified Model

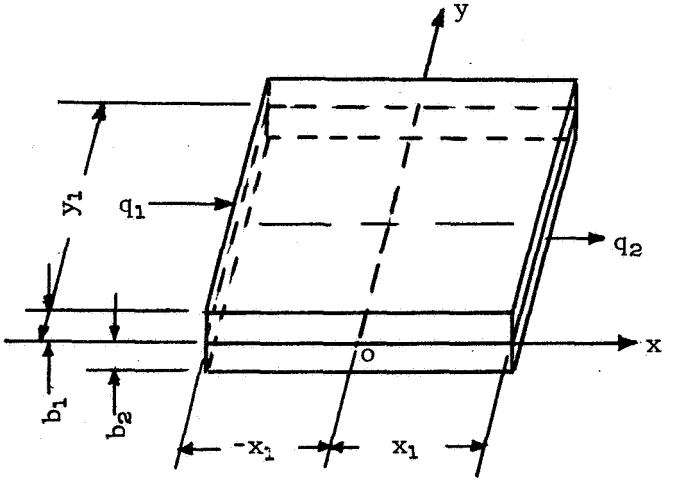

Illustration V-3
Further Simplified Model

A rectilinear coordinate system is employed in Illustration V-3. The top plate is designated "1" and the bottom, "2". The differential equations for the steady-state temperature distribution in the two plates are

$$\frac{\partial^2 T_1}{\partial x^2} + \frac{\partial^2 T_1}{\partial y^2} = \frac{C(x,y)}{k_1 b_1} (T_2 - T_1) + \frac{h_{t_1}}{k_1 b_1} (T_\infty - T_1) \qquad \text{(V-1)}$$

and

$$\frac{\partial^2 T_2}{\partial x^2} + \frac{\partial^2 T_2}{\partial y^2} = \frac{C(x,y)}{k_2 b_2} (T_1 - T_2) + \frac{h_{t_2}}{k_2 b_2} (T_\infty - T_2) \; . \qquad \text{(V-2)}$$

$C(x,y)$ is the interface thermal conductance; h_{t_1} and h_{t_2} are the total heat transfer coefficients for heat exchange with the surroundings. The boundary conditions are:

Plate 1

$$\begin{aligned} x = -x_1 \; ; \quad & \frac{dT_1}{dx} = -\frac{q_1}{k_1} \\ x = x_1 \; ; \quad & \frac{dT_1}{dx} = \frac{h_{e_1}}{k_1} (T_1 - T_\infty) \\ y = 0 \; ; \quad & \frac{dT_1}{dy} = \frac{h_{e_1}}{k_1} (T_1 - T_\infty) \\ y = y_1 \; ; \quad & \frac{dT_1}{dy} = 0 \end{aligned} \qquad \text{(V-3)}$$

Plate 2

$$\begin{aligned} x = -x_1 \; ; \quad & \frac{dT_2}{dx} = \frac{h_{e_2}}{k_2} (T_2 - T_\infty) \\ x = x_1 \; ; \quad & \frac{dT_2}{dx} = -\frac{q_2}{k_2} \\ y = 0 \; ; \quad & \frac{dT_2}{dy} = \frac{h_{e_2}}{k_2} (T_2 - T_\infty) \\ y = y_1 \; ; \quad & \frac{dT_2}{dy} = 0 \end{aligned} \qquad \text{(V-4)}$$

The nature of C, h_{t_1}, and h_{t_2} in equations V-1 and V-2 must first be considered. From Chapter IV, it is apparent that the interface

conductance will exhibit an approximately circular symmetry on account of the symmetry of the bolt stresses and the resulting interface stresses and gap. Thus C(x,y) would have to be approximated by a trigonometric series whose complexity would depend on the nature of the interface stresses. The variables h_{t_1} and h_{t_2} are even more difficult to handle because their radiation components are cubic functions of the temperature. A closed-form solution of equations V-1 and V-2 is most likely not possible. However, a solution is readily obtained if a finite-difference approach is used. Two of the many finite-difference programs now in wide use that were used in this study are described in references 1 and 69.

In order to utilize a finite-difference solution, the two plates must be divided into nodes; the interface conductance must then be described for each pair of interface nodes. As the first step, both the regions of apparent contact and the pressure in these regions must be determined and the interface gap calculated as a function of position. Methods developed to do this have already been discussed in Chapter IV. After the contact areas and pressures and the interface gap thickness are established, the interface conductance must be determined as a function of node location. A method developed to do this will be taken up in the following paragraphs.

B. Thermal Conductance in the Contact Zone

Chapter II contains a lengthy review of the experimental work that has been done to determine the thermal conductance across contacts. Much experimental data exists, but due to the disparities in it, its application is difficult. In reference 48, a recommended approach is

outlined and was employed in this study. This approach, discussed in Chapter II, is only briefly outlined here.

In the contact zone, the thermal conductance is given by equation II-25 as

$$C_t = C_f + C_a = \frac{1.56k_f}{(i_A + i_B)} + 2\bar{n}\bar{a}k_M \quad . \qquad \text{(II-25)}$$

To employ this equation, the thermal conductivity of the joint material, k_M, must be known. The thermal conductivity of the interface fluid, k_f, is usually known or can be readily calculated, as discussed in Chapter II. If the R.M.S. values of surface roughness and waviness are known, then they can be added and $(i_A + i_B)$ determined. If only the roughness values are available, Figure II-7 can be used to obtain an estimate for i_A and i_B. An estimate for the value of $\bar{n}\bar{a}$ can be obtained from Figure II-6, using the computed value of the contact pressure.

In lieu of using equation II-25, the experimental curves compiled in reference 48 can be used. Equation II-25 was employed to calculate the thermal conductances in the contact zone for use in the finite difference analysis discussed in Section E.

C. Thermal Conductance in the Separated Zone

In the discussion on contacts in Chapter II, it was shown that the conductance in the separated zone (interface gap) can be divided into three components. It was shown that, in most cases, convection is not possible and radiation may be neglected. If radiation must be considered, then the gap conductance can be written as

$$C_g = C_R + C_D = k_f \left[\frac{1}{\delta_R} + \frac{1}{\bar{\delta}} \right] \qquad \text{(V-5)}$$

where δ_R is given by equation II-7 as

$$\delta_R = \frac{k_f}{4\sigma T_M^3} \quad . \qquad \text{(II-7)}$$

In the finite difference heat transfer analyses (to be discussed in Section E) of the two joints for which experimental data was obtained, four situations were considered. These four involved both the aluminum and stainless steel joints at ambient pressure and in vacuum. For the ambient pressure cases $\delta_R \simeq 1900\bar{\delta}$ for the aluminum joint and $2000\bar{\delta}$ for the stainless steel joint. Thus there was no question that the heat transfer by radiation across the interface gap could be neglected. For the vacuum cases $\delta_R \simeq 70\bar{\delta}$ for the aluminum joint and $30\bar{\delta}$ for the stainless steel joint. Here again it was possible to neglect interfacial heat transfer by radiation, without introducing an error in the value of C_g greater than about 3 percent.

In cases involving <u>high</u> vacuum conditions the ratio of δ_R to $\bar{\delta}$ is significant and δ_R has to be incorporated into the expression for C_g (equation V-5). In any case, once $\bar{\delta}$ has been determined using the methods developed in Chapter IV, C_g can be calculated.

D. <u>Experimental Measurements--Thermal Conductance of Bolted Joints</u>

A series of heat transfer experiments were conducted under controlled conditions to measure the temperature distribution in two bolted joints for a verification of the analytical methods developed herein to handle such a problem. Two lap joints, one of 6061T6 aluminum and one of 304 stainless steel, were tested.

The aluminum joint consisted of two 7-inch × 2-inch × 1/4-inch plates; the stainless steel plates were the same length and width, but

were only 1/8 inch thick. Each plate had seventeen 0.062-inch diameter holes drilled approximately 1/8 inch deep for connecting Conax 32 gauge copper-constantan grounded thermocouples. The stainless steel and aluminum hot-side plates are shown in Figure V-1; both the hot- and cold-side aluminum plates are shown in Figure V-2. Illustration V-4 is a section

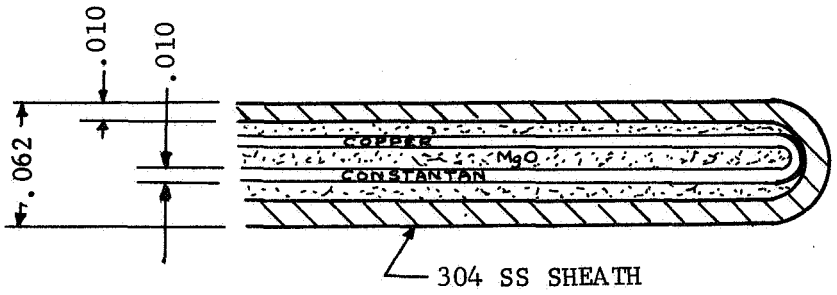

ILLUSTRATION V-4 Cross Section of Conax Thermocouple

of the thermocouples. The assembled aluminum joint, along with the hot-side circular heating element (Chromalox, Inc.), is shown in Figure V-3. The cold-side aluminum plate and its coolant plate are shown in Figure V-4. Cooling water was fed through the coolant plate with the polyethylene tubing that is visible in Figure V-3.

The whole apparatus, with the aluminum joint in place for temperature measurements, is shown in Figures V-5, V-6, and V-7. The aluminum bell jar used for measurements at ambient pressure, as well as in vacuum, is visible in Figure V-6. (More consistent results were obtained with the bell jar in place for measurements at ambient pressure due to the avoidance of air currents created in the room by a circulating fan.)

In Figure V-7, a close-up view of the aluminum joint shows the method of thermocouple installation. This attachment method for these thermocouples does not introduce any significant error because of the

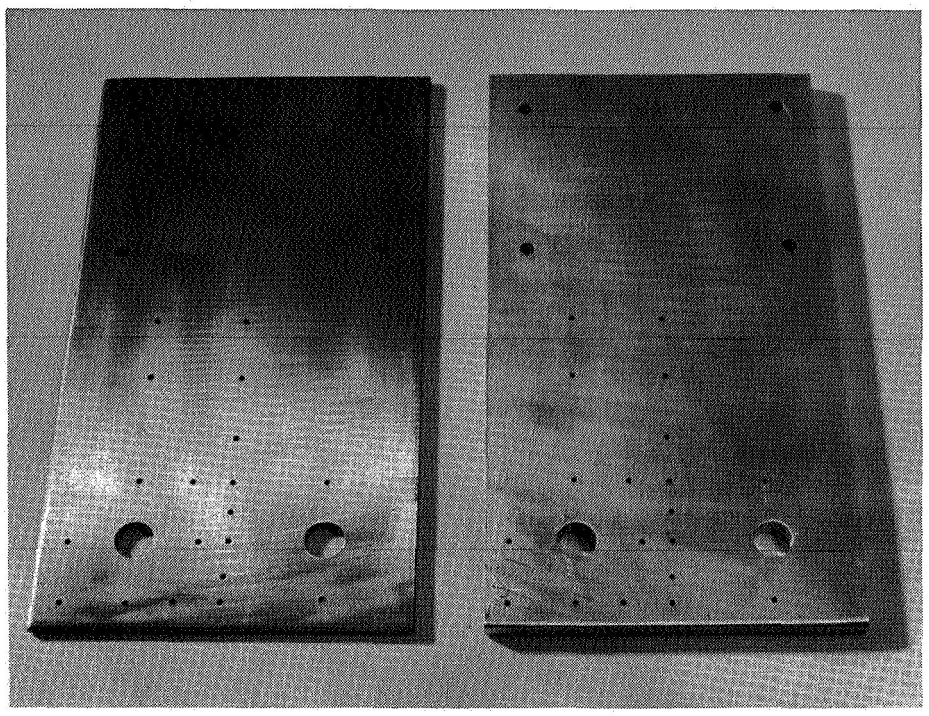

FIGURE V-1 STAINLESS STEEL AND ALUMINUM PLATES FOR HEAT TRANSFER STUDY

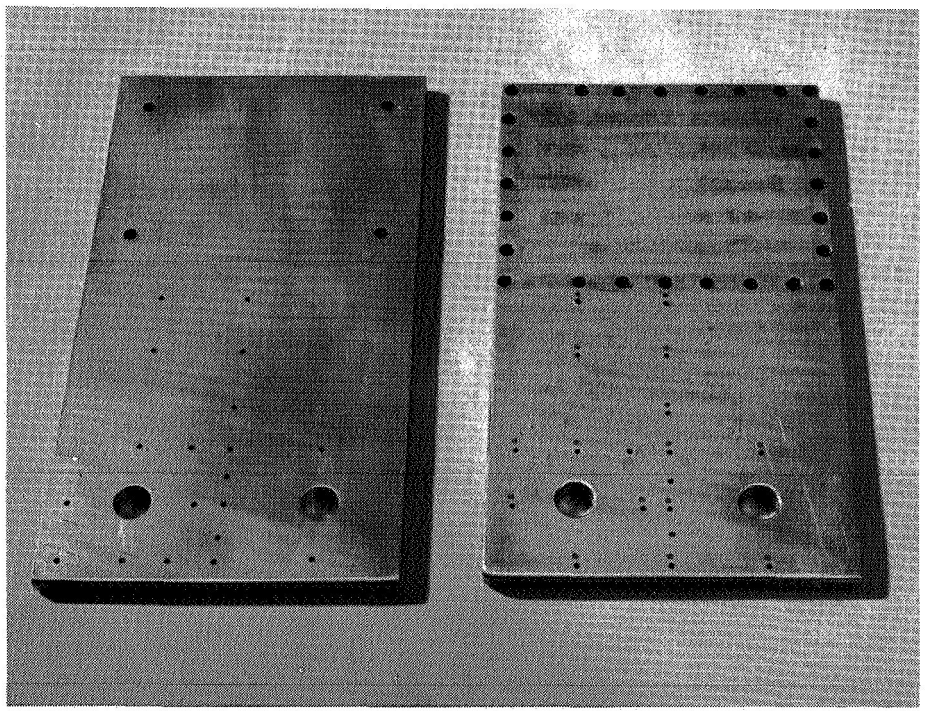

FIGURE V-2 1/4-INCH HOT AND COLD SIDE ALUMINUM PLATES FOR HEAT TRANSFER STUDY

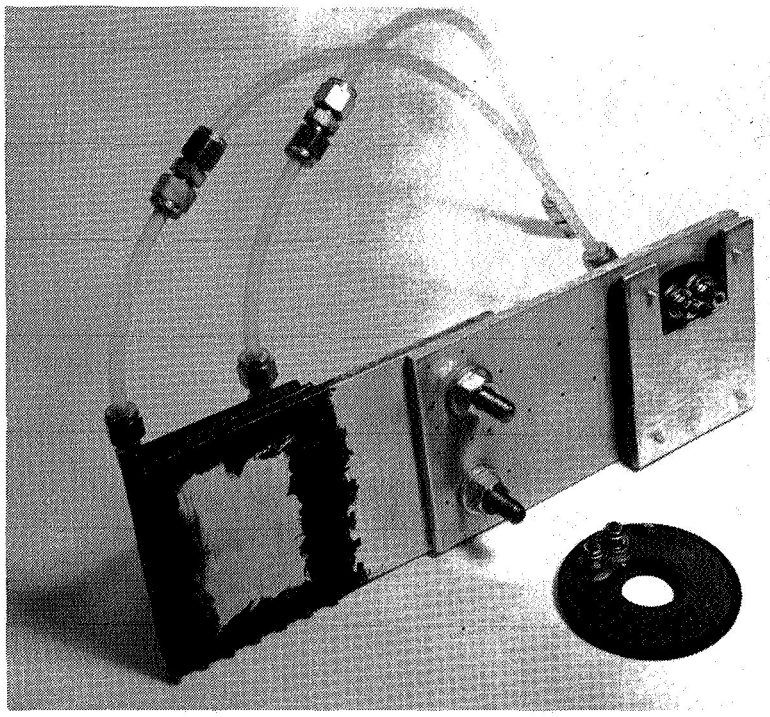

FIGURE V-3 ALUMINUM JOINT USED IN HEAT TRANSFER STUDY

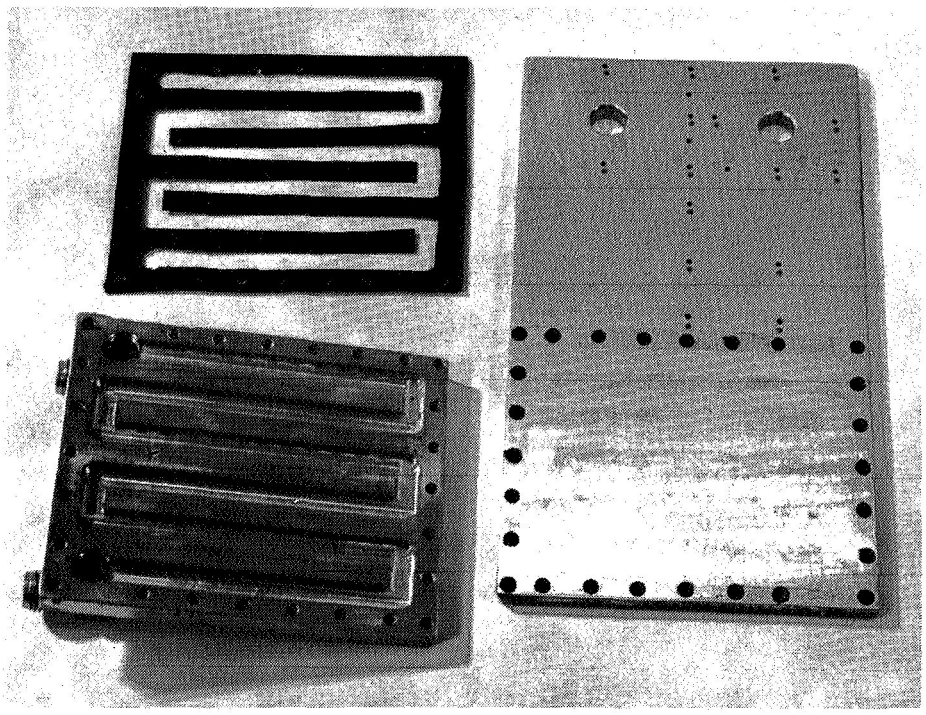

FIGURE V-4 COLD-SIDE PLATE DISASSEMBLED TO SHOW COOLANT PLATE AND GASKET.

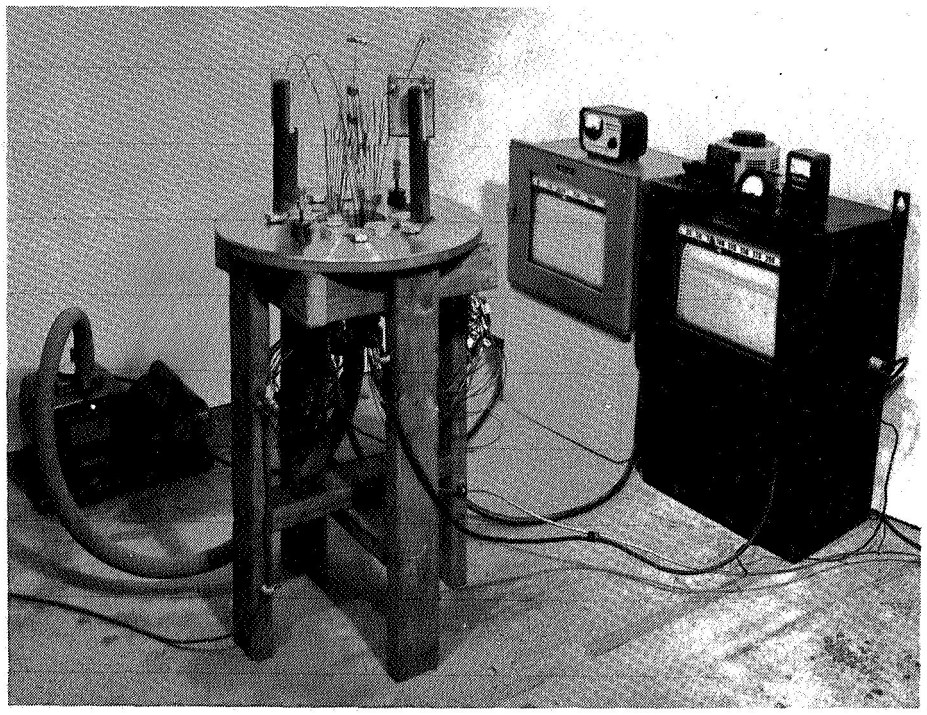

FIGURE V-5 EXPERIMENTAL ARRANGEMENT FOR HEAT TRANSFER STUDY (BELL JAR REMOVED)

FIGURE V-6 EXPERIMENTAL ARRANGEMENT FOR HEAT TRANSFER STUDY (BELL JAR IN PLACE)

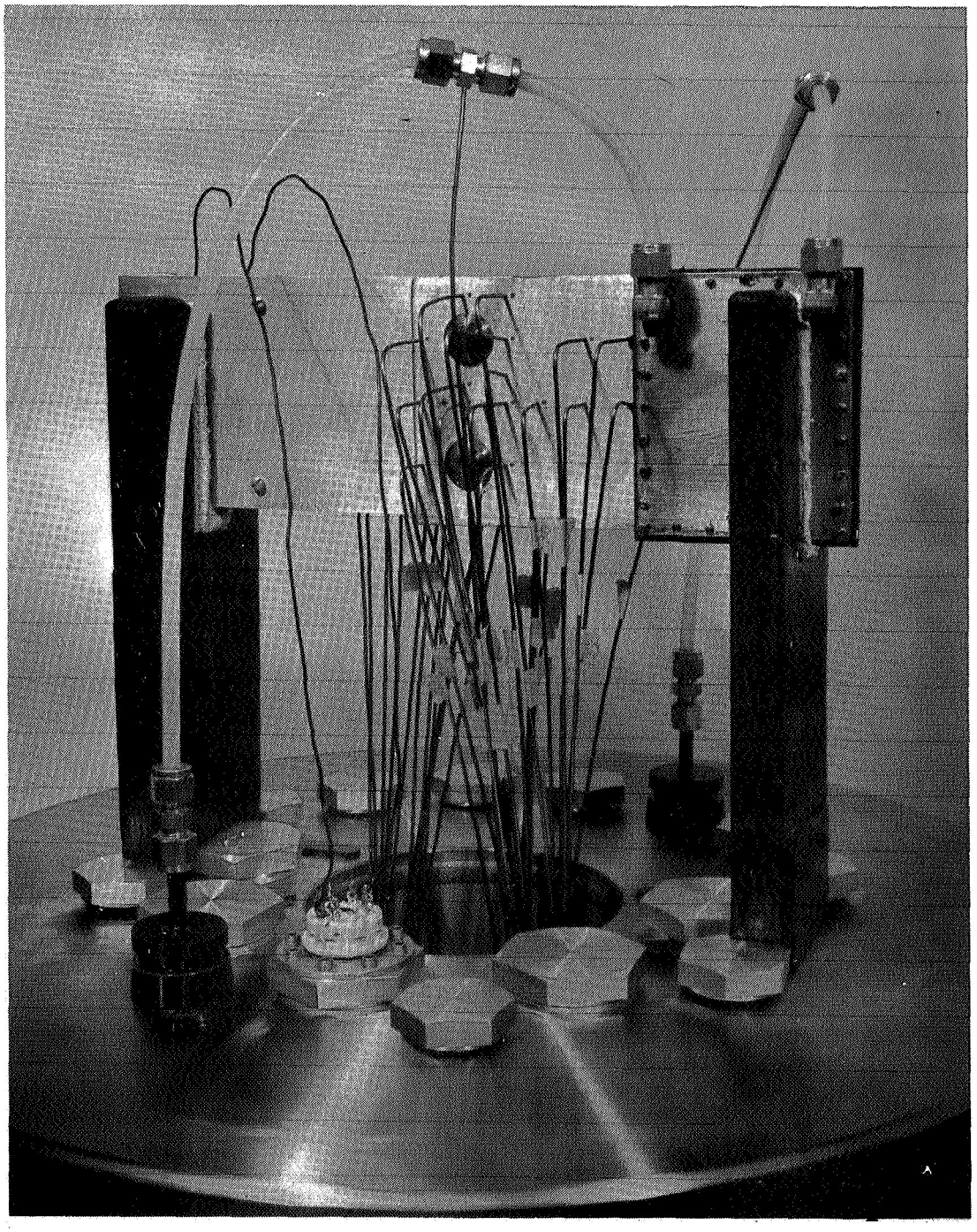

FIGURE V-7 CLOSE-UP VIEW- ALUMINUM JOINT INSTALLED FOR HEAT TRANSFER STUDY

ceramic insulation sheath around the thermocouple wires (Illustration V-4). The holes in the plates were drilled to provide an interference fit for the thermocouple tips. Where the fit was not tight, thin aluminum foil was used to shim the holes.

The flow of the cooling water was regulated by a manually operated valve. The inlet and outlet water temperatures were measured at two brass couplings (insulated during tests) in the polyethylene lines (Figure V-7). The electrical heating element was controlled by a variac with monitoring of the voltage and current. The output from the 36 thermocouples was registered by two Minneapolis-Honeywell recorders. For tests in a vacuum, the bell jar was evacuated to a pressure between 100 and 300 microns of mercury. (Pressures were read with a CVC thermocouple vacuum gauge.)

After the thermocouples had been installed in the bell jar but before they were inserted into the aluminum joint for the first test, the recorder outputs for all of them were checked at 32°F by the insertion of 12 thermocouples at one time into an insulated bath of crushed ice. It was found that the difference between recorders was greater than that between thermocouples. Although the thermocouples had a temperature output variation among themselves of only ± 0.4°F (two thermocouple sets, one set on each recorder), the recorders differed from each other by 1.7°F. (Before installation of the thermocouples the recorder calibrations had been checked.) Because temperatures differences were of prime concern, not absolute temperature measurements, it was concluded that the discrepancy between recorders would not be a serious problem.

The joint was allowed to come to thermal equilibrium before the desired steady-state temperatures were recorded. This equilibrium was

considered attained when temperature measurements were repeatable within ± 0.5°F for at least 30 minutes. As expected, the stainless steel joint required considerably more time (about 2 hours) to reach thermal equilibrium than did the aluminum joint which required only about 30 minutes.

Ten tests were conducted; nine of these provided a complete set of temperature data. Table V-1 summarizes the most important measurements, other than temperature, obtained during these tests. The same torque wrench mentioned in Chapter II was used to tighten the joints.

The steady-state temperature measurements obtained in the 9 tests will not be listed here; they will be given later for comparison with temperatures computed in a finite-difference analysis. First, it is necessary to describe the finite-difference steady-state heat transfer technique used to obtain the computed values of joint temperatures.

Table V-1

SUMMARY OF HEAT TRANSFER TESTS

Test No.	Joint	Torque ft-lbs	Ambient Press. ~ psi	Heater Current ~ amps	Heater Voltage ~ volts	Flow Rate of Water ~ lb_m/min
1	Alum.	15	14.7	0.92	95.	2.34
2	"	8	14.7	0.92	95.	"
3	"	8	0.0058	0.85	86.5	"
4	"	15	0.0039	0.85	86.5	"
5	Stain. Steel	8	14.7	0.625	66.	"
6	"	8	0.0019	0.38	40.	"
7	"	15	14.7	0.64	66.	"
8	"	15	0.0025	0.38	40.5	"
10	"	15	14.7*	0.65	68.	"

*Bell jar not used.

E. Finite-Difference Analysis

The simplest approach to the computation of the temperature distribution in a bolted joint is a finite-difference approach. The three-dimensional steady-state finite-difference analysis described in reference 69 was used to calculate the theoretical values of interface temperature for comparison with the experimental results. As required by the finite-difference method the two joints were divided into a nodal network as shown in Figure V-8. The locations of the 34 thermocouples are designated by the "O" around the node center point to indicate where measured values of the temperature were available.

Nodes 1-37 were treated as variable-temperature nodes (diffusion nodes); nodes 38-65 were treated as fixed-temperature nodes (boundary nodes). Conductors 1-22 were in plate 1, conductors 23-50 were interface conductors, and conductors 51-59 were equivalent conductors for radiation. Since the nodes in plate 2 were fixed temperature nodes, no conductors were necessary in that plate. For handling the convective heat transfer losses and the heat input from the heating element, nodes 1-37 were treated as source nodes.

The thermal conductivity (k) and emittance (ϵ) of the joint materials and the convective heat transfer coefficient (h) were also needed to accurately describe the total heat transfer problem. Because the values given in the literature would only be estimates in this case, 10 thermocouples, located in the two plates outside of the lap area, provided temperature measurements not directly influenced by the interface conductance. From this data, the constants k, ϵ, and h were determined for the aluminum and stainless steel joints. A summary of the computed

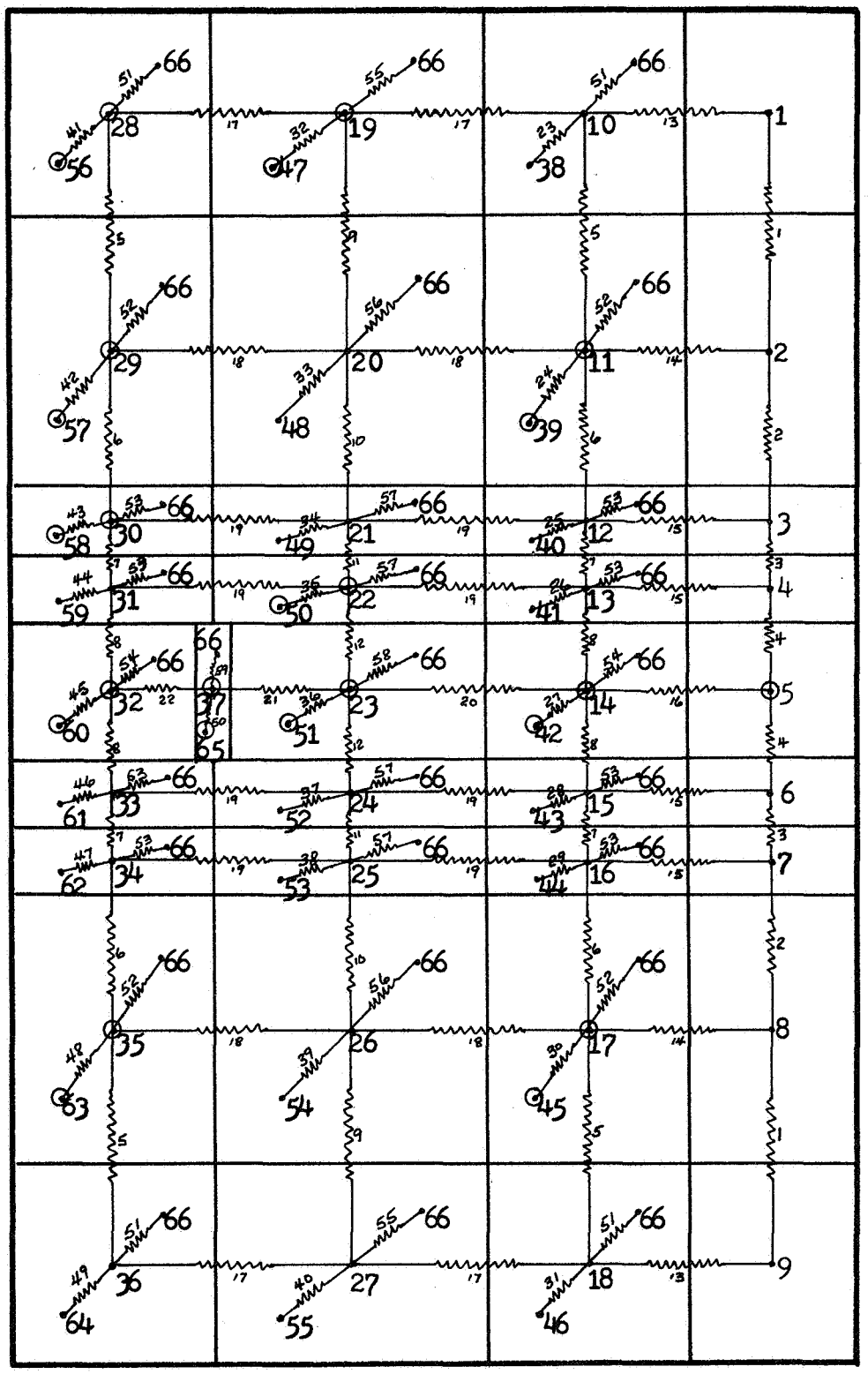

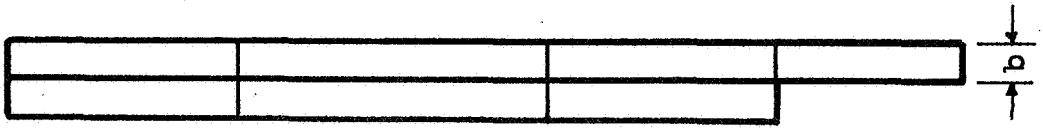

FIGURE V-8 NODAL NETWORK FOR FINITE DIFFERENCE ANALYSES

Table V-2

THERMAL CONDUCTIVITY, EMITTANCE, AND CONVECTIVE FILM COEFFICIENTS

		k BTU/in-min-°F	ε	h BTU/min-in^2-°F
6061 Aluminum	Reference 6		0.10-0.15	
	" 70	0.154		
	" 71	0.138	0.56 (anodized)	
	Joint Data	0.160	0.59	0.80×10^{-4}
	Value Used	0.160	0.15	1.74×10^{-4}
304 Stainless	Reference 6		0.30	
	" 70	0.0133		
	" 71	0.0130-0.0135	0.30-0.41	
	Joint Data	0.0147	0.34	2.55×10^{-4}
	Value Used	0.0147	0.34	2.55×10^{-4}
Reference 6 (p. 172)				1.74×10^{-4}

values is given in Table V-2 along with estimated values taken from the literature.

The measured values of thermal conductivity (k) for both metals and the emittance (ε) for the stainless steel agree within about 10 percent with previously reported values. The emittance for aluminum determined from the joint data, however, appears too high, as compared to the literature value for non-anodized 6061 aluminum. Both values of h appear reasonable, but the value of h determined for the aluminum joint appears too low. This is due to the high value of ε, for the aluminum joint, which was used in calculating a value for h. It is not known whether the differences between the calculated values and the values taken from the literature are normal variations in the properties of the materials,

or due to errors in the temperature and electrical power measurements and the estimate for heat losses around the heating element.

For both the aluminum and stainless steel joints, the emittances were determined from the temperature measurements outside the lap area and the computed heat losses during the tests in vacua. These emittance values were then used in computing the convective heat transfer coefficient from the temperature measurements obtained at ambient pressure. Thus, in the case of the stainless steel joint, a value of 0.34 for ϵ, obtained from the temperature measurements in vacuum, was used to compute a value of 2.55×10^{-4} for h from the temperature measurements at ambient pressure. Both of these values were used in the finite-difference analysis.

Instead of using a value of 0.59 for the emittance of the aluminum joint, a value of 1.74×10^{-4} was assumed for h and a consistent value for ϵ was computed using the temperature measurements at ambient pressure. The value obtained, 0.15, is consistent with that given for aluminum by McAdams (6). These values of ϵ and h were then used in the finite-difference analysis of the aluminum joint.

The actual division of the heat losses into convection and radiation losses, was found to be important in the finite-difference steady-state analysis--as long as the total heat loss was accounted for. In addition, if the total heat loss rate is small compared with the heat transfer rate across the joint, no appreciable error is introduced into the computed interface temperature differences. The computed heat transfer rates to and from the joints for all 10 tests are given in Table V-3.

From Table V-3 it is seen, that for the aluminum joint in vacuum (tests 3 and 4), the heat loss across the joint was only about 11 percent

Table V-3

CALCULATED JOINT HEAT TRANSFER AND LOSS RATES

Test	Input Heat Rate BTU/min	Output Heat Rate BTU/min	Heat Loss Rate across Joint BTU/min
1	4.20	3.53	0.67
2	4.20	3.53	0.67
3	3.74	3.33 (3.64)*	0.41 (0.10)*
4	3.74	3.33 (3.64)*	0.41 (0.10)*
5	0.58	0.13	0.45
6	0.32	0.17	0.15
7	0.64	0.14	0.50
8	0.33	0.18	0.15
9	0.32	0.16	0.16
10	0.75	0.12	0.63

*Value used in finite-difference analysis.

of the heat input. So, in this case, the change in ϵ from a computed value of 0.59 to a computed value of 0.15 reduces this 11 percent to only about 3 percent, since the 11 percent value was used to compute the value of 0.59 for ϵ.

At the joint interface, however, the increase in heat transfer rate due to the change in ϵ of from 0.59 to 0.15 is only 4 percent. For tests 1 and 2, the difference is much less because the value for the total heat loss was retained which means that a higher value of h was used to compensate for a lower value of ϵ. If a change in ϵ had been necessary for the stainless steel joint, the error would have been much

larger; the losses across the joint in tests 6, 8, and 9 were about 50 percent of the input, rather than 11 percent.

To obtain the input rates given in Table V-3, the measured values of the heating element input were corrected for convection and radiation losses about the heating element by use of the calculated values of h and ϵ. The heat transfer loss for all 34 thermocouples inserted in the plates was found to be only 0.008 BTU/min.

With k, ϵ, h, and q_1 determined, the only remaining parameters to be determined for use in the finite-difference analyses were the interface thermal conductances (conductors 23-50). The values of the thermal conductance between pairs of interface nodes were obtained using equation II-25 to calculate C_t in the contact area and equation V-5 to calculate C_g in the gap area. The results for tests 1, 5, and 8 are given in Tables V-4, V-5, and V-6. The values of k_f for these equations were taken from Figures II-3 and II-4, and the values of i_A and i_B (irregularity of the plate surfaces) were measured with a Proficorder (Micrometrical Corporation). The average measured values for the stainless steel and aluminum plates are plotted in Figure II-6 and are seen to fall within the standard deviation of the data from reference 48.

The contact areas for the stainless steel and aluminum joints were determined with values of r_σ from Figure IV-16. The experimental data reported in Chapter III for the 1-inch button-head bolt was extrapolated to the 3/8-inch button-head bolt actually used in the joints. To obtain values of r_σ from Figure IV-16, a value of 0.336 inches for r_h was used rather than the actual bolthead radius of 0.406 inches, in line with the oil pressure and penetration data obtained for button-head bolts in Chapter III.

Table V-4

INTERMEDIATE RESULTS IN THE CALCULATION OF THE NODAL INTERFACE CONDUCTANCES - TEST 1

Conductor Number	$\bar{\delta}$	C_g	Avg Contact Pressure	$\bar{na}$	C_t	Percent C_g	Percent C_t	Nodal Interf. Conductance
	10^{-4} in	$\frac{BTU}{min\ in^2\ °F}$	psi	1/in	$\frac{BTU}{min\ in^2\ °F}$			$\frac{BTU}{min\ in^2\ °F}$
23	6.0	0.041	90.	0.29	0.17	90.	10.	0.055
24	3.9	0.063	650.	1.6	0.59	50.	50.	0.33
25	4.7	0.052	30.	0.12	0.12	75.	25.	0.068
26	5.2	0.047	-	-	-	100.	0.	0.047
27	7.0	0.035	-	-	-	100.	0.	0.035
28	5.2	0.047	-	-	-	100.	0.	0.047
29	4.7	0.052	30.	0.12	0.12	75.	25.	0.068
30	3.9	0.063	650.	1.6	0.59	50.	50.	0.33
31	6.0	0.041	90.	0.29	0.17	90.	10.	0.055
32	4.5	0.054	650.	1.6	0.59	50.	50.	0.33
33	-	-	2700.	5.8	1.9	0.	100.	1.9
34	-	-	800.	2.0	0.72	0.	100.	0.72
35	3.2	0.076	90.	0.29	0.17	50.	50.	0.12
36	3.7	0.066	-	-	-	100.	0.	0.067
37	3.2	0.076	90.	0.29	0.17	50.	50.	0.12
38	-	-	800.	2.0	0.72	0.	100.	0.72
39	-	-	2700.	5.8	1.9	0.	100.	1.9
40	4.5	0.054	650.	1.6	0.59	50.	50.	0.33
41	6.0	0.040	90.	0.29	0.17	90.	10.	0.053
42	3.9	0.061	650.	1.6	0.59	50.	50.	0.33
43	4.7	0.051	30.	0.12	0.12	75.	25.	0.068
44	5.2	0.046	-	-	-	100.	0.	0.046
45	7.0	0.034	-	-	-	100.	0.	0.034
46	5.2	0.046	-	-	-	100.	0.	0.046
47	4.7	0.051	30.	0.12	0.12	75.	25.	0.066
48	3.9	0.061	650.	1.6	0.59	50.	50.	0.33
49	6.0	0.040	90.	0.29	0.17	90.	10.	0.053
50	3.8	0.064	-	-	-	100.	0.	0.062

Table V-5

INTERMEDIATE RESULTS IN THE CALCULATION OF THE NODAL INTERFACE CONDUCTANCES - TEST 5

Conductor Number	$\bar{\delta}$	C_g	Avg Contact Pressure	$\bar{na}$	C_t	Percent C_g	Percent C_t	Nodal Interf. Conductance
	10^{-4} in	$\frac{BTU}{min\ in^2\ °F}$	psi	1/in	$\frac{BTU}{min\ in^2\ °F}$			$\frac{BTU}{min\ in^2\ °F}$
23	2.7	0.085	-	-	-	100.	0.	0.086
24	1.7	0.14	150.	0.45	0.15	90.	10.	0.14
25	2.1	0.11	-	-	-	100.	0.	0.11
26	2.5	0.092	-	-	-	100.	0.	0.092
27	2.6	0.089	-	-	-	100.	0.	0.088
28	2.5	0.092	-	-	-	100.	0.	0.092
29	2.1	0.11	-	-	-	100.	0.	0.11
30	1.7	0.14	150.	0.45	0.15	90.	10.	0.14
31	2.7	0.085	-	-	-	100.	0.	0.086
32	2.0	0.11	150.	0.45	0.14	90.	10.	0.12
33	0.45	0.51	2200.	4.8	0.27	5.	95.	0.28
34	1.1	0.21	150.	0.45	0.14	80.	20.	0.19
35	1.3	0.18	-	-	-	100.	0.	0.17
36	1.6	0.14	-	-	-	100.	0.	0.14
37	1.3	0.18	-	-	-	100.	0.	0.17
38	1.1	0.21	150.	0.45	0.14	80.	20.	0.19
39	0.45	0.51	2200.	4.8	0.27	5.	95.	0.28
40	2.0	0.11	150.	0.45	0.14	90.	10.	0.12
41	2.7	0.083	-	-	-	100.	0.	0.86
42	1.7	0.13	150.	0.45	0.14	90.	10.	0.13
43	2.1	0.11	-	-	-	100.	0.	0.11
44	2.5	0.090	-	-	-	100.	0.	0.092
45	2.6	0.087	-	-	-	100.	0.	0.086
46	2.5	0.090	-	-	-	100.	0.	0.092
47	2.1	0.11	-	-	-	100.	0.	0.11
48	1.7	0.13	150.	0.45	0.14	90.	10.	0.13
49	2.7	0.083	-	-	-	100.	0.	0.86
50	1.7	0.13	-	-	-	100.	0.	0.13

Table V-6

INTERMEDIATE RESULTS IN THE CALCULATION OF THE NODAL INTERFACE CONDUCTANCES - TEST 8

Conductor Number	$\bar{\delta}$	C_g	Avg Contact Pressure	$\bar{na}$	C_t	Percent C_g	Percent C_t	Nodal Interf. Conductance
	10^{-4} in	$\frac{BTU}{min\ in^2\ °F}$	psi	1/in	$\frac{BTU}{min\ in^2\ °F}$			$\frac{BTU}{min\ in^2\ °F}$
23	5.4	0.0012	-	-	-	100.	0.	0.0012
24	3.6	0.0012	200.	0.59	0.019	90.	10.	0.0012
25	4.3	0.0011	-	-	-	100.	0.	0.0011
26	4.8	0.0011	-	-	-	100.	0.	0.0011
27	5.5	0.0012	-	-	-	100.	0.	0.0012
28	4.8	0.0011	-	-	-	100.	0.	0.0011
29	4.3	0.0011	-	-	-	100.	0.	0.0011
30	3.6	0.0012	200.	0.59	0.019	90.	10.	0.0012
31	5.4	0.0012	-	-	-	100.	0.	0.0012
32	4.1	0.0012	200.	0.59	0.019	90.	10.	0.0012
33	0.9	0.00078	4500.	9.0	0.26	5.	95.	0.25
34	2.2	0.0011	200.	0.59	0.019	80.	20.	0.0046
35	3.1	0.0011	-	-	-	100.	0.	0.0011
36	3.4	0.0012	-	-	-	100.	0.	0.0012
37	3.1	0.0011	-	-	-	100.	0.	0.0011
38	2.2	0.0011	200.	0.59	0.019	80.	20.	0.0046
39	0.9	0.00078	4500.	9.0	0.26	5.	95.	0.25
40	4.1	0.0012	200.	0.59	0.019	90.	10.	0.0012
41	5.4	0.0012	-	-	-	100.	0.	0.0012
42	3.6	0.0012	200.	0.59	0.019	90.	10.	0.0012
43	4.3	0.0011	-	-	-	100.	0.	0.0011
44	4.8	0.0011	-	-	-	100.	0.	0.0011
45	5.5	0.0012	-	-	-	100.	0.	0.0012
46	4.8	0.0011	-	-	-	100.	0.	0.0011
47	4.3	0.0011	-	-	-	100.	0.	0.0011
48	3.6	0.0012	200.	0.59	0.019	90.	10.	0.0012
49	5.4	0.0012	-	-	-	100.	0.	0.0012
50	3.4	0.0012	-	-	-	100.	0.	0.0012

Sneddon's theory gives values for r_σ of 0.58 and 0.45 for the aluminum and stainless steel joints respectively, whereas the curve drawn through the experimental data from the present study (Figure IV-16) gives 0.75 and 0.50. Only this latter set of r_σ values was used to calculate contact areas and nodal interface conductance values. However, both sets were used to calculate plate deflections and interface gap thicknesses.

Average values of the interface gap thicknesses, $\overline{\delta}$, were determined from joint plate deflections calculated using the analysis developed in this study and described in Chapter IV, and the digital program given in Appendix A. The pair of r_σ values from Sneddon's curve (Figure IV-16) gave 50 percent smaller plate deflections for the aluminum joint and 10 percent smaller deflections for the stainless steel joint than deflections obtained with r_σ values taken from the new experimental curve in the same figure. For the finite-difference analysis, the values of $\overline{\delta}$ were determined from the new curve for r_σ. The results for tests 1, 5, and 8 are given in Tables V-4, V-5, and V-6.

The contact-area interface pressures were determined with Fernlund's simplified method discussed in Chapter IV. These pressures for tests 1, 5, and 8 are given in Tables V-4, V-5, and V-6. This method was suitable for the joints under consideration because the values of $(r_\sigma - r_s)$ are close to the values of $(r_h - r_s)$. The calculated interface stress distributions, shown in Figures V-9 and V-10, were used to find values of $\overline{na}$ from the curve labeled "arithmetic mean" in Figure II-6.

In Tables V-4, V-5, and V-6, besides the values of C_g, C_t, $\overline{\delta}$, and average contact pressure, the values of $\overline{na}$ read for each of the interface conductors from Figure II-6 are given. Also given in these tables are

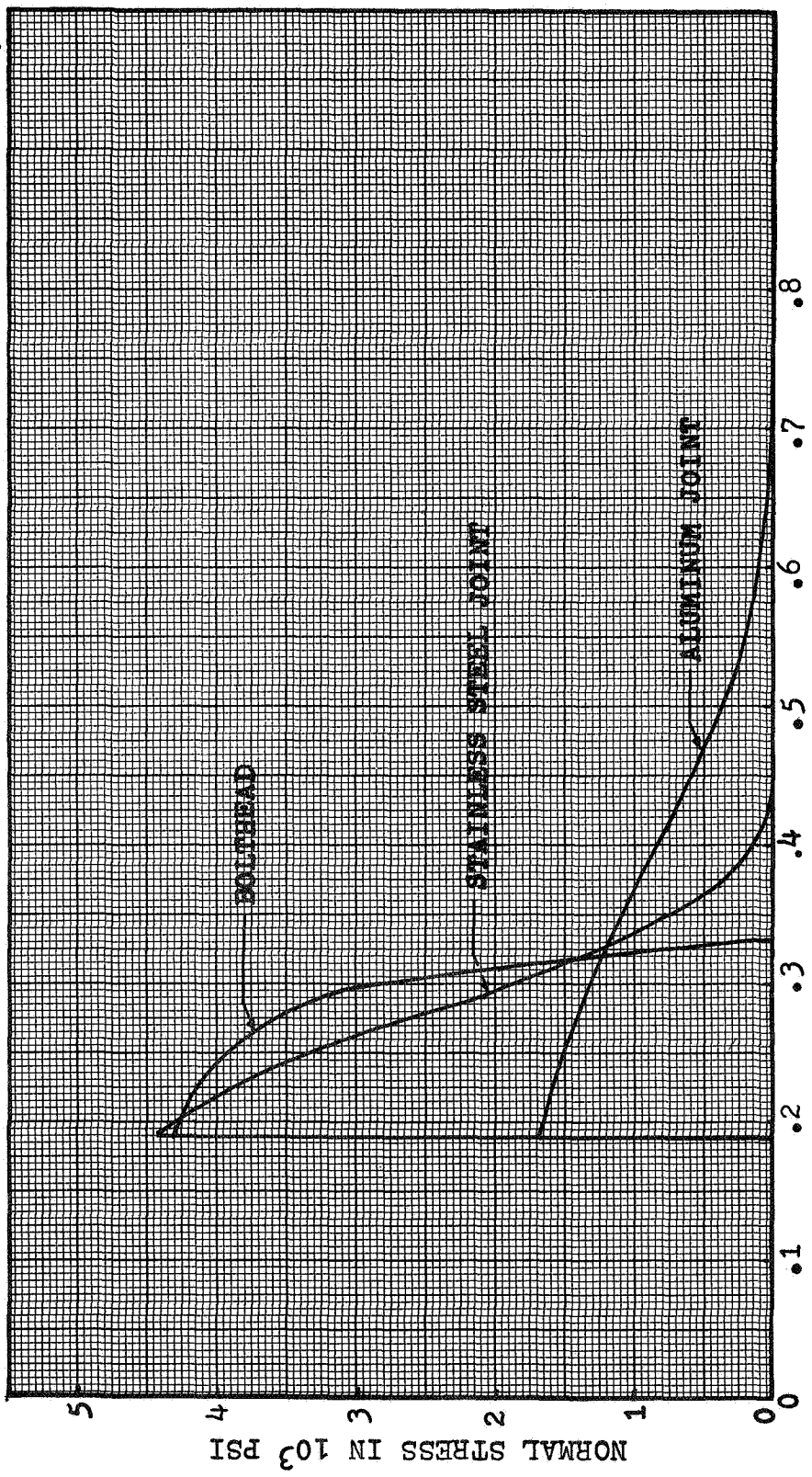

FIGURE V-9 BOLTHEAD AND INTERFACE STRESS DISTRIBUTIONS FOR 7 FT-LBS TORQUE

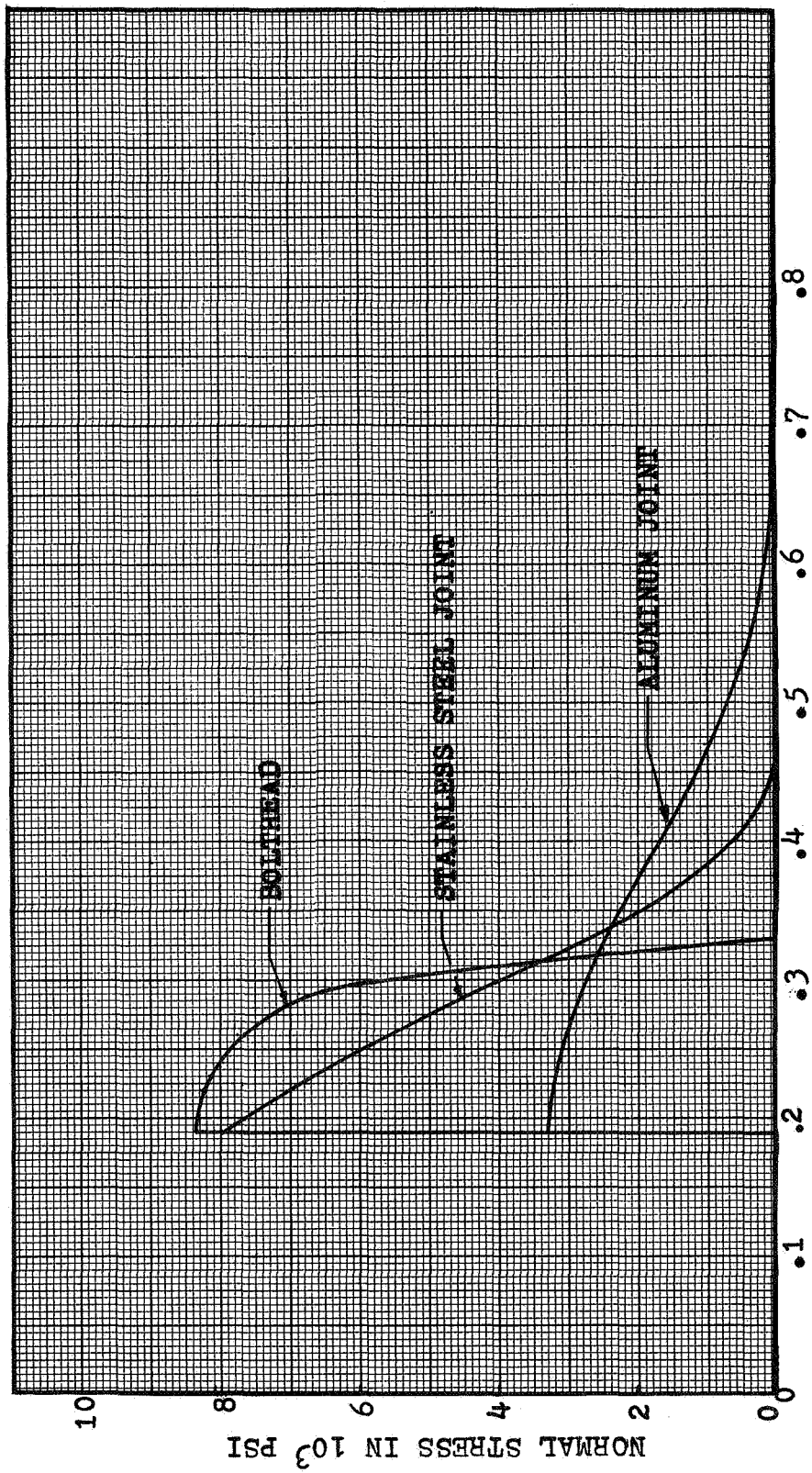

FIGURE V-10 BOLTHEAD AND INTERFACE STRESS DISTRIBUTIONS FOR 15 FT-LBS TORQUE

the percentages of the interface nodal area in which gap conductance (C_g) occurs and in which contact conductance (C_t) occurs.

From the tables, it is apparent that the conductance between most of the interfacial nodal pairs is governed by the equation for C_g. This is especially pronounced in the stainless steel joint (tests 5 and 8). The differences in the average values of the interface gap $\overline{\delta}$ are also apparent from the three tables. The difference in the values of $\overline{\delta}$ for tests 5 and 8 is due to the difference in the applied torque (see Table V-1). A comparison of the values of C_g and nodal interface conductance for tests 5 and 8 reveals the effect of interface fluid pressure on the magnitude of the interface conductance.

The values of the nodal interface conductances resulting from the complete analyses for the 9 tests are shown in Table V-7. These values were used in the finite-difference analyses to determine the interface temperature distributions. The computed values of interface temperatures are given in the next section.

F. Comparison Between Theoretical and Measured Values of Interface Temperatures

Steady-state temperature distributions were calculated with the finite-difference computer program (reference 69) and the nodal arrangement shown in Figure V-8. The temperature distributions were found for each of the 9 tests using the data in Tables V-2, V-3, and V-7.

In Table V-8, the computed temperatures for test 1 are tabulated for comparison with the measured temperatures, which are also tabulated. Similar tables for tests 2-10 are given in Appendix B.

A summary of the differences between theoretical and experimental temperature gradients for all of the tests is given in Table V-9.

Table V-7

THEORETICAL VALUES OF INTERFACE CONDUCTANCE

Conductor No.	Interface Conductance BTU/in^2 - min ^oF								
	Test 1	Test 2	Test 3	Test 4	Test 5	Test 6	Test 7	Test 8	Test 10
23	.055	.092	.0081	.011	.086	.00088	.042	.0012	.042
24	.33	.25	.15	.27	.14	.0025	.073	.0012	.073
25	.068	.092	.057	.012	.11	.00083	.054	.0011	.052
26	.047	.10	.0028	.0018	.092	.00091	.049	.0011	.048
27	.035	.083	.0029	.0019	.088	.00091	.042	.0012	.041
28	.047	.10	.0028	.00018	.092	.00091	.049	.0011	.048
29	.068	.092	.057	.012	.11	.00083	.054	.0011	.052
30	.33	.25	.15	.26	.14	.0025	.073	.0012	.073
31	.055	.092	.0081	.011	.086	.00088	.042	.0012	.042
32	.33	.22	.15	.26	.12	.0023	.064	.0012	.064
33	1.9	1.0	.96	1.86	.28	.13	.39	.25	.39
34	.72	.42	.34	.64	.19	.022	.11	.0046	.11
35	.12	.14	.028	.26	.17	.00093	.075	.0011	.075
36	.067	.13	.0027	.0018	.14	.00093	.067	.0012	.067
37	.12	.14	.028	.049	.17	.00093	.075	.0011	.075
38	.72	.42	.34	.71	.19	.022	.11	.0046	.11
39	1.9	1.0	.96	1.86	.28	.13	.39	.25	.39
40	.33	.22	.15	.26	.12	.0023	.064	.0012	.064
41	.053	.092	.0081	.011	.86	.00088	.042	.0012	.042
42	.33	.25	.15	.26	.13	.0025	.073	.0012	.073
43	.068	.092	.057	.012	.11	.00083	.053	.0011	.051
44	.046	.10	.0028	.0018	.092	.00091	.047	.0011	.046
45	.034	.086	.0029	.0022	.086	.00090	.041	.0012	.040
46	.046	.10	.0028	.0018	.092	.00091	.047	.0011	.046
47	.066	.092	.057	.012	.11	.00083	.053	.0011	.052
48	.33	.25	.15	.26	.13	.0025	.073	.0012	.073
49	.053	.092	.0081	.011	.86	.00088	.042	.0012	.042
50	.062	.14	.0025	.020	.13	.0010	.068	.0012	.065

Table V-8

INTERFACE TEMPERATURES FOR TEST 1

CONDUCTOR NO.	COLD SIDE TEMP. ~ °F	HOT SIDE TEMP. ~ °F		Δ T ACROSS INTERFACE ~ °F		% DEVIATION IN Δ T
		MEASURED	CALCULATED	MEASURED	CALCULATED	
24	178.4	185.2	182.9	6.8	4.5	-34.
27	174.8	185.1	184.4	10.3	9.6	- 6.8
30	176.2	183.5	180.8	7.3	4.6	-37.
32	173.5	175.7	174.6	2.2	1.1	-50.
35	173.3	174.2	174.6	0.9	1.3	44.
36	171.7	174.4	174.0	2.7	2.3	-15.
41	159.6	167.7	167.8	8.1	8.2	- 1.2
42	162.2	167.1	165.8	4.9	3.6	-26.
43	160.6	166.3	167.3	5.7	6.7	18.
45	159.2	168.9	167.6	9.7	8.4	-13.
48	158.9	166.4	163.0	7.5	4.1	-45.
50	165.6	171.6	170.2	6.0	4.6	-23.
		Absolute Average		6.0	4.9	26.

Table V-9

COMPARISON OF THEORETICAL AND EXPERIMENTAL INTERFACE TEMPERATURE DROPS

Conductor Number	Deviation in Interface Temperature Drop ~°F								
	Test 1	Test 2	Test 3	Test 4	Test 5	Test 6	Test 7	Test 8	Test 10
24	-2.3	-2.4	-2.2	-4.4	-3.5	2.2	-2.7	5.4	-2.5
27	-0.7	-2.5	-1.6	-3.3	-3.8	3.0	-4.0	5.8	-1.2
30	-2.7	-4.0	-0.2	-5.3	-1.2	5.6	-2.0	6.2	-0.9
32	-1.1	-2.8	-0.7	-0.7	-1.3	0.3	-1.4	4.1	-1.4
35	0.4	-0.6	-1.7	-3.3	-1.5	-0.2	-0.9	2.8	0.9
36	-0.4	-1.6	-1.5	-3.0	-	1.1	-0.4	2.4	-0.2
41	0.1	-1.8	1.4	-0.6	-0.8	2.1	-2.3	3.2	-2.5
42	-1.3	-1.8	-0.9	-4.6	-1.3	-1.3	-0.4	2.0	-1.7
43	1.0	-0.2	0.6	-0.2	-2.2	0.2	-2.9	2.4	-1.5
45	-1.3	-2.7	-1.5	-0.9	-2.0	-0.6	-2.8	1.3	-1.9
48	-3.4	-3.6	-4.8	-6.4	-5.6	-	-	-	-
50	-1.4	-2.5	1.8	-1.8	-3.6	0.1	-3.1	1.6	-0.3
Average Abs. Dev.	1.3	2.2	1.6	2.9	2.4	1.5	2.1	3.4	1.4
Overall Average Deviation = 2.1°F									

From Table V-8 and Appendix B it is apparent that the average percentage deviation between theoretical and experimental values of ΔT is large in most cases. The overall average deviation is 35 percent. However, it is clear from Table V-9 that the average values of the absolute deviation are on the order of 2°F. This is within the limits of the accuracy of the temperature measurements and the finite-difference analysis, the latter being limited by the knowledge of k, h, and ϵ.

It should be noted that where the temperature gradient across the interface is about 10 degrees, the percentage error is only about half as large as the overall average. (See for example Tables B-2 and B-5.) This fact indicates that the discrepancy between the theoretical and experimental values of ΔT is partly due to the inaccuracies in the temperature measurements. The thermocouples employed are rated at ± 0.75°F over a temperature range of 0 to 200°F. Since a calibration of the thermocouples in place in the bell jar was possible only at 32°F, some error in the readings between thermocouples was expected. However, from Table V-9 it is obvious that in all of the tests the deviations are either mostly positive or mostly negative. One would expect the errors resulting from the thermocouple readings to have more of a random nature. Thus it appears that most of the 2°F deviation should be attributed to the finite-difference analysis and specifically, to the uncertainties in k, h, and ϵ.

In reviewing the literature, large discrepancies were found between and within sets of experimental data for interface thermal conductance. Agreement to within 35 percent was rarely found. Difficulties inherent

in the experimental measurements are part of the reason. In light of this, the analytical method developed in this study provides a better method of obtaining estimates of interface thermal conductance values for design purposes.

CHAPTER VI

SUMMARY OF RESULTS AND RECOMMENDATIONS

The primary objective of this investigation was the development of a practical analytical method of determining the interface thermal conductance of a bolted joint from a minimum of design information. Such a method was developed and its validity demonstrated with experimental data.

In reviewing the literature, it was found that the development of a completely analytical method was hampered by a number of factors. These included the lack of; (1) experimental data for the stress distribution under boltheads, (2) an experimentally verified method for obtaining the stress distribution in the interface of a bolted joint and the region of apparent contact, and (3) a theoretical method for predicting the interface gap when the stresses are known. A comprehensive program combining experimental analysis with theory and digital computer calculations was undertaken to eliminate the unknowns and to provide the necessary analytical techniques.

A. Stress Analysis and Plate Deflection

The normal stress distributions under 1-inch button- and fillister-head bolts were obtained from oil penetration and oil pressure measurements. (There is not available at this time any other data of this type with which to compare the results of these measurements.) It was found that the normal stress distribution under a thick fillister-head bolt was very nearly uniform under the entire head. Data obtained for a button-head bolt and a thin fillister-head bolt exhibited non-uniform distributions with a zone of near-zero stress close to the head perimeter.

Data obtained for a 5/8-inch button-head bolt indicated that an approximately linear scale factor existed for defining the zero-stress zone for button-head bolts smaller than 1-inch in diameter.

Information on the interface stress distribution between circular and rectangular plates was obtained from oil penetration and oil pressure measurements. The values obtained for r_σ, the radial extent of the interface stress, represent the first extensive experimental data of this kind and were found to disagree with results obtained from Sneddon's (61) theory. This disagreement was shown to be important when values of r_σ are applied in the calculation of plate deflection. Fernlund's (60) simplified method to obtain interface stress distributions, previously verified for thick plates, was shown to be invalid for thin plates. An approximate method was developed for use in place of Fernlund's simplified method, and was shown to yield adequate results if r_σ is known to within 2-3 percent.

An analytical technique, employing the method of superposition, was developed to describe the deflection of thin circular plates with center holes, subject to non-uniform partial loading. The resulting equations were programmed for digital solution. This analysis was shown to agree well with results from the literature when applied to cases involving uniform continuous loading. Plate deflections calculated with this program were shown to disagree with Lieb's (42) simplified analysis in several important cases. The program was also employed in a parametric study to demonstrate the extreme sensitivity of the deflection of bolted plates to the value of r_σ.

B. Heat Transfer Results

The information obtained from the study of bolthead and interface stress distributions, combined with the plate deflection program, was used in equations previously developed for the contact region and the interface gap to calculate theoretical values of interface conductance for two bolted joints. This was done for aluminum and stainless steel joints in air and in vacuum. These computed conductances were then used in finite-difference steady-state heat transfer analyses to calculate the temperature gradients across the joint interfaces.

Interface temperature gradients were measured for the aluminum and stainless steel joints in 5 tests in air at ambient pressure and 4 tests in vacuum. The measured gradients were found to agree with the computed gradients within about 2°F. The average deviation between measured and computed gradients was 35 percent. This deviation was attributed partly to the errors in temperature measurement, but mostly to the uncertainties in the values of k, h and ϵ used in the finite-difference analysis.

C. Recommendations

There are two areas in which more experimental data is needed. The first of these is the determination of r_σ as a function of $(r_h - r_s)/b$. The second is interface temperature gradients.

In Chapter IV the importance of knowing r_σ very accurately was demonstrated. In order to obtain the needed accuracy over a range of values of $(r_h - r_s)/b$ it is believed that the methods employed in this study will not be adequate and that three-dimensional photoelastic methods should be employed in an attempt to determine r_σ to within a few percent.

More accurate measurements of the temperature drop across the interface of bolted joints are needed to establish a reliable experimental baseline with which the theoretical results can be compared. Great care needs to be taken in the fabrication of the experimental plates. The plates should be made from thick flat stock and ground down to eliminate any possible warping. The mating surfaces should be lapped if possible to insure the best possible mating. The thermal conductivity and emittance of the plates should be measured to within a few percent in separate, closely controlled experiments in order to provide accurate data for calculating heat losses. A complete finite-difference analysis should be performed to estimate the heat losses. This analysis should consider the heating element, cooling plate, and the support structure in order to more accurately determine the heat losses from the element and the heat transfer across the joint. The thermocouple calibration should be checked (in place) at a temperature above the ice point, if possible. This would require a small electrically-heated well-insulated portable vessel.

Larger temperature gradients across the interface would possibly reduce the percentage error in the measurements; however, the heat losses would probably be greater. If all of the heat losses can be accurately accounted for in a finite-difference heat transfer analysis, higher heating rates and temperature gradients would prove beneficial.

Considerable improvement in the analysis of interface stress distribution could be obtained if Fernlund's (60) exact method was adapted to non-uniformly loaded plates. This might be possible by using a method of superposition to describe the non-uniform loading. This could best

be done using a digital computer. Such an analysis would permit a theoretical determination of r_σ which might prove better than any experimental method.

LITERATURE CITED

(1) No Author - "Boeing Thermal Analyzer", Boeing Document AS 0315, August 21, 1963.

(2) Coulbert, C. D. and C. Liu, "Thermal Resistance of Aircraft Structure Joints", Wright Air Development Center, TN 53-50, June 1953.

(3) Eckert, E. R. G. and R. M. Drake. Heat and Mass Transfer, McGraw-Hill Book Company, Inc., New York, (1959). p. 404.

(4) Minzner, R. A., K. S. W. Champion, and H. L. Pond. "The ARDC Model Atmosphere, 1959", Air Force Cambridge Research Center TR-59-267, August 1959.

(5) Jacob, M. Heat Transfer, Vol - 1, John Wiley and Sons, New York, (1949), pp. 534-539.

(6) McAdams, W. H. Heat Transmission, McGraw-Hill Book Company, Inc., New York, (1954), pp. 181-182.

(7) Lindh, K. G., B. A. Lieb, E. L. Knuth, T. Ishimoto, and H. Kaysen. "Studies in Heat Transfer in Aircraft Structure Joints", University of California, Los Angeles, Report 57-50, May 1957.

(8) Stubstad, W. R. "Measurements of Thermal Contact Conductance in Vacuum", ASME Reprint 63-WA-150, November 1963.

(9) Dushman, S. Scientific Foundations of Vacuum Technique, John Wiley and Sons, New York, (1961), pp. 47-50.

(10) Northrup, E. F. "Some Aspects of Heat Flow", Trans. Amer. Electrochem. Soc., XXIV, (1913), pp. 85-103.

(11) Taylor, T. A. "The Thermal Conductivity of Insulating and Other Materials", Trans. ASME, 41, (1919), pp. 605-621.

(12) Van Dusen, M. S. "A Simple Apparatus for Comparing the Thermal Conductivity of Metals and Very Thin Specimens of Poor Conductors", J. Optical Soc. of Amer., VI, (1922), pp. 739-743.

(13) Jacobs, R. B. and C. Starr. "Thermal Conductance of Metallic Contacts", Review of Scientific Instruments, 10, (1939), pp. 140-141.

(14) Bowden, F. P. and D. Tabor. "The Area of Contact Between Stationary and Moving Surfaces", Proc. Royal Soc. of London, A 169, (1939), pp. 391-413.

(15) Kouwenhoven, W. B. and J. Tampico. "Measurement of Contact Resistance", Paper presented at the annual meeting of the American Welding Society, Cleveland, Ohio, October 21-25, 1940.

(16) Kouwenhoven, W. B. and J. Tampico. "Surface Polish and Contact Resistance", The Welding Journal Research Supplement, VI, (1941), pp. 468-471.

(17) Tampico, J. "Measurement of Contact Resistance", Ph.D. Dissertation at Johns Hopkins, (1941).

(18) Karush, W. "Temperature of Two Metals in Contact", AEC Report AECD-2967, December 22, 1944.

(19) Atkins, H. L. "Bibliography on Thermal Metallic Contact Conductance", NASA TM x-53227, April 15, 1965.

(20) Minges, M. L. "Thermal Contact Resistance - A Review of the Literature", Air Force Materials Laboratory, AFML-TR-65-375-Volume I, Wright-Patterson A.F.B., Ohio, April 1966.

(21) Fried, E. and H. L. Atkins. "Interface Thermal Conductance in a Vacuum", J. of Spacecraft and Rockets, 2 No. 4, (July-August 1965), pp. 591-593.

(22) Fried, E. "Thermal Conductance of Metallic Contacts in a Vacuum", Amer. Inst. of Aeronautics and Astronautics Reprint 65-661, September 1965.

(23) Fry, E. M. "Measurement of Contact Coefficients of Thermal Conductance", Amer. Inst. of Aeronautics and Astronautics Reprint 65-662, September 1965.

(24) Stubstad, W. R. "Thermal Contact Resistance Between Thin Plates in Vacuum", ASME Reprint 65-HT-16, August 1965.

(25) Yovanovich, M. M. "Theoretical and Experimental Study of Thermal Conductance of Wavy Surfaces", Semi-annual Status Report, NASA Research Grant No. NGR-22-009-065, June 1965.

(26) Yovanovich, M. M. "Thermal Contact Conductance in a Vacuum", Massachusetts Institute of Technology Mechanical Engineering Thesis, February 1966.

(27) Yovanovich, M. M. and H. Fenech. "Thermal Contact Conductance of Nominally-Flat, Rough Surfaces in a Vacuum Environment", Amer. Inst. of Aeronautics and Astronautics, Reprint 66-42, January 1966.

(28) Koh, B. and J. E. John. "The Effect of Interfacial Metallic Foils on Thermal Contact Resistance", the ASME Reprint 65-HT-44, August 1965.

(29) Williams, A. "Heat Transfer Through Metal to Metal Joints", Inst. of Mech. Engineers Reprint No. 125, August 1966.

(30) Mendelsohn, A. P. "Contact Effectiveness in a Space Radiator", J. of Spacecraft and Rockets, 2, No. 6, (Nov. - Feb. 1965), pp. 995-996.

(31) Blum, H. A. and C. J. Moore, Jr. "Transient Phenomena in Heat Transfer Across Surfaces in Contact", ASME Reprint 65-HT-59, August 1965.

(32) Dutkiewicz, R. "Interfacial Gas Gap for Heat Transfer Between Randomly Rough Surfaces", Inst. of Mech. Engineers Reprint No. 126, August 1966.

(33) Yovanovich, M. M. "Thermal Contact Resistance Between Smooth Rigid Isothermal Planes Separated by Elastically Deformed Smooth Spheres", Amer. Inst. of Aeronautics and Astronautics Reprint 66-461, June 1966.

(34) Hultberg, J. A. "Thermal Joint Conductance", JPL Space Program Summary Report No. 37-38, IV, (April 1966), pp. 61-63.

(35) Ozisik, M. N. and D. Hughes. "Thermal Contact Conductance of Smooth-to-Rough Contact Joints", ASME Reprint 66-WA/HT-54, November 1966.

(36) Jelinek, D. "Heat Transfer of Proposed Structural Joints in the Rocket Package for the F-86D Airplane", North American Aviation Lab Report No. NA-49-831, September 30, 1949.

(37) Coulbert, C. D. and C. Liu. "Thermal Resistance of Aircraft Structure Joints", Wright Aeronautical Development Center TN 53-50, June 1953.

(38) Lindh, K. G. "Measurement of Thermal Contact Resistance", UCLA Service to Industry Report C14-53, June 1953.

(39) Lindh, K. G. "Thermal Contact Resistance Study", UCLA Service to Industry Report C15-53, August 1953.

(40) Ambrosio, A. and K. G. Lindh. "Thermal Contact Resistance of Riveted Joints", UCLA Service to Industry Report C55-4, February 1955.

(41) Ambrosio, A. and K. G. Lindh. "Thermal Contact Resistance of Spot Welded Titanium Joints", UCLA Service to Industry Report C55-12, March 1955.

(42) Lindh, K. G., B. A. Lieb, E. L. Knuth, T. Ishimoto, and H. M. Kaysen. "Studies in Heat Transfer in Aircraft Structure Joints", UCLA Report 57-50, May 1957.

(43) Holloway, G. F. "The Effect of an Interface on the Transient Temperature Distribution in Composite Aircraft Joints", Syracuse University M. S. Thesis, December 1954.

(44) Ashmead, F. A. H. "Thermal Resistance of Joints", College of Aeronautics Diploma Thesis, Great Britian, May 1955.

(45) Griffith, G. E. and G. H. Miltonberger. "Some Effects on Joint Conductivity on the Temperature and Thermal Stresses in Aerodynamically Heated Skin Stiffner Combinations", NACA Technical Note 3699, June 1956.

(46) Gateweed, B. E. "Effect of Thermal Resistance of Joints upon Thermal Stresses", Air Force Institute of Technology Report 56-6 (AD 106-014), May 1956.

(47) Barber, A. D., H. H. Weiner, and B. Boley. "An Analysis of the Effect of Thermal Contact Resistance in a Sheet Stringer Structure", J. of Aeronautical Sciences, 23:3, (March 1957), pp. 232-234.

(48) Fontenot, J. E. "Thermal Conductance of Contacts and Joints", Boeing Document D5-12206, The Boeing Company, Huntsville, Alabama, December 1964.

(49) Andrews, I. D. C. "An Investigation of the Thermal Conductance of Bolted Joints", Royal Aircraft Establishment Technical Note WE.46, January 1964.

(50) Anderson, R. R. "Interface Thermal Conductance Tests of Riveted Joints in a Vacuum", Douglas Aircraft Company Report TU24871, Douglas Aircraft Company, Tulsa, Oklahoma, February 6, 1964.

(51) Bevans, J. T. et al. "Bimonthly Progress Reports Nos. 1-5, Prediction of Space Vehicle Thermal Performance", TRW Space Technology Laboratory Reports 4182-600 1 to 5-SU-000, August 1964 - May 1965.

(52) Elliott, D. H. "Thermal Conductance Across Aluminum Bolted Joints", ASME Reprint 65-HT-53, August 1965.

(53) Maerschalk, J. C. "The Effects of Creep on Thermal Contact Conductance Between Thin Plates in a Vacuum", Collins Radio Company Report 523-0757819-00181M, April 15, 1965.

(54) Fenech, H. and W. H. Rohsenow. "Prediction of Thermal Conductance of Metallic Surfaces in Contact", J. of Heat Transfer, 85:1, (February 1963), pp. 15-24.

(55) Centinkale, T. N. and M. Fishenden. "Thermal Conductance of Metal Surfaces in Contact", General Discussion on Heat Transfer, IME and ASME, (1951), pp. 271-294.

(56) Laming, L. C. "Thermal Conductance of Machined Contacts", International Developments in Heat Transfer, The American Society of Mechanical Engineers, New York, (1963), pp. 65-76.

(57) Boeschoten, F. and E. F. M. Van der Held. "The Thermal Conductance of Contacts Between Aluminum and Other Metals", Physica, XXIII, (1957), pp. 37-44.

(58) Graff, W. J. "Thermal Conductance Across Metal Joints", Machine Design, 32:19, (September 15, 1960), pp. 166-172.

(59) Holm, R. Electrical Contacts, Almquist and Wiksells Akademiska Hanbocker, Stockhom., Sweden, (1946).

(60) Fernlund, I. "A Method to Calculate the Pressure Between Bolted or Riveted Plates", Chalmers University of Technology Report No. 245, Gothenburg, Sweden, (1961).

(61) Sneddon, I. N. Fourier Transforms, McGraw-Hill Book Company, New York, N. Y. (1962), pp. 479-480.

(62) Coker, E. H. and L. N. G. Filon. A Treatise on Photo-Elasticity, Cambridge University Press, London, England (1957).

(63) Aron, W. and G. Colombo. "Controlling Factors of Thermal Conductance Across Bolted Joints in a Vacuum Environment", ASME Paper No. 63-WA-196, (November 1963).

(64) No author. Torque Manual, P. A. Sturtevant Co., Addison, Illinois (1966).

(65) Bumgardner, H. M., Jr. "A Study of Load Distributions Under Bolt Heads", Louisiana State University Masters Thesis, (August 1967).

(66) Timoshenko, S. and S. Woinowsky-Krieger. Theory of Plates and Shells, McGraw-Hill Book Company, New York, N. Y. (1959).

(67) Timoshenko, S. and J. N. Goodier. Theory of Elasticity, McGraw-Hill Book Company, New York, N. Y. (1951).

(68) Wahl, A. M. and G. Lobo. "Stresses and Deflections in Flat Circular Plates With Central Holes", Transactions of ASME, 52, (1930), pp. APM 29-43.

(69) Gaski, J. D. and D. R. Lewis. "Chrysler Improved Numerical Differencing Analyzer", Chrysler Corporation Space Division TN-AP-66-15, New Orleans, La. (April 1966).

(70) No author. "Material Selector Issue", Materials in Design Engineering, 54:5 (October 1961).

(71) Belleman, G. "Thermophysical Properties of Materials", The Boeing Company, Document No. D-16103-1, Seattle, Washington (March 1961).

APPENDIX A

Computer Program for Plate Deflection

```
C     THIN PLATE THEORY - METHOD OF SUPERPOSITION
C
C     THIS PROGRAM IS WRITTEN IN FORTRAN IV COMPUTER LANGUAGE FOR AN IBM
C     7040 DIGITAL COMPUTER.  IT WILL CALCULATE THE DEFLECTION OF A THIN
C     CIRCULAR PLATE SUBJECT TO NON-UNIFORM PARTIAL LOADING.  THE METHOD
C     OF SUPERPOSITION IS USED IN CONJUNCTION WITH MATCHED BOUNDARY CON-
C     DITIONS.  WITHIN THE PROGRAM THERE IS AN OPTIONAL PROCEDURE FOR
C     OBTAINING THE COEFFICIENTS THAT ARE USED IN THE POLYNOMIAL EQUA-
C     TIONS THAT DESCRIBE THE STRESS DISTRIBUTIONS APPLIED TO THE PLATE.
C     THE FIRST OPTION SPECIFIES THAT THE COEFFICIENTS BE PREDETERMINED
C     AND READ INTO THE PROGRAM AS INPUT DATA.  THE SECOND OPTION SPECI-
C     FIES THAT COORDINATES FROM THE STRESS DISTRIBUTION CURVE BE READ
C     IN AS INPUT DATA.  THE PROGRAM THEN CURVE FITS THESE COORDINATES
C     BY USING A POLYNOMIAL CURVE FIT SUBROUTINE WHICH IS LOCATED IN THE
C     SYSTEMS LIBRARY OF THE IBM 7040 COMPUTER BEING USED.  THE OUTPUT
C     OF THIS SUBROUTINE IS THE COEFFICIENTS OF THE POLYNOMIAL EQUATION.
C     FOR ANY GIVEN CASE, THE UPPER STRESS ON THE PLATE MAY USE THE
C     FIRST OPTION WHILE THE LOWER STRESS MAY USE THE SECOND, OR VICE
C     VERSA.  THERE IS ANOTHER PROCEDURAL OPTION WHICH ALLOWS THE CALCU-
C     LATION OF THE DEFLECTION CAUSED ONLY BY THE UPPER OR LOWER STRESS
C     INSTEAD OF THE SUPERIMPOSED DEFLECTION CAUSED BY THE UPPER AND
C     LOWER STRESSES ACTING TOGETHER.
C
C
C     DIMENSION VARIABLES
      DIMENSION B(20),W(30),R(20)
      DIMENSION XX(50),YY(50),YYC(50),COEFS(50),ERROR(50)
C     SET COUNT VARIABLE FOR CASE NUMBER AND PRINT
      KKK = 0
 1000 KKK = 1+ KKK
      PRINT 80,KKK
 80   FORMAT(1H1/49X,12H****CASE NO.,I4,4H****///)
C     READ OPTION CONTROL VARIABLE WHICH CHOOSES BETWEEN SUPERIMPOSED
C     DEFLECTION AND DEFLECTION FROM A SINGLE STRESS.
C     IF IJK = 1, CALCULATE DEFLECTION CAUSED BY A SINGLE STRESS
C     IF IJK = 2, CALCULATE DEFLECTION CAUSED BY UPPER STRESS, CALCULATE
```

```
C                  DEFLECTION CAUSED BY LOWER STRESS, AND CALCULATE THE
C                  TOTAL DEFLECTION BY THE METHOD OF SUPERPOSITION
      READ 25,IJK
 25   FORMAT(I10)
      LM = 0
      IF(IJK-1)51,51,52
 51   MIN = 1
      GO TO 53
 52   MIN = 2
 53   DO 200 KIJ = 1,MIN
      IF(IJK-1)11,11,12
C     PRINT TYPE OF STRESS BEING CALCULATED
 12   IF(KIJ-1)13,13,14
 13   PRINT 92
 92   FORMAT(53X,12HUPPER STRESS)
      GO TO 11
 14   PRINT 93
 93   FORMAT(///53X,12HLOWER STRESS)
C     READ OPTION CONTROL VARIABLE WHICH DESIGNATES WHETHER THE COEFFI-
C     CIENTS USED IN THE POLYNOMIAL ARE TO BE READ IN OR CALCULATED BY
C     THE CURVE FIT SUBROUTINE.
C     IF ME = 1,THE COEFFICIENTS ARE TO BE READ IN
C     IF ME= 2, THE COEFFICIENTS ARE TO BE CALCULATED
 11   READ 25,ME
C     READ HEADER CARD (INPUT DATA)
C     MAT = VARIABLES WHICH INDICATES TYPE OF METAL BEING USED
C         1 FOR STAINLESS STEEL, 2 FOR ALUMINUM, 3 FOR TITANIUM
C     XB = PLATE THICKNESS
C     RR = RADIUS OF THE PLATE
C     RS = RADIUS OF THE SHANK OF THE BOLT
C     RL = RADIUS OF THE LOADED AREA
C     N = DEGREE OF POLYNOMIAL BEING USED
C     LTYPE - DESIGNATES WHETHER PLATE HAS A FREE OUTER EDGE OR
C         A FIXED OUTER EDGE
C         1 FOR FREE EDGE
C         2 FOR FIXED EDGE (EDGE OF ZERO SLOPE)
```

```
      READ 10,MAT,XB,RR,RS,RL,N,LTYPE
 10   FORMAT(I1,4F10.0,2I10)
      IF(ME-1)63,63,64
C     IF COEFFICIENTS ARE TO BE CALCULATED, READ HEADED CARD TO THE CO-
C     ORDINATE INPUT DATA.
C     NNN = NUMBER OF PAIRS OF COORDINATES TO BE READ IN (INPUT TO SUBROUTINE)
C     TOL = MAXIMUM TOLERANCE REQUESTED (MUST BE SET MUCH LOWER THAN
C           OBTAINABLE SO THAT PROGRAM CAN SEARCH FOR MINIMUM STANDARD
C           ERROR) (INPUT TO SUBROUTINE)
C     LL = MAXIMUM DEGREE POLYNOMIAL DESIRED (INPUT TO SUBROUTINE)
 64   READ 62,NNN,TOL,LL
 62   FORMAT(I10,F10.0,I10)
C     READ COORDINATES FROM STRESS DISTRIBUTION CURVE
      READ 61,(XX(IN),YY(IN),IN=1,NNN)
 61   FORMAT(2F10.0)
      JC = LL
      NJ = JC + 1
C     CALCULATE STANDARD ERROR FOR EACH DEGREE OF POLYNOMIAL FROM 1 TO LL
 67   CALL CURVEF(NNN,TOL,LL,XX,YY,SE,YYC,COEFS,INDIK)
C     XX = ARRAY OF X COORDINATES TO BE FITTED (INPUT TO SUBROUTINE)
C     YY = ARRAY OF Y COORDINATES TO BE FITTED (INPUT TO SUBROUTINE)
C     SE = STANDARD ERROR OF POLYNOMIAL CURVE TO INPUT CURVE (OUTPUT OF
C          SUBROUTINE)
C     YYC = ARRAY OF YY CALCULATED VALUES (OUTPUT OF SUBROUTINE)
C     COEFS = ARRAY OF COEFFICIENTS FOR THE POLYNOMIAL EQUATION (OUTPUT
C          OF SUBROUTINE)
C     INDIK = AN INDICATOR WHICH SPECIFIES WHETHER A LESSER DEGREE POLY-
C          NOMIAL THAN LL HAS A STANDARD ERROR LESS THAN THE TOLER-
C     ANCE SPECIFIED BY TOL (OUTPUT OF SUBROUTINE - NOT USED HERE)
      NJ = NJ - 1
      ERROR(NJ) = SE
      IF(LL-1)65,65,66
 66   LL = LL- 1
      GO TO 67
 65   NJ = JC
C     PRINT STANDARD ERRORS
```

```
      PRINT 57
 57   FORMAT(///32X,33HSTANDARD ERRORS FOR DEGREES 1-LL ,
     *23HOF POLYNOMIAL CURVE FIT)
      PRINT 56,(ERROR(JF),JF = 1,5)
      PRINT 56,(ERROR(JF),JF = 6,JC)
 56   FORMAT(//9X,5E19.7)
C     SEARCH FOR BEST STANDARD ERROR
 55   KB = NJ
      NJ = NJ - 1
      IF(ERROR(NJ)-ERROR(KB))8,9,9
 8    GO TO 55
C     CALCULATE COEFFICIENTS FOR DEGREE YIELDING BEST STANDARD ERROR
 9    LL = KB
      CALL CURVEF(NN,TOL,LL,XX,YY,SE,YYC,COEFS,INDIK)
 63   CONTINUE
C     SET PROPERTIES OF METAL BEING USED
C     E = MODULUS OF ELASTICITY
C     U = POISSONS RATIO
      IF(MAT-2)1,2,3
C     PROPERTIES OF STAINLESS STEEL
 1    E=29000000.0
      U=.25
      GOTO4
C     PROPERTIES OF ALUMINUM
 2    E=10500000.0
      U=.33
      GOTO4
C     PROPERTIES OF TITANIUM
 3    E=16000000.0
      U=.30
C     CALCULATE CONSTANTS
C     D = PLATE MODULUS OF RIGIDITY
C     RHOR, RHOS, ALPHA, BETA, AND GAMMA - PARAMETERS DEVELOPED IN TEXT
 4    D=(E*X8**3)/(12.0*(1.0-U**2))
      RHOR=RR/RL
      RHOS=RS/RL
```

```
      ALPHA=(1.0-(1.0+U)/(1.0-U)*RHOR**2)/(1.0+(1.0+U)/(1.-U)*RHOR**2)
      BETA=(1.0-RHOS**2)/(1.0+RHOS**2)
      GAMMA=(RHOR**2+1.0)/(RHOR**2-1.0)
C     EVALUATE SUMMATIONS
      S1=0.0
      S2=0.0
      S3=0.0
      S4=0.0
      S5=0.0
      S6=0.0
      IF(NE-1)72,72,73
 73   J = LL + 1
      GO TO 77
 72   J=N+1
 77   DO100K=1,J
      I=K-1
      XI=I
      IF(NE-1)68,68,69
C     SET VALUE OF A = COEFS(K) IF COEFFICIENTS ARE CALCULATED
 69   A = COEFS(K)
      GO TO 71
C     READ VALUE OF A IF COEFFICIENTS ARE READ IN
 68   READ20,A
 20   FORMAT(F20.0)
 71   S1=((A*(XI+3.0))/((XI+2.0)**2*(XI+4.0)))*(RL**(I+3))*(1.0+RHOS
     ***(I+4))+S1
      S2=(A/(4.0*(XI+2.0)))*(RL**(I+3))*(RHOS**2*(1.0-2.0*ALOG(RS))-
     *(1.0+2.0*ALOG(RL)))+S2
      S3=-(A*(XI+2.0)/((XI+2.0)**2*(XI+4.0)))*(RL**(I+3))*(1.0-RHOS**(I+4))+S3
      S4=(A/(4.0*(XI+2.0)))*(RL**(I+3))*(RHOS**2*(1.0-2.0*ALOG(RS))-
     *(1.0-2.0*ALOG(RL)))+S4
      S5=-(A/((XI+2.0)**2*(XI+4.0)**2))*(RL**(I+3))*(1.0-RHOS**(I+4)
     **(1.0-(XI+4.0)*ALOG(RHOS)))+S5
      S6=-(A/(4.0*(XI+2.0)))*(RL**(I+3))*((1.0-ALOG(RL))+RHOS**2*
     *((1.0-2.0*ALOG(RS))*ALOG(RHOS)-(1.0-ALOG(RS))))+S6
      B(K)=A
```

```
 100  CONTINUE
      S1=S1/D
      S2=S2/D
      S3=S3/D
      S4=S4/D
      S5=S5/D
      S6=S6/D
C     PRINT INPUT DATA
      PRINT 30,MAT,XB,RR,RS,RL,N,LTYPE
 30   FORMAT(///14X,5HMAT =,I3,5X,3HB =,F6.3,5X,4HRR =,F5.2,5X,4HRS =,
     *F6.3,5X,4HRL =,F5.2,5X,3HN =,I3,5X,6HTYPE =,I3///)
C     PRINT COEFFICIENTS
      PRINT 74
 74   FORMAT(59X,1HA/)
      DO 250 NM = 1,J
      PRINT 75,B(NM)
 75   FORMAT(45X,E20.5)
 250  CONTINUE
C     PRINT CARRIAGE CONTROLL FOR SPACING
      PRINT 76
 76   FORMAT(//1H )
C     PRINT SUMMATIONS
      PRINT 40,S1,S2,S3,S4,S5,S6
 40   FORMAT(16X,10HS1 TO S6 =,4X,6E12.3///)
C     PRINT CONSTANTS
      PRINT 50,D,RHOR,RHOS,ALPHA,BETA,GAMMA
 50   FORMAT(15X,3HD =,E9.2,3X,6HRHOR =,F5.2,3X,6HRHOS =,F6.3,3X,
     *7HALPHA =,F6.3,3X,6HBETA =,F6.3,3X,7HGAMMA =,F7.4///)
C     PRINT HEADINGS FOR COLUMNS OF OUTPUT
      PRINT 60
 60   FORMAT(15X,2HRB,7X,5HSIGMA,13X,2HSL,12X,2HWL,12X,1HR,11X,1HW,
     *15X,3HRHO/)
      DO200L=1,10
      LM = 1 + LM
      XL=L
C     SET INCREMENTS OF RB FOR CALCULATING SIGMA
```

```
      SIGMA=0.0
      DO300M=1,J
      RB=RS+XL*(RL-RS)/10.0
C     CALCULATE SIGMA (STRESS AT A GIVEN POINT ON THE STRESS DISTRIBUTION
C     CURVE)
 300  SIGMA=B(M)*RB**(M-1)+SIGMA
C     SET INCREMENTS OF R FOR CALCULATING W FOR FREE EDGE AND FOR
C     FIXED EDGE.
      R(L) = RS+XL*(RR-RS)/10.0
      RHO=R(L)/RL
      IF(LTYPE-1)5,5,6
C     CALCULATE CONSTANTS FOR W FREE EDGE
C     SL = SLOPE AT RL
C     WL = DEFLECTION AT RL
 5    SL=(S3+S4+(S1+S2)*BETA)/(1.0-ALPHA*BETA)
      WL=(S5+S6+((1.0-RHOS**2*(1.0-2.0*ALOG(RHOS)))/(2.0*(1.0+RHOS**2
     *)))*(S1+S2+ALPHA*SL))*RL
C     CALCULATE W FOR FREE EDGE
      W(LM)=WL+SL*RL*(ALOG(RHO)+(RHO**2-(1.0+2.0*ALOG(RHO)))/(2.0*(((1.0
     *+U)/(1.0-U))*RHOR**2+1.0)))
      GOTO7
C     CALCULATE CONSTANTS FOR W FIXED EDGE
 6    SL=(S3+S4+(S1+S2)*BETA)/(1.0+GAMMA*BETA)
      WL=(S5+S6+((1.0-RHOS**2*(1.0-2.0*ALOG(RHOS)))/(2.0*(1.0+RHOS**2
     *)))*(S1+S2-GAMMA*SL))*RL
C     CALCULATE W FOR FIXED EDGE
      W(LM)=WL+SL*RL*(ALOG(RHO)-(RHO**2-(1.+2.0*ALOG(RHO)))/(2.0*(RHOR**
     *2-1.0)))
 7    CONTINUE
C     PRINT RESULTS
      PRINT 70,RB,SIGMA,SL,WL,R(L),W(LM),RHO
 70   FORMAT(13X,F5.2,03X,0PE10.3,07X,E10.3,04X,E10.3,5X,F6.2,03X,E12.4,
     *6X,E10.3)
 200  CONTINUE
      IF(IJK-1)15,15,16
 16   PRINT 94
```

```
 94    FORMAT(1Y//43X,1HR,24X,4HWSUM/)
C      CALCULATE WSUM BY SUPERIMPOSING THE DEFLECTIONS CAUSED BY THE
C      UPPER AND LOWER STRESSES
       DO 500 MM = 1,10
       NN = MM + 10
       WSUM = W(MM) + W(NN)
       PRINT 95,R(MM),WSUM
 95    FORMAT(40X,F6.2,E30.4)
 500   CONTINUE
       PRINT 90
 90    FORMAT(1H1)
       GO TO 1000
C      PRINT CARRIAGE CONTROL
 15    CONTINUE
       PRINT 90
       GOTO1000
       END
```

****CASE NO. 1****

UPPER STRESS

STANDARD ERRORS FOR DEGREES 1-LL OF POLYNOMIAL CURVE FIT

0.1039821E 04	0.7033394E 03	0.4329979E 03	0.2210252E 03	0.1152397E 03
0.4935722E 02	0.6606985E 02	0.5234340E 02	0.4051367E 02	0.5391077E 02

MAT = 2 B = 0.250 RR = 1.00 RS = 0.188 RL = 0.33 N = 0 TYPE = 1

A

0.45988E 03
0.12405E 06
-0.14832E 07
0.72941E 07
-0.13625E 08
0.56381E 08
-0.54892E 09
0.17786E 10
-0.12401E 10
-0.16406E 10

S1 TO S6 = 0.187E-02 0.272E-02 -0.502E-03 -0.185E-02 -0.911E-04 -0.454E-03

D = 0.15E 05 RHOR = 3.05 RHOS = 0.573 ALPHA = -0.897 BETA = 0.505 GAMMA = 1.2411

RB	SIGMA	SL	WL	R	W	RHO
0.20	0.416E 04	-0.192E-04	-0.480E-05	0.27	-0.3570E-05	0.821E 00
0.22	0.413E 04	-0.192E-04	-0.480E-05	0.35	-0.5223E-05	0.107E 01
0.23	0.407E 04	-0.192E-04	-0.480E-05	0.43	-0.6567E-05	0.132E 01
0.24	0.399E 04	-0.192E-04	-0.480E-05	0.51	-0.7714E-05	0.156E 01
0.26	0.387E 04	-0.192E-04	-0.480E-05	0.59	-0.8729E-05	0.181E 01
0.27	0.371E 04	-0.192E-04	-0.480E-05	0.68	-0.9652E-05	0.206E 01
0.29	0.344E 04	-0.192E-04	-0.480E-05	0.76	-0.1051E-04	0.231E 01
0.30	0.293E 04	-0.192E-04	-0.480E-05	0.84	-0.1131E-04	0.255E 01
0.31	0.193E 04	-0.192E-04	-0.480E-05	0.92	-0.1208E-04	0.280E 01
0.33	-0.418E 00	-0.192E-04	-0.480E-05	1.00	-0.1282E-04	0.305E 01

LOWER STRESS

MAT = 2 B = 0.250 RR = 1.00 RS = 0.188 RL = 0.58 N = 4 TYPE = 1

A

0.37842E 04
-0.85505E 05
0.37488E 06
-0.60775E 06
0.33824E 06

****CASE NO. 2****

MAT = 1 B = 0.125 RR = 1.00 RS = 0.188 RL = 0.45 N = 4 TYPE = 1

A

0.25945E 05
-0.46084E 06
0.21550E 07
-0.39205E 07
0.24924E 07

S1 TO S6 = -0.110E-01 -0.890E-02 0.260E-02 0.123E-01 0.369E-03 0.454E-02

D = 0.50E 04 RHOR = 2.20 RHOS = 0.414 ALPHA = -0.780 BETA = 0.707 GAMMA = 1.5193

RB	SIGMA	SL	WL	R	W	RHO
0.21	-0.717E 04	0.540E-03	0.153E-03	0.27	0.3016E-04	0.593E 00
0.24	-0.641E 04	0.540E-03	0.153E-03	0.35	0.9092E-04	0.772E 00
0.27	-0.539E 04	0.540E-03	0.153E-03	0.43	0.1405E-03	0.951E 00
0.29	-0.426E 04	0.540E-03	0.153E-03	0.51	0.1831E-03	0.113E 01
0.32	-0.314E 04	0.540E-03	0.153E-03	0.59	0.2210E-03	0.131E 01
0.35	-0.213E 04	0.540E-03	0.153E-03	0.68	0.2557E-03	0.149E 01
0.37	-0.130E 04	0.540E-03	0.153E-03	0.76	0.2881E-03	0.167E 01
0.40	-0.675E 03	0.540E-03	0.153E-03	0.84	0.3188E-03	0.184E 01
0.43	-0.274E 03	0.540E-03	0.153E-03	0.92	0.3483E-03	0.202E 01
0.45	-0.674E 02	0.540E-03	0.153E-03	1.00	0.3769E-03	0.220E 01

S1 TO S6 = -0.340E-02 -0.776E-03 0.123E-02 0.232E-02 0.287E-03 0.107E-02

D = 0.15E 05 RHOR = 1.72 RHOS = 0.324 ALPHA = -0.710 BETA = 0.810 GAMMA = 2.0139

RB	SIGMA	SL	WL	R	W	RHO
0.23	-0.252E 04	0.107E-03	0.507E-04	0.27	0.6442E-05	0.464E 00
0.27	-0.218E 04	0.107E-03	0.507E-04	0.35	0.2109E-04	0.604E 00
0.31	-0.173E 04	0.107E-03	0.507E-04	0.43	0.3300E-04	0.744E 00
0.34	-0.126E 04	0.107E-03	0.507E-04	0.51	0.4316E-04	0.884E 00
0.38	-0.829E 03	0.107E-03	0.507E-04	0.59	0.5216E-04	0.102E 01
0.42	-0.475E 03	0.107E-03	0.507E-04	0.68	0.6033E-04	0.116E 01
0.46	-0.222E 03	0.107E-03	0.507E-04	0.76	0.6791E-04	0.130E 01
0.50	-0.718E 02	0.107E-03	0.507E-04	0.84	0.7504E-04	0.144E 01
0.54	-0.969E 01	0.107E-03	0.507E-04	0.92	0.8186E-04	0.158E 01
0.58	-0.439E-02	0.107E-03	0.507E-04	1.00	0.8843E-04	0.172E 01

R	WSUM
0.27	0.2872E-05
0.35	0.1587E-04
0.43	0.2643E-04
0.51	0.3545E-04
0.59	0.4343E-04
0.68	0.5068E-04
0.76	0.5740E-04
0.84	0.6373E-04
0.92	0.6977E-04
1.00	0.7561E-04

APPENDIX B

Heat Transfer Data

Table B-1 Interface Temperatures for Test 2

CONDUCTOR NO.	COLD SIDE TEMP. ~ °F	HOT SIDE TEMP. ~ °F		Δ T ACROSS INTERFACE ~ °F		% DEVIATION IN Δ T
		MEASURED	CALCULATED	MEASURED	CALCULATED	
24	177.4	184.0	181.6	6.6	4.2	-38.
27	173.6	183.9	181.4	10.3	7.8	-24.
30	173.2	182.7	178.7	9.5	5.5	-42.
32	169.5	174.4	171.6	4.9	2.1	-57.
35	172.5	173.3	172.7	0.8	0.2	-75.
36	170.9	173.7	172.1	2.8	1.2	-57.
41	159.3	167.1	165.3	7.8	6.0	-23.
42	161.4	166.8	165.0	5.4	3.6	-33.
43	159.7	165.5	165.3	5.8	5.6	- 3.4
45	158.1	167.5	164.8	9.4	6.7	-29.
48	157.5	165.5	161.9	8.0	4.4	-45.
50	164.7	170.2	167.7	5.5	3.0	-45.
		Absolute Average		6.4	4.2	39.

Table B-2 Interface Temperatures for Test 3

CONDUCTOR NO.	COLD SIDE TEMP. ~ °F	HOT SIDE TEMP. ~ °F		Δ T ACROSS INTERFACE ~ °F		% DEVIATION IN Δ T
		MEASURED	CALCULATED	MEASURED	CALCULATED	
24	186.9	195.7	193.5	8.8	6.6	-25.
27	182.8	197.0	195.4	14.2	12.6	-11.
30	183.9	194.6	194.4	10.7	10.5	- 1.9
32	181.4	183.4	184.1	2.0	2.7	35.
35	178.3	185.4	183.7	7.1	5.4	-24.
36	179.1	185.1	183.6	6.0	4.5	-25.
41	166.0	177.8	179.2	11.8	13.2	12.
42	167.5	177.1	176.2	9.6	8.7	- 9.4
43	166.7	176.4	177.0	9.7	10.3	6.2
45	163.9	179.4	177.9	15.5	14.0	- 9.7
48	164.8	177.1	172.3	12.3	7.5	-39.
50	173.5	178.6	180.4	5.1	6.9	35.
		Absolute Average		9.4	8.6	19.

Table B-3 Interface Temperatures for Test 4

CONDUCTOR NO.	COLD SIDE TEMP. ~ °F	HOT SIDE TEMP. ~ °F		Δ T ACROSS INTERFACE ~ °F		% DEVIATION IN Δ T
		MEASURED	CALCULATED	MEASURED	CALCULATED	
24	185.7	194.2	189.8	8.5	4.1	-52.
27	181.7	195.5	192.2	13.8	10.5	-24.
30	182.8	193.6	188.3	10.8	5.5	-49.
32	180.2	181.9	181.2	1.7	1.0	-41.
35	177.6	183.6	180.3	6.0	2.7	-55.
36	177.9	184.0	181.0	6.1	3.1	-49.
41	165.3	176.3	175.7	11.0	10.4	- 5.5
42	166.2	176.0	171.4	9.8	5.2	-47.
43	165.5	174.7	174.5	9.2	9.0	- 2.2
45	162.8	176.7	175.8	13.9	13.0	- 6.5
48	164.0	176.5	170.1	12.5	6.1	-51.
50	172.3	179.8	178.0	7.5	5.7	-24.
		Absolute Average		9.2	6.4	34.

Table B-4 Interface Temperatures for Test 5

CONDUCTOR NO.	COLD SIDE TEMP. ~ °F	HOT SIDE TEMP. ~ °F		Δ T ACROSS INTERFACE ~ °F		% DEVIATION IN Δ T
		MEASURED	CALCULATED	MEASURED	CALCULATED	
24	137.1	142.6	139.1	5.5	2.0	-64.
27	136.8	142.9	139.1	6.1	2.3	-62.
30	134.8	138.8	137.6	4.0	2.8	-30.
32	130.9	133.1	131.8	2.2	0.9	-59.
35	129.4	131.4	129.9	2.0	0.5	-75.
36	131.4	130.2	131.1	---	---	---
41	122.0	123.2	122.4	1.2	0.4	-67.
42	124.2	126.0	124.7	1.8	0.5	-72.
43	121.9	125.2	123.0	3.3	1.1	-67.
45	119.3	125.0	123.0	5.7	3.7	-35.
48	119.4	125.2	119.6	5.8	0.2	-96.
50	114.3	128.2	124.6	13.9	10.3	-26.
		Absolute Average		4.7	2.2	60.

Table B-5 Interface Temperatures for Test 6

CONDUCTOR NO.	COLD SIDE TEMP. ~ °F	HOT SIDE TEMP. ~ °F		Δ T ACROSS INTERFACE ~ °F		% DEVIATION IN Δ T
		MEASURED	CALCULATED	MEASURED	CALCULATED	
24	156.6	171.3	173.5	14.7	16.9	15.
27	156.6	174.1	177.1	17.5	20.5	17.
30	158.6	170.1	175.7	11.5	17.1	49.
32	151.8	157.6	157.9	5.8	6.1	5.2
35	151.5	157.5	157.3	6.0	5.8	-3.3
36	154.1	157.8	158.9	3.7	4.8	30.
41	138.9	150.3	152.4	11.4	13.5	18.
42	143.0	151.7	150.4	8.7	7.4	-15.
43	139.8	151.6	151.8	11.8	12.0	1.7
45	138.9	153.5	152.9	14.6	14.0	-4.1
48	139.5	-----	151.4	----	11.9	-----
50	145.4	155.3	155.4	9.9	10.0	1.0
		Absolute Average		10.5	12.5	14.

Table B-6 Interface Temperatures for Test 7

CONDUCTOR NO.	COLD SIDE TEMP. ~ °F	HOT SIDE TEMP. ~ °F		Δ T ACROSS INTERFACE ~ °F		% DEVIATION IN Δ T
		MEASURED	CALCULATED	MEASURED	CALCULATED	
24	139.6	144.3	141.6	4.7	2.0	-57.
27	137.6	144.8	140.8	7.2	3.2	-56.
30	136.1	140.4	138.4	4.3	2.3	-46.
32	132.4	134.9	133.5	2.5	1.1	-56.
35	130.3	133.2	132.3	2.9	2.0	-31.
36	132.1	133.2	132.8	1.1	0.7	-36.
41	123.8	127.0	124.7	3.2	0.9	-66.
42	126.0	127.1	126.7	1.1	0.7	-36.
43	123.3	126.6	123.7	3.3	0.4	-88.
45	120.9	126.5	123.7	5.6	2.8	-50.
48	119.3	-----	119.9	---	0.6	----
50	125.2	129.0	125.9	3.8	0.7	-82.
		Absolute Average		3.6	1.5	55.

Table B-7 Interface Temperature for Test 8

CONDUCTOR NO.	COLD SIDE TEMP. ~ °F	HOT SIDE TEMP. ~ °F		Δ T ACROSS INTERFACE ~ °F		% DEVIATION IN Δ T
		MEASURED	CALCULATED	MEASURED	CALCULATED	
24	152.8	168.6	174.0	15.8	21.2	34.
27	151.5	168.9	174.7	17.4	23.2	34.
30	153.7	166.7	172.9	13.0	19.2	48.
32	147.8	153.2	157.3	5.4	9.5	76.
35	147.2	153.4	156.2	6.2	9.0	45.
36	148.6	154.4	156.8	5.8	8.2	41.
41	136.5	148.0	151.2	11.5	14.7	28.
42	140.3	148.0	150.0	7.7	9.7	26.
43	136.9	148.0	150.4	11.1	13.5	22.
45	135.8	149.2	150.5	13.4	14.7	9.7
48	135.2	-----	148.2	----	13.0	----
50	141.3	151.4	153.0	10.1	11.7	16.
		Absolute Average		10.7	14.0	35.

Table B-8 Interface Temperature for Test 10

CONDUCTOR NO.	COLD SIDE TEMP. ~ °F	HOT SIDE TEMP. ~ °F		Δ T ACROSS INTERFACE ~ °F		% DEVIATION IN Δ T
		MEASURED	CALCULATED	MEASURED	CALCULATED	
24	128.4	133.4	130.9	5.0	2.5	-50.
27	128.0	132.9	131.7	4.9	3.7	-24.
30	126.1	129.5	128.6	3.4	2.5	-26.
32	122.0	123.4	122.0	1.4	0.0	-100.
35	121.5	122.0	121.1	0.5	-0.4	-----
36	120.6	120.9	120.7	0.3	0.1	-67.
41	113.7	116.8	114.3	3.1	0.6	-32.
42	114.6	116.5	114.8	1.9	0.2	-89.
43	113.0	115.4	113.9	2.4	0.9	-62.
45	113.1	115.5	113.6	2.4	0.5	-79.
48	112.1	-----	112.4	---	0.3	----
50	115.8	117.7	117.4	1.9	1.6	-16.
		Absolute Average		2.5	1.1	55.